

ULTIMATE LOAD CAPACITY OF OPTIMALLY DESIGNED
CELLULAR BEAMS

A THESIS SUBMITTED TO
THE GRADUATE SCHOOL OF NATURAL AND APPLIED SCIENCES
OF
MIDDLE EAST TECHNICAL UNIVERSITY

BY

FERHAT ERDAL

IN PARTIAL FULFILLMENT OF THE REQUIREMENTS
FOR
THE DEGREE OF DOCTOR OF PHILOSOPHY
IN
ENGINEERING SCIENCES

FEBRUARY 2011

Approval of the thesis:

**ULTIMATE LOAD CAPACITY OF OPTIMALLY DESIGNED
CELLULAR BEAMS**

submitted by **FERHAT ERDAL** in partial fulfillment of the requirements for
the degree of **Doctor of Philosophy in Engineering Sciences Department,**
Middle East Technical University by,

Prof. Dr. Canan ÖZGEN _____
Dean, Graduate School of Natural and Applied Sciences

Prof. Dr. Turgut TOKDEMİR _____
Head of Department, **Engineering Sciences**

Prof. Dr. Turgut TOKDEMİR _____
Supervisor, **Engineering Sciences Dept., METU**

Prof. Dr. Mehmet Polat SAKA _____
Co-Supervisor, **Engineering Sciences Dept., METU**

Examining Committee Members:

Prof. Dr. Ayşe DALOĞLU _____
Civil Engineering Dept., KTU

Prof. Dr. Turgut TOKDEMİR _____
Engineering Sciences Dept., METU

Prof. Dr. Murat DİCLELİ _____
Engineering Sciences Dept., METU

Assoc. Prof. Dr. Oğuzhan HASANÇEBİ _____
Civil Engineering Dept., METU

Assist. Prof. Dr. Ferhat AKGÜL _____
Engineering Sciences Dept., METU

Date: .../.../.....

I hereby declare that all information in this document has been obtained and presented in accordance with academic rules and ethical conduct. I also declare that, as required by these rules and conduct, I have fully cited and referenced all material and results that are not original to this work.

Name, Surname : Ferhat ERDAL

Signature :

ABSTRACT

ULTIMATE LOAD CAPACITY OF OPTIMALLY DESIGNED CELLULAR BEAMS

Erdal, Ferhat
Ph.D., Engineering Sciences Department
Supervisor: Prof. Dr. Turgut Tokdemir
Co-Supervisor: Prof. Dr. M. Polat Saka

February 2011, 184 Pages

Cellular beams became increasingly popular as an efficient structural form in steel construction since their introduction. Their sophisticated design and profiling process provides greater flexibility in beam proportioning for strength, depth, size and location of circular holes. The purpose of manufacturing these beams is to increase overall beam depth, the moment of inertia and section modulus, which results in greater strength and rigidity. Cellular beams are used as primary or secondary floor beams in order to achieve long spans and service integration. They are also used as roof beams beyond the range of portal-frame construction, and are the perfect solution for curved roof applications, combining weight savings with a low-cost manufacturing process.

The purpose of the current research is to study optimum design, ultimate load capacity under applied load and finite element analysis of non-composite

cellular beams. The first part of the research program focuses on the optimum design of steel cellular beams using one of the stochastic search methods called “harmony search algorithm”. The minimum weight is taken as the design objective while the design constraints are implemented from the Steel Construction Institute. Design constraints include the displacement limitations, overall beam flexural capacity, beam shear capacity, overall beam buckling strength, web post flexure and buckling, vierendeel bending of upper and lower tees and local buckling of compression flange. The design methods adopted in this publication are consistent with BS5950. In the second part of the research, which is the experimental work, twelve non-composite cellular beams are tested to determine the ultimate load carrying capacities of these beams under using a hydraulic plug to apply point load. The tested cellular beam specimens have been designed by using harmony search algorithm. Finally, finite element analysis program is used to perform elastic buckling analysis and predict critical loads of all steel cellular beams. Finite element analysis results are then compared with experimental test results for each tested cellular beam.

Keywords: Web-expanded beams, cellular beams, steel structures, optimum structural design, minimum weight, stochastic search techniques, harmony search algorithm, particle swarm method, failure modes of beams and finite element method

ÖZ

OPTİMUM BOYUTLANDIRILMIŞ DAİRESEL GÖZENEKLİ PETEK KİRİŞLERİN YÜK TAŞIMA KAPASİTESİ

Erdal, Ferhat

Doktora, Mühendislik Bilimleri Bölümü

Tez Danışmanı: Prof. Dr. Turgut Tokdemir

Ortak tez Danışmanı: Prof. Dr. M. Polat Saka

Şubat 2011, 184 Sayfa

Dairesel gözenekli petek kirişler başlangıçlarından beri çelik yapılarda etkin bir yapı modeli olarak artan bir popüleriteye sahip oldular. Gelişmiş tasarımları kendilerine dayanım, derinlik, boyut ve dairesele boşlukların yerleri için diğer kirişlere oranla daha fazla esneklik sağlar. Bu kirişlerin üretiminin asıl amacı; kirişin derinliği, atalet momenti ve kesit katsayısını arttırmaktır. Artan atalet momenti ve kesit katsayısı kirişin dayanımının ve rijiditesinin yükselmesini sağlar. Dairesel gözenekli petek kirişler büyük açıklıkları rahat geçebilmek için birincil yada ikinci derecede olan döşeme kirişleri olarak kullanılır. Bu kirişler ayrıca çerçeve sundurmaların ötesinde çatı kirişleri olarak kullanılır ve eğimli çatı uygulamalarında ağırlık ve maliyet düşürülmesiyle mükemmel sonuçlar verirler.

Bu çalışmanın amacı; dairesel gözenekli çelik kirişlerin optimum boyutlandırılması, uygulanan yük altında taşıma kapasitesinin ölçülmesi ve sonlu elemanlar yöntemiyle modellenmesidir. Araştırmanın ilk aşaması dairesel petek kirişlerin algıya dayalı arama yöntemlerinden biri olan harmoni arama tekniği kullanılarak optimum boyutlandırılmasına odaklanmıştır. Harmoni arama yöntemi UB kesitleri arasından uygun profili seçer böylece SCI (Steel Construction Institute)'da tanımlanan tasarım sınırlamaları sağlanır ve sistemin ağırlığı minimuma indirgenir. Tasarım sınırlayıcıları olarak deplasman kısıtlayıcısı, kiriş profilin esneklik kapasitesi, kiriş kesme kapasitesi, kiriş gövdesi esneklik ve burkulma kapasitesi, kirişin alt ve üst parçalarının vierendeel (ikincil) eğilme kapasitesi ve üst flanşda bölgesel burkulma alınır. Çalışmanın ikinci aşaması olan deneysel süreçte; ilk kısımda harmoni arama yöntemi kullanılarak optimizasyonu yapılan 12 adet NPI kesit çelik dairesel gözenekli petek kirişlerin hidrolik güç üniteli basınç silindiri altında dayanımı test edilecektir. Son olarak, bütün kiriş numunelerinin elastik burkulma analizi ve taşıyabilecekleri kritik yükleri sonlu eleman programı kullanılarak yapıldıktan sonra herbir kiriş için sonlu eleman analizi sonuçları deneysel çalışmadan elde edilen sonuçları ile kıyaslanır.

Anahtar Kelimeler: Gövdesi genişletilmiş kirişler, dairesel gözenekli petek kirişler, çelik yapılar, yapının optimum boyutlandırılması, minimum ağırlık, harmoni arama yöntemi, parçacık sürü optimizasyonu yöntemi, kirişlerin göçme durumları ve sonlu eleman yöntemi

*To my family,
For your endless support and love*

ACKNOWLEDGEMENTS

I would like to express my deepest gratitude to my thesis supervisor Prof. Dr. M. Polat SAKA for his guidance, understanding, kind support, encouraging advices, criticism, and valuable discussions throughout my thesis.

I am greatly indebted to Prof. Dr. M. Ruşen GEÇİT and Prof. Dr. Turgut TOKDEMİR for their guidance and providing me every opportunity to use in Engineering Sciences Department.

My special thanks are due to Assoc. Prof. Dr. Oğuzhan Hasańebi from METU Engineering Faculty Civil Engineering Department for his great advices and discussions in performing this research.

I would sincerely thank to Erkan DOĐAN, Hakan BAYRAK, Memduh KARALAR, Fuat KORKUT, Serdar ÇARBAŞ, Refik Burak TAYMUŞ and Semih ERHAN for their endless friendship, making my stay in METU happy and memorable and being always right beside me.

I would also like to thank to my friends, Selman SAĐLAM, Mehmet DOĐAN, Özgür AKTÜRK, Fatih GÖKÇE, Kaveh Hassanzehtap and Ali Sinan DİKE for cooperation and friendship, and helping me in all the possible ways.

My greatest thanks go to my parents, Mehmet ERDAL and Habba ERDAL for their support, guidance and inspiration all through my life, my brother Fatih ERDAL, my sisters Filiz and Fidan ERDAL who are always there for me.

I owe thanks to the most special person in my life Aslı BUGAY for her boundless moral support giving me joy of living. This life would have never been meaningful without her.

TABLE OF CONTENTS

ABSTRACT	iiv
ÖZ.....	vi
ACKNOWLEDGEMENTS.....	ix
TABLE OF CONTENTS	x
LIST OF TABLES.....	xiv
LIST OF FIGURES.....	xvi
LIST OF ABBREVIATIONS.....	xxi
CHAPTERS	
1 WEB-EXPANDED BEAMS IN GENERAL.....	1
1.1 Introduction to Web-Expanded Beams	1
1.2 Castellated Beams	2
1.3 Cellular Beams	3
1.3.1 Applications of Cellular Beams	6
1.4 Literature Review	10
1.5 Objective and Scope of Research	24
2 THE DESIGN OF CELLULAR BEAMS	26
2.1 Failure Modes of Web-Expanded Beams.....	26
2.1.1 Formation of a Vierendeel Bending Mechanism.	27
2.1.2 Lateral Torsional Buckling.....	29
2.1.3 Web-Post Buckling.....	30
2.1.4 Rupture of Welded Joints.....	31

2.1.5	Flexure Mechanism.	32
2.2	Design Process of Cellular Beams	33
2.2.1	Overall Beam Flexural Capacity.	34
2.2.2	Beam Shear Capacity.	34
2.2.3	Flexural and Buckling Strength of Web-Post.....	36
2.2.4	Vierendeel Bending of Upper and Lower Tees.....	37
2.2.5	Classification of Cellular Beams.....	39
2.2.6	Deflection of Cellular Beams	41
3	THE DESIGN OPTIMIZATION OF CELLULAR BEAMS	
	USING META-HEURISTIC SEARCH TECHNIQUES	44
3.1	Optimum Design Problem of Cellular Beams.....	44
3.2	Stochastic Search Techniques in Optimization.....	47
3.2.1	Harmony Search Method.....	49
3.2.2	Particle Swarm Optimization Method.....	54
3.2.3	The Comparison of HS and PSO Algorithms with An Example	57
3.2.3.1	Cellular Beam with 4-m Span	58
3.3	Design Examples	64
3.3.1	Cellular Beam with NPI-240 Section.....	65
3.3.2	Cellular Beam with NPI-260 Section	69
3.3.3	Cellular Beam with NPI-280 Section	73
4	EXPERIMENTAL TESTS ON OPTIMALLY DESIGNED	
	STEEL CELLULAR BEAMS.....	77
4.1	Experimental Studies on Steel Cellular Beams.....	77
4.2	Fabrication of Optimally Designed Cellular Test Beams.....	80
4.3	Load Cell Calibration	84
4.4	Flexural Bending Testing with Hydraulic Power Unit.....	89
4.5	Experimental Test Program of Optimally Designed Cellular Beams	91
4.5.1	Test Specimens.....	92

4.5.2	Test Arrangement	92
4.5.3	Instrumentation of Tests	92
4.5.4	Test Procedure	93
4.5.5	Material Properties of Specimens.....	94
4.5.6	Flexural Bending Tests of Cellular Beams.....	94
4.5.6.1	NPI_240 Section Cellular Beams.....	94
4.5.6.2	NPI_260 Section Cellular Beams.....	102
4.5.6.3	NPI_280 Section Cellular Beams.....	108
5	TENSILE TESTS ON OPTIMALLY DESIGNED STEEL	
	CELLULAR BEAM SPECIMENS	114
5.1	Sample Requirements.....	114
5.2	Test Setup and Equipment.....	119
5.3	The Objective of Tension Test	120
5.4	The Procedure of Tensile Testing	120
5.5	Tensile Test Results.....	122
6	NONLINEAR FINITE ELEMENT ANALYSIS ON OPTIMALLY	
	DESIGNED STEEL CELLULAR BEAMS.....	126
6.1	Introduction to Finite Element Modeling.....	126
6.2	Finite Element Modeling of Cellular Beams.....	128
6.2.1	Element and Material Modeling on ANSYS Program.....	131
6.2.2	Mesh Generations on Cellular Beams with ANSYS.....	133
6.2.3	Setting Contact Analysis Parameters	137
6.2.4	Identification Contact and Target Surface.....	137
6.2.4.1	Types of Contact	138
6.2.4.1.1	Frictional Contact	139
6.2.4.1.2	Frictionless Contact.....	139
6.2.4.1.3	Rough Contact.....	139
6.2.4.1.4	Contact without Separation	140

6.2.4.1.5	Bonded Contact	140
6.2.4.2	Behaviour of Contact.....	140
6.2.4.3	Contact Analysis Algorithm.....	141
6.2.4.3.1	Penalty Method.....	141
6.2.4.3.2	Multipoint Constraint Method.....	141
6.2.4.3.3	Pure Lagrangian Method	141
6.2.4.3.4	Augmented Lagrangian Method.....	142
6.3	Nonlinear Finite Element Model of Cellular Beams.....	142
6.3.1	Definition of Static Structural Analysis Settings	142
6.3.2	Nonlinear Solution of NPI_240 Cellular Beam	146
6.3.3	Nonlinear Solution of NPI_260 Cellular Beam	153
6.3.4	Nonlinear Solution of NPI_280 Cellular Beam	160
7	SUMMARY AND CONCLUSIONS.....	167
7.1	Overview and Summary of the Thesis	167
7.2	Conclusions	169
	REFERENCES	172
	VITA	180

LIST OF TABLES

TABLES

Table 1.1	An investigation of open web expanded beams	11
Table 1.2	An experimental investigation of open-web beams	12
Table 1.3	The plastic behaviour of castellated beams	14
Table 1.4	Tests on Castellated beams.....	15
Table 1.5	Failure of castellated beams due to rupture of welded joints	16
Table 1.6	Optimum expansion ratio of castellated beams.....	18
Table 1.7	Web buckling in thin webbed castellated beams.....	19
Table 1.8	Ultimate strength designs of beams with multiple openings.....	21
Table 2.1	Limiting width to thickness ratios	39
Table 3.1	The initial feasible designs selected by PSO and HS algorithms	59
Table 3.2	Feasible designs obtained after 32 iterations by PSO and HS algorithms	60
Table 3.3	Feasible designs obtained after 780 iterations by PSO and HS algorithms	61
Table 3.4	Comparison of optimum designs for 4-m simply supported beam	62
Table 3.5	Feasible designs obtained after 650 iterations by HS algorithms.....	66
Table 3.6	Optimum Design of NPI_240 Cellular beam with 3-m span	67
Table 3.7	Feasible designs obtained after 900 iterations by HS algorithms.....	70
Table 3.8	Optimum Design of NPI_260 Cellular beam with 3-m span	71
Table 3.9	Feasible designs obtained after 1200 iterations by HS algorithms.....	74
Table 3.10	Optimum Design of NPI_280 Cellular beam with 3-m span	75
Table 4.1	The variation of setting weight with minimum division set 100.....	86
Table 4.2	The variation of setting weight with minimum division set 50.....	87
Table 4.3	The variation of setting weight with minimum division set 20.....	88
Table 4.4	Dimensional Properties an Ultimate Load of NPI_240.....	95

Table 4.5	Ultimate Load Capacities and Failure Modes of NPI_240 Sections ..	101
Table 4.6	Dimensional Properties an Ultimate Load of NPI_260.....	102
Table 4.7	Ultimate Load Capacities and Failure Modes of NPI_260 Sections ..	107
Table 4.8	Dimensional Properties an Ultimate Load of NPI_280.....	108
Table 4.9	Ultimate Load Capacities and Failure Modes of NPI_280 Sections ..	113
Table 5.1	Dimensions for Standart Tension Test Specimens	116
Table 6.1	Numbers of Nodes and Elements for Mesh Types	133
Table 6.2	Displacement Values at The Middle of NPI-240 Cellular Beam	147

LIST OF FIGURES

FIGURES

Figure 1.1	Basic Process of Castellated Beam	2
Figure 1.2	Basic Process of Cellular Beam	4
Figure 1.3	The comparison of cellular and original I-beams	5
Figure 1.4	Reduction of Beam Depth by Placing Service Integrations in Holes	5
Figure 1.5	Premier Place with 15 m clear span	6
Figure 1.6	ASTA shopping center	7
Figure 1.7	A curving roof cellular beam application	7
Figure 1.8	Blackpool Car Park	8
Figure 1.9	Cambridge Car Park	8
Figure 1.10	Stamford Bridge Stadiums	9
Figure 1.11	Cantilever design of cellular beam in stadium	9
Figure 2.1	High bending in the cellular beam	27
Figure 2.2	High shears in the cellular beam	28
Figure 2.3	Lateral torsional buckling along beam	29
Figure 2.4	Web buckling on web-expanded beams	30
Figure 2.5	Rupture of welded joints on web-expanded beams	31
Figure 2.6	Geometrical parameters of a cellular beam	33
Figure 2.7	Horizontal shear in the web post of cellular beam	35
Figure 2.8	Olander's curved beam approach	38
Figure 3.1	Loading of 4-m simply supported beam	58
Figure 3.2	The design history graph for 4-m cellular beam	63
Figure 3.3	Typical cross section of beam with 3-m for NPI-240	65
Figure 3.4	The design history graph for NPI_240 cellular beam	67
Figure 3.5	Optimum Shape of NPI-240 after 10,000 Iterations	68

Figure 3.6	Typical cross section of beam with 3-m for NPI-260.....	69
Figure 3.7	The design history graph for NPI_260 cellular beam.....	71
Figure 3.8	Optimum Shape of NPI-260 after 10,000 Iterations.	72
Figure 3.9	Typical cross section of beam with 3-m for NPI-280.....	73
Figure 3.10	The design history graph for NPI_280 cellular beam.....	75
Figure 3.11	Optimum Shape of NPI-280 after 10,000 Iterations.....	76
Figure 4.1	Cellular Beam in Test Frame.....	78
Figure 4.2	Experimental set up and load introduction.	79
Figure 4.3	The appearance of the computer drawing of the cellular beam.....	80
Figure 4.4	The first flame cutting process of original I-section beam.....	81
Figure 4.5	The second flame cutting process of original I-section beam.....	81
Figure 4.6	The separation of tee sections of the beam.....	82
Figure 4.7	The assembling of the tee sections.....	82
Figure 4.8	The welding of upper and lower tees of the cellular beam.....	83
Figure 4.9	The appearance of cellular beam after cutting and re-weld process.....	83
Figure 4.10	Canister Load Cell for heavy duty design.....	84
Figure 4.11	NT-501A Indicator for calibration.....	84
Figure 4.12	The variation of setting weight for minimum division set 100.....	86
Figure 4.13	The variation of setting weight for minimum division set 50.....	87
Figure 4.14	The variation of setting weight for minimum division set 20.....	88
Figure 4.15	NPI-200 beam under point loading in the self-reaction frame.....	91
Figure 4.16	Demonstration of transducers on beam.....	93
Figure 4.17	NPI-240 Cellular Beam with Eight Openings.....	95
Figure 4.18	Lateral torsional buckling on NPI-240_TEST1.....	96
Figure 4.19	Load-Deflection Graphic for NPI-240_TEST1.....	96
Figure 4.20	Lateral torsional buckling on NPI-240_TEST2.....	97
Figure 4.21	Load-Deflection Graphic for NPI-240_TEST2.....	97
Figure 4.22	Web-post Buckling on NPI-240_TEST3.....	99
Figure 4.23	Load-Deflection Graphic for NPI-240_TEST3.....	99
Figure 4.24	Web-post Buckling on NPI-240_TEST4.....	100

Figure 4.25	Load-Deflection Graphic for NPI-240_TEST4	100
Figure 4.26	Vierendeel Bending and Web Buckling on NPI-260_TEST1	103
Figure 4.27	Load-Deflection Graphic for NPI-260_TEST1	103
Figure 4.28	Vierendeel Bending and Web Buckling on NPI-260_TEST2	104
Figure 4.29	Load-Deflection Graphic for NPI-260_TEST2	104
Figure 4.30	Vierendeel Bending and Web Buckling on NPI-260_TEST3	105
Figure 4.31	Load-Deflection Graphic for NPI-260_TEST3	105
Figure 4.32	Vierendeel Bending and Web Buckling on NPI-260_TEST4	106
Figure 4.33	Load-Deflection Graphic for NPI-260_TEST4	106
Figure 4.34	Web buckling on NPI-280_TEST1	109
Figure 4.35	Load-Deflection Graphic for NPI-280_TEST1	109
Figure 4.36	Web Buckling on NPI-280_TEST2	110
Figure 4.37	Load-Deflection Graphic for NPI-280_TEST2	110
Figure 4.38	Web Buckling on NPI-280_TEST3	111
Figure 4.39	Load-Deflection Graphic for NPI-280_TEST3	111
Figure 4.40	Web Buckling on NPI-280_TEST4	112
Figure 4.41	Load-Deflection Graphic for NPI-280_TEST4	112
Figure 5.1	Standard Dimensions for Tensile Test Specimen	115
Figure 5.2	Cutting process of standart test specimen with CNC method.....	117
Figure 5.3	Standart Tension Test Specimen from NPI Profiles	118
Figure 5.4	Dimensions for rectangular coupon from cellular beam specimen.....	118
Figure 5.5	Universal Testing Machine.	119
Figure 5.6	Rectangular Test Specimens under Tension.	121
Figure 5.7	View of Test Specimens after Rupture	121
Figure 5.8	One of Test Specimens after Tension Test	122
Figure 5.9	Stress-Strain Graph of Tensile Test of NPI_240 Profiles	123
Figure 5.10	Stress-Strain Graph of Tensile Test of NPI_260 Profiles	124
Figure 5.11	Stress-Strain Graph of Tensile Test of NPI_280 Profiles	125
Figure 6.1	Finite Element Model of Non-composite Cellular Beam	126
Figure 6.2	The Geometry of Cellular Beam with Solidworks.....	128

Figure 6.3	Structural Properties of NPI_240 Steel Cellular Beam.....	129
Figure 6.4	Alternating Stress Curve of NPI_240 Steel Cellular Beam	130
Figure 6.5	Strain-Life Parameter Graph of NPI_240 Steel Cellular Beam	130
Figure 6.6	Tetrahedron Volume Element Node Patterns	131
Figure 6.7	3-D Contact Element Geometry.....	132
Figure 6.8	TARGE-170 Element Geometry.....	133
Figure 6.9	Different Types of Mesh Generations.....	135
Figure 6.10	Different Mesh Sizes and Stress Values	136
Figure 6.11	Tetrahedron Mesh Model with 25-mm Size	137
Figure 6.12	Contacts and Target Surface.	138
Figure 6.13	Contact Types	138
Figure 6.14	Analysis Settings for Cellular Beam.....	143
Figure 6.15	Load-Diagram and Steps for NPI_240 Cellular Beam Section	144
Figure 6.16	Plasticity Properties of NPI_240 Steel Section.....	145
Figure 6.17	Applying Load to NPI_240 Cellular Beam.....	146
Figure 6.18	Linear and Nonlinear Load-Deflection Diagram for NPI_240 Cellular Beam.....	148
Figure 6.19	Equivalent Stress Values on NPI_240 Cellular Beam.....	149
Figure 6.20	Deformation Values on NPI_240 Cellular Beam	149
Figure 6.21	Normal Stress Values on NPI_240 Cellular Beam	150
Figure 6.22	Shear Stress Values on NPI_240 Cellular Beam	150
Figure 6.23	Load-deflection-curve for upper flange of NPI_240_TEST3.....	151
Figure 6.24	Load-deflection-curve for lower flange of NPI_240_TEST3.....	151
Figure 6.25	Load-deflection-curve for upper flange of NPI_240_TEST4.....	152
Figure 6.26	Load-deflection-curve for lower flange of NPI_240_TEST4.....	152
Figure 6.27	Applying Load to NPI_260 Cellular Beam.....	153
Figure 6.28	Equivalent Stress Values on NPI_260 Cellular Beam.....	154
Figure 6.29	Deformation Values on NPI_260 Cellular Beam	154
Figure 6.30	Normal Stress Values on NPI_260 Cellular Beam	155
Figure 6.31	Shear Stress Values on NPI_260 Cellular Beam	155

Figure 6.32	Load-deflection-curve for upper flange of NPI_260_TEST1	156
Figure 6.33	Load-deflection-curve for lower flange of NPI_260_TEST1	156
Figure 6.34	Load-deflection-curve for upper flange of NPI_260_TEST2.....	157
Figure 6.35	Load-deflection-curve for lower flange of NPI_260_TEST2.....	157
Figure 6.36	Load-deflection-curve for upper flange of NPI_260_TEST3.....	158
Figure 6.37	Load-deflection-curve for lower flange of NPI_260_TEST3.....	158
Figure 6.38	Load-deflection-curve for upper flange of NPI_260_TEST4.....	159
Figure 6.39	Load-deflection-curve for lower flange of NPI_260_TEST4.....	159
Figure 6.40	Applying Load to NPI_260 Cellular Beam.....	160
Figure 6.41	Equivalent Stress Values on NPI_260 Cellular Beam.....	161
Figure 6.42	Deformation Values on NPI_260 Cellular Beam	161
Figure 6.43	Normal Stress Values on NPI_260 Cellular Beam	162
Figure 6.44	Shear Stress Values on NPI_260 Cellular Beam	162
Figure 6.45	Load-deflection-curve for upper flange of NPI_260_TEST1	163
Figure 6.46	Load-deflection-curve for lower flange of NPI_260_TEST1	163
Figure 6.47	Load-deflection-curve for upper flange of NPI_260_TEST2.....	164
Figure 6.48	Load-deflection-curve for lower flange of NPI_260_TEST2.....	164
Figure 6.49	Load-deflection-curve for upper flange of NPI_260_TEST3.....	165
Figure 6.50	Load-deflection-curve for lower flange of NPI_260_TEST3.....	165
Figure 6.51	Load-deflection-curve for upper flange of NPI_260_TEST4.....	166
Figure 6.52	Load-deflection-curve for lower flange of NPI_260_TEST4.....	166

LIST OF ABBREVIATIONS

d_g	Overall depth of the section
b_f	Width of flange
t_w	Thickness of web
t_f	Thickness of flange
e	Length of welded joint
h_0	Height of hole
S	Distance between hole centers
φ	Angle of castellation
F_y	Yield Stress
M_U	Maximum moment under applied load combinations
M_P	Plastic moment capacity of the cellular beam
A_{LT}	Cross sectional area of lower tee
P_Y	Design strength of steel
H_U	Distance between centrals of upper tee and lower tee
P_{VY}	Vertical shear capacity of the beam
P_{VH}	Horizontal shear capacity of the beam
A_{WUL}	Total cross sectional areas of webs of tees
A_{WP}	Minimum area of the web post
V	Shear force
T	Axial force
M	Bending moment at the cross section
x_0	Distance between the axial forces to flange.
M_{MAX}	Maximum allowable web post moment and

M_E	Web post capacity at section
D_0	Diameter of the web holes
C_1, C_2, C_3	Constants
t_w	Web thickness
P_O	Force on the section
M	Moment on the section
P_U	Area of critical section $\times P_Y$
M_P	The plastic modulus of critical section $\times P_Y$ in plastic sections or elastic section modulus of critical section $\times P_Y$ in other sections
S_x	Plastic modulus of section
Z_x	Elastic modulus of section
ε	Constant in connection with limiting with to thickness ratios
λ_F	Slenderness ratio for I-shaped member flanges and the thickness
λ_w	Slenderness ratio for beam web
T_i	The axial forces in tees
V_h	Horizontal forces in tees
h	Distance between the centroids of upper and lower tees
$\frac{\overline{V}_i}{2}, \overline{N}_i, \overline{V}_h$	Internal forces under a unit load
y_{mt}	Deflection due to bending moment in tee
y_{wp}	Deflection due to bending moment in web post of beam
y_{at}	Deflection due to axial force in tee
y_t	Deflection due to shear in tee
y_w	Deflection due to shear in web post
E	Elasticity modulus of steel cellular beam

I_T	Total moment of inertia of cell beam
G	Shear modulus of steel
X	Web post form factor
y_T	Total deflection of a single opening under load conditions
I	Integer design vector
I_1	Sequence number of for the rolled beam section
I_2	Sequence number for the hole diameter
I_3	Total number of holes in the cellular beam
W_{CB}	Weight of the cellular beam,
ρ_s	Density of steel
A_{CB}	Total cross-sectional area of a steel profile
L_{CB}	Span of the cellular beam
N_{hole}	Number of holes in the beam
V_{MAXSUP}	Shear stresses computed at the supports
P_V	Allowable shear stresses
V_{OMAX}	Shear stresses at the web openings
P_{VY}	Allowable vertical shear stresses
V_{HMAX}	Horizontal shear stresses
P_{VH}	Allowable horizontal shear stresses
M_{A-AMAX}	Maximum moment determined at A-A section
M_{WMAX}	Maximum allowable web post moment
V_{TEE}	Vertical shear on the tee at $\theta = 0$ of web opening
y_{MAX}	Maximum displacement
hms	Harmony memory size
$hmcr$	Harmony memory considering rate
par	Pitch adjusting rate
N_{cyc}	Maximum search number

v	Velocity of particle
μ	Number of particles
I_{\max}	Total number of values in the discrete set
x_k^i	Design space positions.
p_k^i	Optimum particle position
p_k^g	Global optimum particle position
r_1, r_2	Random numbers between 0 and 1
p_k^i	Best position found by particle i
p_k^g	Best position in the swarm at time k
w	Inertia of the particle
c_1, c_2	Trust parameters in the swarm
<i>SCI</i>	Steel Construction Institute
<i>BS</i>	British Standard
<i>ASD-AISC</i>	American Institute of Steel Construction-Allowable Stress Design
<i>LRFD</i>	Load and Resistance Factor Design
<i>FEM</i>	Finite Element Model
<i>HEA</i>	I-shaped steel beam according DIN 1025 and Euro-norm 53-62
<i>UB</i>	Universal Beam Sections according British Standard
<i>NPI</i>	I-shaped cross-section beams according Eurocode
<i>HS</i>	Harmony Search Algorithm
<i>PSO</i>	Particle Swarm Optimization
<i>CB</i>	Cellular Beam

CHAPTER 1

WEB-EXPANDED BEAMS IN GENERAL

1.1 Introduction to Web-expanded Beams

Structural engineers have always tried to find new ways to improve the practices in the design and construction of steel and composite buildings so that the overall cost can be decreased. Beams with web openings and open web-expanded steel beams are some of these ways. Web openings with different geometrical properties have been used for many years to pass duct work or utilities through the web holes in order to decrease floor height and constructional cost of large scale buildings. This is because; decrease in story height reduces interior volume and exterior surface of building and these results in cost saving. Furthermore, in comparison with solid web beams, web-expanded beams can easily increase the shear capacities, vertical bending stiffness and capacities of structure.

Steel I-beam sections can be modified to intensify their strength by creating an open-web expanded section from an original solid beam. This is achieved by cutting the web of a solid beam in a certain pattern and then re-welding the two parts to each other. As a result of these cutting and re-welding processes, the overall beam depth increases which in return causes increase in the capacity of the original section. There are two common types of open web expanded beams: with hexagonal openings, also called castellated beams and beams with

circular openings referred to as cellular beams. Castellated and cellular beams have been used in various types of constructions for many years. The most common structure types built using these beams are office buildings, car parks, shopping centers and any structure with a suspended floor. Web-expanded beams provide a very economical solution for producing tapered members, which have been used extensively in big sports stadiums.

1.2 Castellated Beams

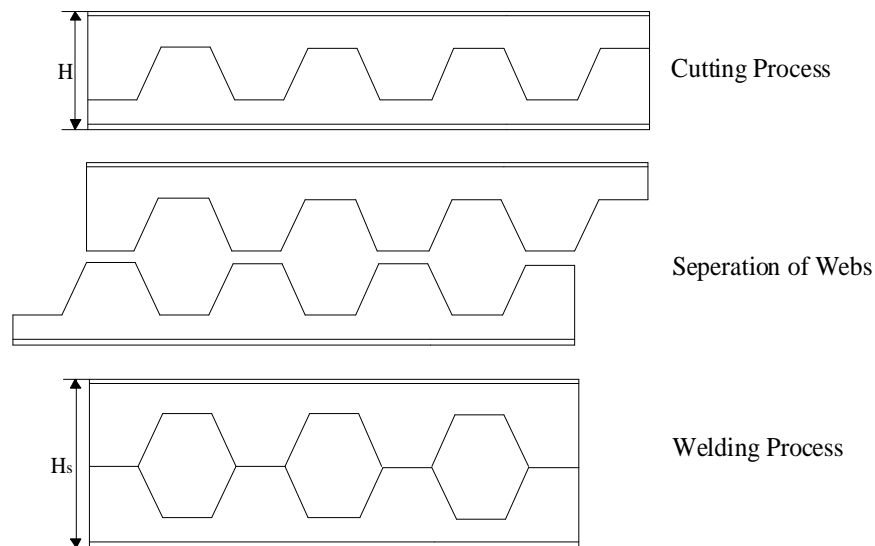


Figure 1.1 Basic process of castellated beam

Castellated beams are steel sections with hexagonal openings that are made by cutting a saw tooth pattern along its centerline in the web of a rolled I-beam section along the length of its span. The two parts of original beam are then welded together to produce a beam of greater depth with halves of hexagonal holes in the steel section as shown above in Figure 1.1.

The cutting and re-welding processes increase the overall beam depth, moment of inertia and section modulus of the original rolled beam, while reducing the overall weight of the beam. Since the 1940s the high strength to weight ratio of castellated beams has been a desirable item to structural engineers in their efforts to design even lighter and more cost efficient steel structures [1].

1.3 Cellular Beams

The emergence of cellular beams was firstly for architectural application, where exposed steelwork with circular web openings in the beam was considered aesthetically pleasing more than castellated beams. Cellular beams are steel sections with circular web openings that are made by twice cutting an original rolled beams web in a half circular pattern along its centerline, separating two tee parts and re-welding these two halves of hot rolled steel sections as shown in Figure 1.2. This circular opening up of the original rolled beam increases the overall beam depth, moment of inertia and section modulus, while reducing the overall weight of the beam.

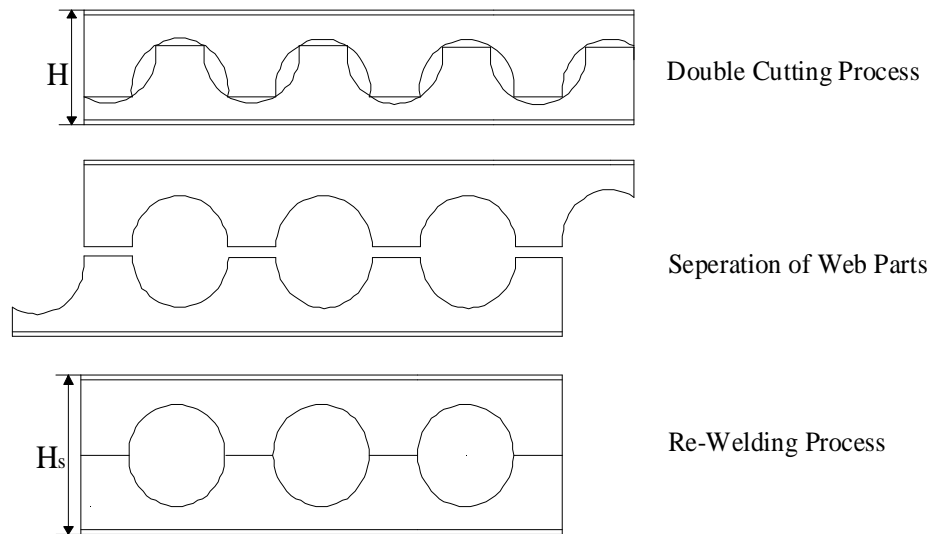


Figure 1.2 Basic process of cellular beam

Cellular beams have been used in over 3500 projects in all around the world [1]. The most common building types for the cellular beams are office buildings, car parks, shopping centers and structures with a suspended floor. Cellular beams are also used as roof beams beyond the range of portal-frame construction, and are perfect solutions for curved roof applications, combining weight savings with a low-cost manufacturing process. Cellular beams are a very economical means of producing tapered members, which have been used extensively in sports halls. They can also be used as gable columns and wind-posts at practical applications.

Cellular beams always produce a more cost-effective solution than castellated beams as a result of their flexible geometry. Although the profile for any castellated beam section is standard or fixed, the major dimensions which are the final depth, cell diameter and spacing are completely flexible in cellular beams. The production process of cellular beams improves the section

properties of the original beam used, thus saving enormous weight compared to plain original beams. Figure 1.3 shows that cellular beams are approximately 40-60% deeper and 40-60% stronger than the original member while reducing the overall weight [2]. As a result of using cellular beams, structures are lightened, spans are increased, and pulling spaces helps us to save in overall height. This flexibility goes together with the functionality of allowing utilization of the web openings as passages for pipes and ducts services through the web holes shown in Figure 1.4.

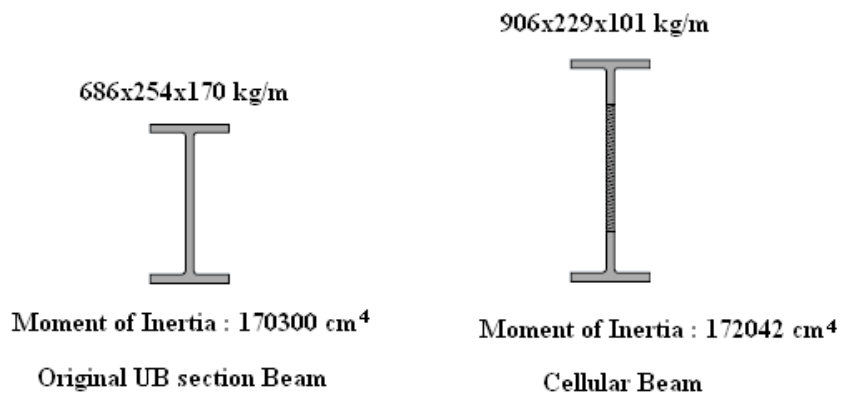


Figure 1.3 The comparison of cellular and original I-beams

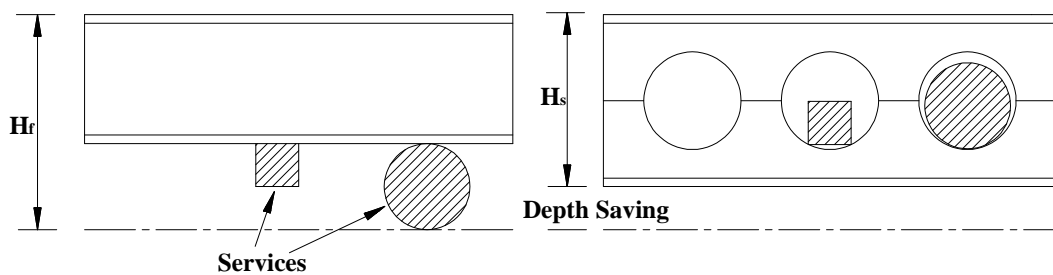


Figure 1.4 Reduction of beam depth by placing service integrations in holes

1.3.1 Applications of Cellular Beams

Cellular beams have been used in various designs of structural buildings. Some of them are office buildings, car parks, shopping centers, hospitals and any structure with a suspended floor. Cellular beams provide long clear spans and great flexibility for service integration, when they are used as floor beams as shown in Figure 1.5.



Figure 1.5 Premier place with 15 m clear span, London

Cellular beams can be used as roof beams because of their low cost. They are the perfect solution for roof applications shown in Figure 1.6 and 1.7, combining a considerable weight saving and providing a building with minimal internal columns compared with original beam sections.



Figure 1.6 ASTA shopping center, Tamworth



Figure 1.7 A curving roof cellular beam application, Winchester

Cellular beams are efficient structural members under car park loadings with long clear spans. Besides their lighter weight, cellular beams provide exact beam depth and a light and airy interior to improve personal security for modern parking constructions (Figure 1.8 and 1.9).



Figure 1.8 Blackpool car park, Cork



Figure 1.9 Cambridge car park

The low cost and structural efficiency of cellular beams in clear long span structures make these beams extensively suitable for use in big sports stadiums shown in Figure 1.10 ad 1.11. They are much lighter and shallower than original solid beams and much less costly than lattice beams.



Figure 1.10 Stamford bridge stadiums, London



Figure 1.11 Cantilever design of cellular beam in stadium, Dumferline

1.4 Literature Review

Web-expanded steel beams were firstly used by engineers in the 1940's to decrease the cost of steel structures [1]. Increasing the stiffness of original beam without any increase of weight of the steel beam has been the purpose of the selection of these beams from designers. Reviews on non-composite web-expanded beams have been extensively reported in the literature. An outline of previous experimental and theoretical studies on these beams is reported here in chronological order with the objective of describing the main purposes of each investigation.

Web-expanded non-composite beams were firstly studied by Altifillisch et al. in 1957. The main focus of this study was to investigate the structural behaviour, strength and failure modes of castellated beams under two concentrated loads both in elastic and plastic ranges [3]. Simply supported 10B11.5 three different types fabricated beams were tested to search the influence of beam depth, web opening geometry and expansion ratio for these experiments. The first type beam with fully bearing stiffeners, 10B11.5-I, was failed through extensive yielding of the tee section and local compression flange buckling. Three tests were performed for the second type of beam, 10B11.5-II, but one of these tests, involved loading to destruction of beam, were excluded from experiments on account of the inadequacy of lateral bracing system. Stress and deflection analysis of other two test beams was substantiated under elastic range loads. In a similar manner with 10B11.5-II beams, the last type of beams with short bearing stiffeners, 10B11.5-III, were tested in the elastic range for the first two tests and the other one was loaded to destruction of beams. Yielding at the corner of the web holes in the shear span and local buckling of the compression flange were defined after applied loads. They concluded that by expanding the depth of beam may be carried 10% to

%35 more moment in comparison with original beam. Data and results of tested beams are given with more detail in Table 1.1.

Table 1.1 An investigation of open web expanded beams (1957).

Beam	10B11.5-I	10B11.5-II	10B11.5-III
d_g	330.20 mm	374.65 mm	412.75 mm
b_f	100.33 mm	100.33 mm	100.33 mm
t_w	4.57 mm	4.57 mm	4.57 mm
t_f	5.18 mm	5.18 mm	5.18 mm
e	85.73 mm	88.90 mm	251 mm
h₀	158.75 mm	247.65 mm	323.85 mm
s	330.20 mm	425.45 mm	501.65 mm
φ	45 ⁰	45 ⁰	45 ⁰
F_{y-web}	326.81 MPa	326.81 MPa	326.81 MPa
F_{y-flange}	297.51 MPa	297.51 MPa	297.51 MPa
Ultimate Loads	199.6 kN	-	252.5 kN
Type of Failure	Flange Buckling	No Result	Flange Buckling

Toprac and Cooke tested ten 8B10 rolled section beams under four concentrated point loads to investigate load carrying capacity and optimum expansion ratio of castellated beams [4]. Experimental results of these tests were then compared with theoretical computations. Excessive lateral buckling at the first two specimens caused the failure so they were excluded from the study. Although ultimate load of third specimen was recorded, but there was not given detail about this test. When the load was reached to maximum, compression flange buckling was observed at 8B10-IV specimen. At the same manner, yielding and flange buckling mode in the pure bending region was

described for 8B10-V specimen. As for specimen 8B10-VI, local buckling of the compression flange in the constant moment region was observed as failure mode. The next specimen, 8B10-VII, failed due to high shear forces across the web openings called vierendeel mechanism. Buckling of compression flange in the constant moment region and vierendeel bending in the highest shear region were observed for the 8B10-VIII and 8B10-IX specimens respectively. The test data and results of these beams are shown with more detail in Table 1.2.

Table 1.2 An experimental investigation of open-web beams (1959).

Beam	8B10-I	8B10-II	8B10-III	8B10-IV	8B10-V
d_g	266.70	281.94	297.94	335.28	330.96
b_f	101.60	101.60	100.33	101.60	100.33
t_w	4.57	4.50	4.83	4.34	4.70
t_f	5.13	5.08	5.13	5.08	5.11
e	57.15	57.15	57.15	57.15	57.15
h_0	133.10	143.26	196.34	247.40	264.92
s	247.40	257.56	310.64	361.70	379.22
ϕ	45	45	45	45	45
$F_{y\text{-web}}$	274.14	274.14	274.14	290.10	290.10
$F_{y\text{-flange}}$	274.14	274.14	274.14	290.10	290.10
Ultimate Loads	-	-	-	215.1 kN	287.3 kN
Type of Failure	No Result	No Result	No Result	Flange Buckling	Flange Buckling

Beam	8B10-VI	8B10-VII	8B10-VIII	8B10-IX	8B10-X
d_g	297.18	330.20	295.91	354.33	200.91
b_f	99.06	101.60	100.33	100.33	100.33
t_w	4.70	4.72	4.45	4.70	4.70
t_f	5.08	5.08	5.16	5.13	5.11
e	57.15	76.20	38.10	38.10	N.A.
h₀	195.58	264.16	194.31	309.63	N.A.
s	347.98	416.56	270.51	385.63	N.A.
φ	45	45	45	45	N.A.
F_{y-web}	290.10	296.41	296.41	296.41	N.A.
F_{y-flange}	290.10	296.41	296.41	296.41	N.A.
Ultimate Loads	-	320.6 kN	274.1 kN	406.8 kN	-
Type of Failure	No Result	Shear Mechanism	Flange Buckling	Shear Mechanism	No Result

In 1966, Shelbourne designed a test program for seven specimens consisting of simply supported beams with bearing stiffeners. The objective of these tests was to examine the interaction of shear forces and moments on the behavior of castellated beams under varying load combinations [5]. The first specimen, Beam_A1, failed through extensive yielding of the mid-depth of the post between the first and second hole under single concentrated load at mid-span. The effect of pure moment investigated at second specimen, Beam_A2, under two concentrated point loads. Failure of Beam_A2 was associated with extensive yielding in the end zones experiencing both shear and moment forces. Beam_A3 was subjected to two point loads and failed through web buckling in the zone of maximum shear. The effect of pure shear across the holes was studied at Beam_ A4 and web buckling observed as failure mode. In addition to these four tests, Shelbourne tested three more specimens under pure

bending moments. The first two tests were reported to fail by flexural mechanisms. The last one was also reported to fail by flexural mechanism; however, lateral torsional buckling was also associated with the failure mode. The test data and results of these beams are given with more detail in Table 1.3.

Table 1.3 The plastic behaviour of castellated beams (1966).

Beam	Beam_A1	Beam_A2	Beam_A3	Beam_A4
d_g	228.60	228.60	228.60	228.60
b_f	76.20	76.20	76.20	76.20
t_w	5.84	5.84	5.84	5.84
t_f	9.58	9.58	9.58	9.58
e	38.10	38.10	38.10	38.10
h₀	152.40	152.40	152.40	152.40
s	164.59	164.59	164.59	164.59
φ	60.00	60.00	60.00	60.00
F_{y-web}	283.00	283.00	283.00	283.00
F_{y-flange}	283.00	283.00	283.00	283.00
Ultimate Loads	338.2 kN	366.8 kN	382.5 kN	362.9 kN
Type of Failure	Mid-Post Yielding	Mid-Post Yielding	Web Buckling	Web Buckling

Later, Bazile and Texier were tested two different types of beams to develop a further understanding of different beam characteristics and properties, geometry and expansion ratios of web-expanded beams in 1968 [6]. To

accomplish this, simply supported HEA_360 and IPE_270 type castellated beams were tested under eight concentrated loads. The different phases of load-deflection diagram of each beam also described under test loads. Two specimens were not included to further study due to failed by lateral torsional buckling. Failure of other three beams (Beam_T1, Beam_T2 and Beam_T3) was associated with web buckling in the zone of maximum shear. The test data and results of these beams are tabulated in Table 1.4.

Table 1.4 Tests on Castellated beams (1968).

Beam	Beam_T1	Beam_T1	Beam_T1
d_g	500.00	600.00	500.00
b_f	300.00	300.00	135.00
t_w	10.00	10.00	6.60
t_f	17.50	17.50	10.20
e	168.00	168.00	138.00
h₀	300.00	370.00	320.00
s	504.00	504.00	414.00
φ	60.80	55.00	52.50
F_{y-web}	370.00	302.00	336.00
F_{y-flange}	299.00	245.00	249.00
Ultimate Loads	295.7 kN	251.1 kN	211.9 kN
Type of Failure	Web Buckling	Web Buckling	Web Buckling

In 1971, Husain and Speirs were tested six simply supported beams under various load conditions to study the yielding and rupture of welded joints of castellated beams [7]. Sufficient lateral bracings and bearing stiffeners were provided to lateral torsional buckling of each beam. Beam_H1 and Beam_S1

were subjected to a single concentrated load and as for that Beam_H2, Beam_H3, Beam_S2 and Beam_S3 were subjected to two concentrated loads. Yield and ultimate shear stress values are recorded for each beam. Due to the strain hardening, measured shear stress values were higher than stress values would have been expected from tensile tests. The test data and results of these beams are given with more detail in Table 1.5. Husain and Speirs also investigated the effects of opening geometry on the strength of web-expanded beams [8]. They concluded that narrowing the throat width increases the performance of these beams.

Table 1.5 Failure of castellated beams due to rupture of welded joints (1971).

Beam	Beam_H1	Beam_S1
d_g	381.00	381.00
b_f	101.60	101.60
t_w	4.88	5.33
t_f	6.83	6.83
e	68.33	50.55
h_0	254.00	254.00
s	390.53	247.65
ϕ	45.00	60.00
F_y	248.21	248.21
Ultimate Loads	441.0 kN	330.1 kN
Type of Failure	Web Buckling	Web Buckling

Beam	Beam_H2	Beam_H3	Beam_S2	Beam_S3
d_g	381.00	381.00	381.00	381.00
b_f	101.60	101.60	101.60	101.60
t_w	4.88	4.88	4.88	4.88
t_f	6.83	6.83	6.83	6.83
e	68.33	68.33	68.33	68.33
h₀	254.00	254.00	254.00	254.00
s	390.53	390.53	390.53	390.53
φ	45.00	45.00	45.00	45.00
F_y	248.21	248.21	248.21	248.21
Ultimate Loads	407.5 kN	407.0 kN	478.1 kN	344.3 kN
Type of Failure	Web Buckling	Web Buckling	Web Buckling	Web Buckling

Four castellated beams fabricated from W10x15 sections were tested by Galambos et al in 1975. The objective of these experiments was to confirm a numerical analysis approach to determine the optimum expansion ratio based on both elastic and plastic methods of analysis [9]. A single concentrated load was applied at mid-span of all beams. The span and weld lengths of beams were taken as constants, but the depth of beams were varied based upon distinct expansion ratios. Ultimate load capacity values of each test beams were recorded, but no further discussion about the modes of failure was given. The test data and results of these beams are shown with more detail in Table 1.6.

Table 1.6 Optimum expansion ratio of castellated beams (1975).

Beam	W10x15-I	W10x15-II	W10x15-III	W10x15-IV
d_g	302.65	354.58	381.00	381.00
b_f	101.60	101.60	101.60	101.60
t_w	5.84	5.84	5.84	5.84
t_f	6.86	6.86	6.86	6.86
e	152.40	152.40	152.40	152.40
h₀	100.89	202.59	176.58	302.51
s	425.45	425.45	425.45	425.45
φ	39.9	59.30	55.68	68.30
F_y	333.43	333.43	333.43	333.43
Ultimate Loads	225.2 kN	244.6 kN	238.9 kN	266.8 kN
Type of Failure	Web Buckling	Web Buckling	Web Buckling	Web Buckling

Then, Zaarour and Redwood tested fourteen castellated beams to examine the buckling of the web post between openings [10]. Some of these beams had plates welded between the halves at the web-post. A single concentrated point load was applied at mid-span of all light beams. The ultimate strength values of each beam were measured depended upon load capacities. The first two tests were reported to fail by local buckling of the tee-section above the holes through greatest bending moments taken placed. Web buckling failure mode was described for other ten specimens. Finally, last two experiments omitted from consideration because of lateral torsional buckling. Finite element model analysis was also used to predict ultimate web buckling load and compared with experimental results. The test data and results of these beams are tabulated in Table 1.7.

Table 1.7 Web buckling in thin webbed castellated beams (1996).

Beam	B8-I	B8-II	B8-III	B8-IV
d_g	302.64	359.66	307.34	358.90
b_f	59.44	58.42	58.42	58.93
t_w	3.43	3.48	3.51	3.48
t_f	4.69	4.72	4.57	4.72
e	48.51	48.26	57.40	58.67
h₀	222.25	270.26	222.25	270.00
s	224.02	222.25	342.90	342.90
φ	60.1	60.1	44.00	44.00
F_y	374.40	374.40	374.40	374.40
Ultimate Loads	248.6 kN	178.4 kN	205.9 kN	145.4 kN
Type of Failure	Shear Mech.	Web Buckling	Shear Mech.	Web Buckling

Beam	B10-I	B10-II	B10-III	B10-IV
d_g	370.59	417.83	376.43	425.45
b_f	69.09	69.85	70.61	70.61
t_w	3.58	3.61	3.61	3.68
t_f	4.39	3.98	4.45	4.27
e	58.17	57.66	57.91	58.93
h₀	245.87	295.15	260.53	308.10
s	254.00	254.00	368.30	368.30
φ	60.30	60.30	45.40	45.40
F_y	357.10	357.10	357.10	357.10
Ultimate Loads	217.6 kN	190.6 kN	213.8 kN	182.9 kN
Type of Failure	Shear Mech.	Web Buckling	Shear Mech.	Web Buckling

Beam	B12-I	B12-II	B12-III	B12-IV
d_g	476.25	527.81	449.58	501.65
b_f	78.49	77.98	78.23	77.98
t_w	4.69	4.59	4.62	4.69
t_f	5.33	5.36	5.35	5.33
e	73.41	74.42	71.37	68.33
h₀	352.81	403.86	302.51	349.75
s	355.60	355.60	438.15	438.15
φ	59.90	59.90	45.20	45.20
F_y	311.60	311.60	311.60	311.60
Ultimate Loads	214.4 kN	217.3 kN	192.8 kN	189.0 kN
Type of Failure	Web Buckling	Web Buckling	Web Buckling	Web Buckling

In 1998, Redwood and Demirdijan focused to examine the buckling of the web post between holes and to investigate the effects of moment-to-shear ratio on the mode of failure in their experiments [11]. Four castellated beams with same cross sectional but different number of openings were tested. All beams were simply supported and subjected to a central point loading. Two identical beams with four openings, 10_4B1 and 10_4B2, and beam with six openings, 10_6B, were failed by web-post buckling mode. Beam with eight openings, 10_8B, was excluded from study since failed by lateral torsional buckling. Elastic finite element analysis was then used to simulate beams tested and compare the buckling loads were reported between experimental and finite element analysis results. The test data and results of these beams are shown with more detail in Table 1.8.

Table 1.8 Ultimate strength designs of beams with multiple openings (1998).

Beam	Beam_10A	Beam_10B	Beam_10C	Beam_10D
d_g	380.50	380.50	380.50	380.50
b_f	66.90	66.90	66.90	66.90
t_w	3.56	3.56	3.56	3.56
t_f	4.59	4.59	4.59	4.59
e	77.80	77.80	77.80	77.80
h_0	266.20	266.20	266.20	266.20
s	306.40	306.40	306.40	306.40
ϕ	60.20	60.20	60.20	60.20
$F_{y\text{-web}}$	352.90	352.90	352.90	352.90
$F_{y\text{-flange}}$	345.60	345.60	345.60	345.60
Ultimate Loads	338.2 kN	366.8 kN	382.5 kN	362.9 kN
Type of Failure	Web Buckling	Web Buckling	Flange-Tee Buckling	-

Lastly, Erdal and Saka studied optimum design algorithm which based on one of the recent meta-heuristic technique called harmony search method for castellated beams in 2009 [12]. The design problem of castellated beams is formulated as optimum design problem. The minimum weight is taken as the design objective while the design constraints are implemented from The Steel Construction Institute (SCI). The design methods adopted in this publication are consistent with BS5950. Discrete programming problem comes out when the design problem of steel castellated beams are formulated considering the design limitations mentioned in the previous publication. The design algorithm

presented selects the optimum UB steel section to be used in the production of a cellular beam subjected to a general loading, the optimum hexagonal hole dimensions and number of holes in the castellated beams.

In comparison with castellated beams; there are limited theoretical and experimental studies on cellular beams. These beams were firstly used on full scale destructive tests to confirm structural integrity and design criteria at Bradford University in 1988 with supervision of steel construction institute (SCI). After several tests, web post buckling was described as failure mode at cellular beams. Afterwards, the evaluation of results were performed of design methods for web beams and analytical studies were undertaken using non-linear finite element analysis to seek the capacity of the web posts and the upper and lower tees [13].

Then, design for simply supported steel and composite cellular beams as used in structures was presented by Ward J.K. in 1990 [14]. Design procedures were associated with British Standard 5950: Part I and Part 3.1 provisions. The behaviour of these beams was described and flexural, local, web-post strengths and bending modes of non-composite and composite cellular beams were also derived from parametric study involving detailed finite element analysis. On the basis of plastic analysis of cellular beams at ultimate loads and elastic analysis at serviceability loads, design procedures were applied to beams.

Later, the stress distribution around the holes of cellular beams under load combinations are investigated by Dionisio et al. in 2004 [15]. The main objective of this research was to describe the critical location around a typical circular cell under load conditions. The study consisted of experimental tests and analytical modeling using finite element modeling. In the experimental part of research, twelve simply supported cellular beams were subjected to monotonically loading. Primary and vierendeel bending stress around circular

holes were defined as failure modes. 3D finite element model of tested cellular beams were then built up in ANSYS to compare with experimental results.

In 2006, in addition to an overview of cellular beams, stress distribution around the web openings and effect of cope geometry to failure of cellular beams were studied by Hoffman et al. In this research [16], linear elastic for service loadings and nonlinear buckling finite element analysis of cellular beams were evaluated and then compared with experimental results. For this purpose, eighteen A570 steel cellular beams with span of 4.57-m were tested in a self reacting frame. Ultimate load and vertical displacement values for every beam were recorded to compare with FEM results. Web-post buckling around first holes and regional buckling between the edge of cope and the edge of the first hole were determined as failure modes in experimental tests.

The optimum design algorithm which based on one of the recent meta-heuristic technique called harmony search method was presented for cellular beams by Erdal and Saka in 2008 [17]. The design problem of cellular beams is formulated as optimum design problem. The minimum weight is taken as the design objective while the design constraints are implemented from SCI publication number 100. The design methods adopted in this publication are consistent with BS5950 part 1 and 3. Discrete programming problem comes out when the design problem of cellular beams are formulated considering the design limitations mentioned in the previous publication. The design algorithm presented selects the optimum HEA section to be used in the production of a cellular beam subjected to a general loading, the optimum holes diameter and the optimum number of these holes in the cellular beam. Furthermore, this selection is also carried out such that the design limitations are satisfied and the weight of the cellular beam is the minimum. Erdal et al. were then adopted particle swarm optimizer to cellular beams and evaluated performance of

harmony search algorithm and particle swarm optimizer for steel cellular beams [18].

1.5 Objective and Scope of Research

The current dissertation research encompasses an investigation into the optimum design, experimental research and finite element studies of non-composite cellular beams. In this dissertation thesis, chapters are arranged as follows;

In Chapter 1, a general definition is given about web-expanded beams. Then, the common types of open web expanded beams: beams with hexagonal openings and beams with circular openings are explained respectively. Lastly, a literature survey on the web opening beams is included in a historical order and the practical applications of cellular beams are shown with some pictures.

Chapter 2 presents failure modes of web-expanded beams and then the first phase of the research with focus on the design process of cellular beams according to BS5950 provisions to prevent the failure of these beams. The design procedure of cellular beams is taken from The Steel Construction Institute (SCI) Publication No: 100 titled “Design of Composite and Non-composite Cellular Beams”.

The design equations of cellular beams are explained in Chapter 3. This chapter also contains the general concepts of harmony search and particle swarm optimization methods in a detailed manner and includes general information about these stochastic-based optimum design techniques. Furthermore, simply supported cellular beams are subjected to different types

of external loading are designed using the algorithms developed in this thesis and the results are presented.

The experimental part of the research is presented in Chapter 4. In the experimental phase of the study, 12 optimally designed non-composite cellular beams are tested in a self reacting frame. The tested cellular beam specimens have been designed using harmony search optimization technique.

In chapter 5, three tension test coupons from web of the every NPI steel cellular beams are tested. Besides modulus of elasticity, yield and ultimate stress values obtained from tensile tests are then used in finite element analysis of these beams.

The last part of the thesis study, Chapter 6, focuses on performing a numerical study on steel cellular beams utilizing finite element analysis. The finite element code, ANSYS, is used to perform elastic buckling analysis and predict critical loads for all tested specimens. Finite element analysis results of these optimally designed steel cellular beams are compared with the experimental results.

Finally, in the last chapter, some brief discussions and conclusions are presented.

CHAPTER 2

THE DESIGN OF CELLULAR BEAMS

Structural design is one of the primary tasks of a structural engineer. The aim of structural designer is to come up a structure that fulfills the criteria set by the owner or builder of a building. The structure must also satisfy the safety requirements regulated by the provisions of design codes and in the mean time it should be economical to be constructed. Design of a steel structure in particular requires a meticulous attention to design of steel members as well as the details of their connections. Non-composite web-expanded steel beams are no exception to this procedure. Structural designer has to consider all cases of failure that can occur in such beam so that safety is assured in their life time. The failure modes that can take place in web-expanded steel beams are explained in the following subsections with more details.

2.1 Failure Modes of Web-Expanded Beams

There are mainly six different failure modes of these beams according to experimental tests carried out by Kerdal and Nethercot on web-expanded beams [19]. These failure modes are caused by beam geometry, web slenderness, type of loading, and provision of lateral supports. Under applied load conditions, failure is likely to occur due to one the following modes:

- Formation of a Vierendeel mechanism
- Lateral torsional buckling of the entire span
- Lateral torsional buckling of the web post
- Rupture of the welded joint
- Web post buckling
- Formation of a flexure mechanism

2.1.1 Formation of a Vierendeel Bending Mechanism

This failure mode is associated with transferring high shear forces across the web holes, parallel to rate of change of bending moment along the beam. The formation of a Vierendeel mechanism often occurs in web-expanded beams with long horizontal opening lengths.

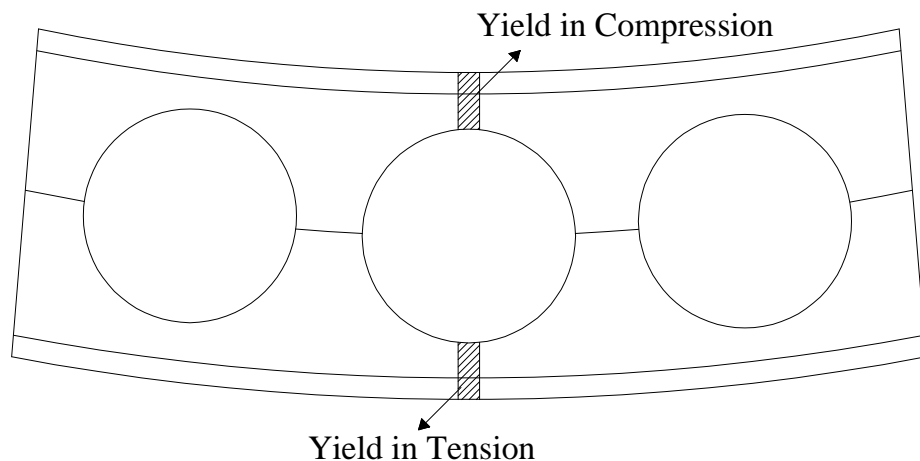


Figure 2.1 High bending in the cellular beam

The collapse of web-expanded beam has two reasons in the absence of regional or overall instability. Firstly plastic tension and compression stresses in the upper and lower tee parts in regions of high overall bending may lead to such a collapse, shown in Figure 2.1. The second cause of collapse of these beams is formation of plastic hinges at the all corners of the holes in regions of high shear called Vierendeel bending moment, shown below in Figure 2.2.

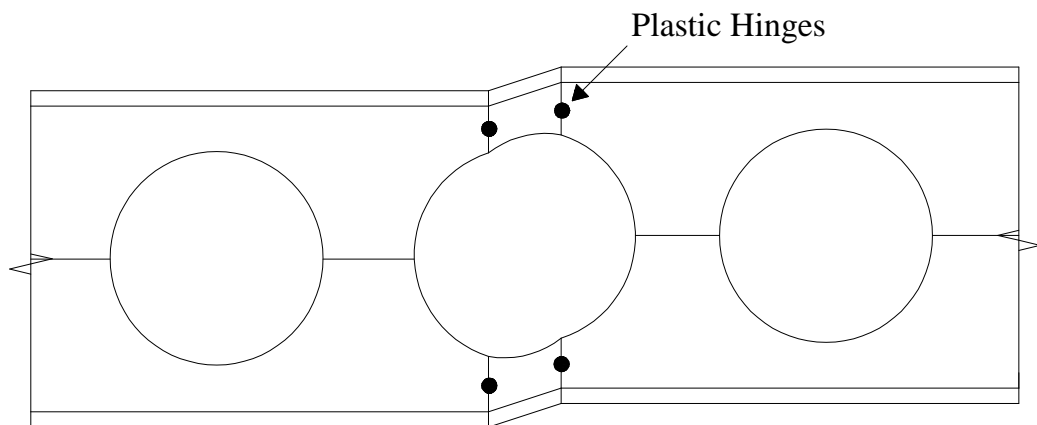


Figure 2.2 High shears in the cellular beam

When a web-expanded beam is subjected to a shear, the top and bottom tee sections must carry the applied shear, as well as the primary and secondary stresses. The primary stress is the formal bending moment on the beam cross-section. This stress is applied uniformly over the areas of the upper and lower part of tees. The secondary stress, also called the Vierendeel bending, comes from the transfer of shear force in the tee sections over the horizontal length of the web opening. The resulting overall stress is the sum of the primary and secondary stresses.

2.1.2 Lateral Torsional Buckling

This mode of failure is mainly brought about by out of plane motions of the beam which does not have web distortions in original web beams. Lateral torsional buckling, as shown in Figure 2.3, is usually associated with longer span beams with inadequate lateral support to the compression flange. The reduced torsional stiffness of the web-expanded beam, which is a result of relatively deeper and slender section properties, contributes to lateral buckling mode.



Figure 2.3 Lateral torsional buckling along beam

This mode of failure was first investigated in 1982 by Nethercot and Kerdal [20]. After experimental tests, they concluded that web openings only had a negligible effect on the overall lateral torsional buckling behavior of the web-expanded beams. Furthermore, they stated that due to the reduced cross sectional properties, web-expanded beams can be subjected to the same design procedures as original solid beams, to settle the lateral buckling strength.

2.1.3 Web-Post Buckling

Web post buckling has been a subject matter for many analytical and experimental studies on web-expanded beams. This failure type is caused by concentrated loading or reaction points applied directly over a web-post of beam. Horizontal shear in the web-post of the beam is due to double curvature bending over the depth of the web-post.



Figure 2.4 Web buckling on web-expanded beams

Web buckling is also related with on web thickness and the ratio of pitch opening and hole diameter. The first inclined edge of the opening is stressed in tension and the other edge of the hole in compression, all of which in a twisting effect of the web post along its depth, shown in Figure 2.4.

2.1.4 Rupture of Welded Joints

This mode of failure depends upon the length of the welded joint. Hussain and Speirs [7] have found this mode after tested six castellated beams with short welded throat. These tests showed that if the horizontal shear stresses exceed the yield strength of the welded throat, weld joint depth of the web between two openings could be ruptured.

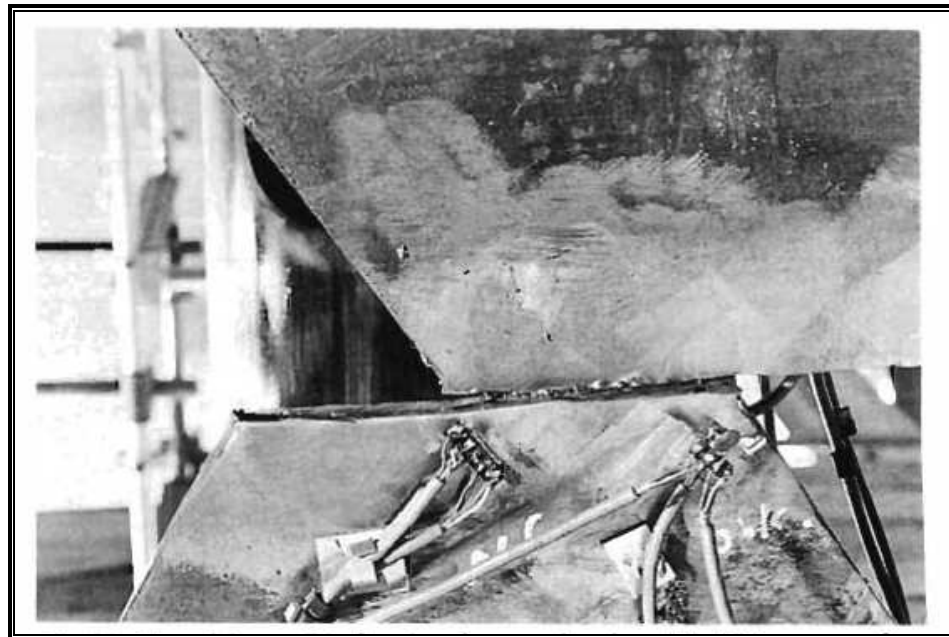


Figure 2.5 Rupture of welded joints on web-expanded beams

Figure 2.5 demonstrates that the failure of welded joints owing to high horizontal shear and short weld length at web-expanded beam. The horizontal length of the openings is equal to the weld length, and if the distance between these openings is reduced to decrease secondary moments, the welded throat of the web-post becomes more vulnerable to failure in this mode.

2.1.5 Flexure Mechanism

Under pure bending conditions, provided the section is compact, which means that the beam does not exhibit buckling behavior, the tee sections above and below the openings yield in tension and compression until they become fully plastic. This mode of failure was reported in the works of Toprac and Cooke (1959) [4]. They concluded that yielding in the tee sections above and below the openings of a web-expanded beam was similar to that of an original solid beam under applied pure bending forces.

2.2 Design Process of Cellular Beams

The design process of a cellular beam consists of checks such that the above mentioned failure modes do not occur. The strength of a beam with various web openings shall be determined based on the interaction of flexure and shear at the web opening. Design constraints include the displacement limitations, overall beam flexural capacity, beam shear capacity, overall beam buckling strength, web post flexure and buckling, Vierendeel bending of upper and lower tees, local buckling of compression flange and practical restrictions between cell diameter and the spacing between cells.

The design procedure given here is taken from The Steel Construction Institute (SCI) Publication No: 100 titled “*Design of Composite and Non-composite Cellular Beams*” [14]. The design methods are consistent with *BS5950* part 1 and 3, [21].

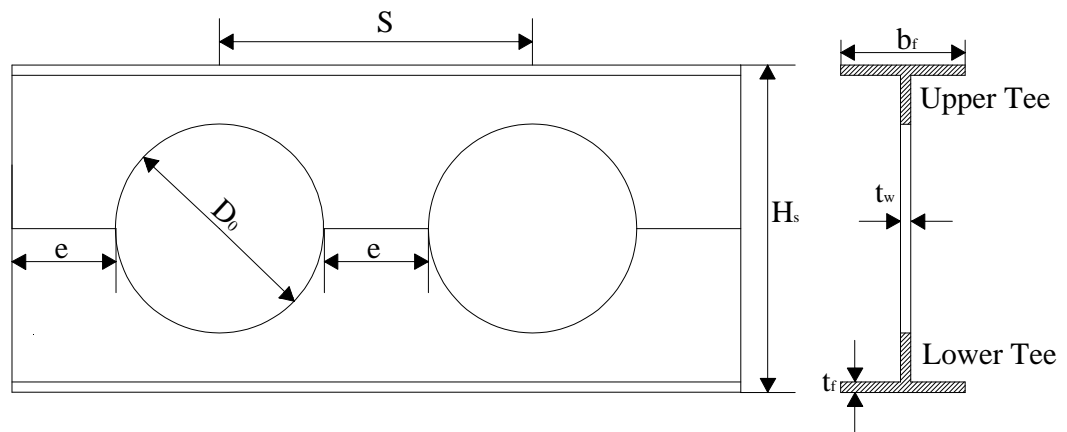


Figure 2.6 Geometrical parameters of a cellular beam

The basic geometry and notations used for cellular beams are shown in Figure 2.6. Although the diameter of holes and spacing between their centers are left to designer to select the following ratios are required to be observed.

$$1.08 < \frac{S}{D_0} < 1.5 \quad (2.1)$$

$$1.25 < \frac{H_s}{D_0} < 1.75 \quad (2.2)$$

2.2.1 Overall Beam Flexural Capacity

Under unfavorable applied load combinations the cellular beam should have sufficient flexural capacity to be able to resist the external loading. That is the maximum moment M_U under applied load combinations should not exceed plastic moment capacity M_P of the cellular beam.

$$M_U = A_{LT} P_Y H_U \leq M_P \quad (2.3)$$

Where A_{LT} is the cross sectional area of lower tee, P_Y is the design strength of steel and H_U is distance between centrals of upper tee and lower tee.

2.2.2 Beam Shear Capacity

It is necessary to check two shear failure modes in cellular beams. The first one is the vertical shear capacity check in the beam. The sum of the shear capacities of the upper and lower tees gives the vertical shear capacity of the beam. The factored shear force in the beam should not exceed P_{VY} :

$$P_{vY} = 0.6 P_Y (0.9 A_{wUL}) \quad (2.4)$$

Where A_{wUL} is the total cross sectional areas of webs of tees. The other check is for the horizontal shear failure. The horizontal shear is developed in the web post due the change in axial forces in the tee as shown in Figure 2.7. The horizontal shear capacity in the web post of beam should not exceed P_{vH} where:

$$P_{vH} = 0.6 P_Y (0.9 A_{wP}) \quad (2.5)$$

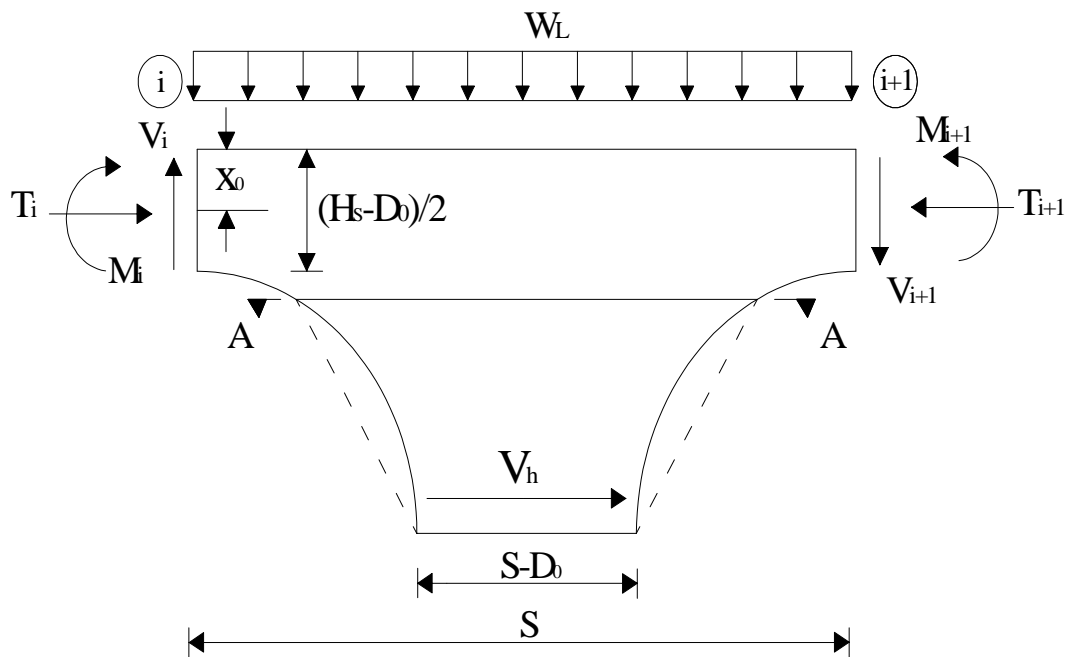


Figure 2.7 Horizontal shear in the web post of cellular beam

Where A_{wP} is the minimum area of the web-post. Neglecting the effect of the applied load and considering the vertical equilibrium and the rate of the

variation of bending moment as shown in Figure 2.7, then the following equations can be written for cellular beams.

$$V_{i+1} = V_i \quad (2.6)$$

$$M_i = T_i \times (H_s - 2x_0) \quad (2.7)$$

$$V_{i+1} = \frac{dM}{dx} = \frac{M_{i+1} - M_i}{S} = (T_{i+1} - T_i) \times \frac{(H_s - 2x_0)}{S} \quad (2.8)$$

For horizontal equilibrium:

$$V_h = T_{i+1} - T_i = V_{i+1} \frac{S}{H_s - 2x_0} \quad (2.9)$$

Where V is shear force, T is axial force and M is bending moment at the cross section of the cellular beam, S is distance between circular opening centers, x_0 is the distance between the axial force to flange.

2.2.3 Flexural and Buckling Strength of Web-Post

In this dissertation study the compression flange of the cellular beam is assumed to be sufficiently restrained by the floor system it is attached to. Hence the overall buckling strength of non-composite cellular beam is omitted from the design consideration. Instead the web post flexural and buckling capacity is checked using equation 2.10.

$$\frac{M_{MAX}}{M_E} = \left[C_1 \left(\frac{S}{D_0} \right) - C_2 \left(\frac{S}{D_0} \right)^2 - C_3 \right] \quad (2.10)$$

Where M_{MAX} is the maximum allowable web post moment and M_E is the web post capacity at section A-A of Figure 3 which is computed as elastic section capacity of design strength P_Y of the steel. S is the spacing between the centers of circular openings and D_0 is the circular opening diameter. Both should be substituted in the equation in mm unit. C_1, C_2 and C_3 are constants evaluated from the following expressions where t_w is the web thickness.

$$C_1 = 5.097 + 0.1464 \left(\frac{D_0}{t_w} \right) - 0.00174 \left(\frac{D_0}{t_w} \right)^2 \quad (2.11)$$

$$C_2 = 1.441 + 0.0625 \left(\frac{D_0}{t_w} \right) - 0.000683 \left(\frac{D_0}{t_w} \right)^2 \quad (2.12)$$

$$C_3 = 3.645 + 0.0853 \left(\frac{D_0}{t_w} \right) - 0.00108 \left(\frac{D_0}{t_w} \right)^2 \quad (2.13)$$

2.2.4 Vierendeel bending of upper and lower tees

The flexural capacity of the upper and lower tees under Vierendeel bending is critical. The transfer of shear forces across a single web opening causes secondary bending stresses. The Vierendeel bending stresses around the hole may be calculated using Olander's approach [22]. Olander utilizes a circular section for the position of the critical section and the ultimate resistance of the tees shown in Figure 2.8.

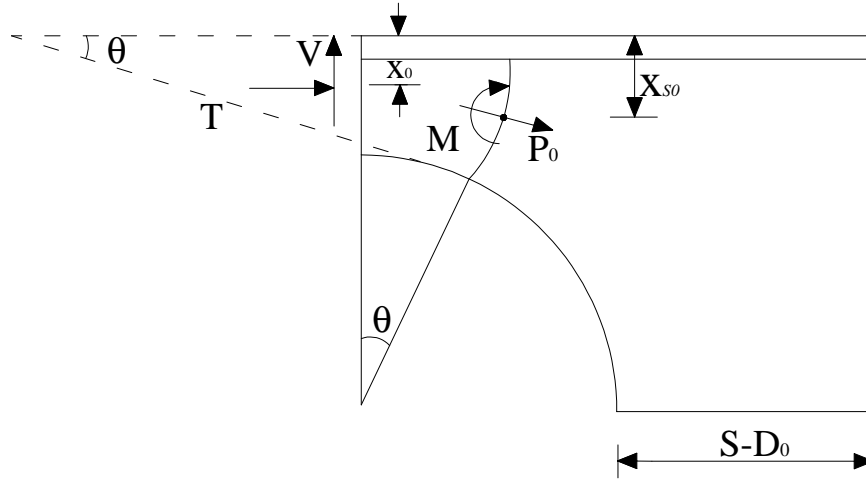


Figure 2.8 Olander's curved beam approach

For asymmetrical sections, the shear force is resisted by the upper and lower web sections in proportion to their depth squared. For symmetrical sections, the shear force is divided equally between upper and lower web sections. The interaction between Vierendeel bending moment and axial force for the critical section in the tee should be checked as follows:

$$\frac{P_o}{P_U} + \frac{M}{M_p} \leq 1.0 \quad (2.14)$$

$$P_o = T \cos \theta - \frac{V}{2} \sin \theta \quad (2.15)$$

$$M = T(x_{s0} - x_0) + \frac{V}{2} \left(\frac{H_s}{2} - x_{s0} \right) \quad (2.16)$$

Where P_o and M are the force and the moment on the section respectively.

P_U is equal to area of critical section $\times P_Y$, M_p is calculated as the plastic

modulus of critical section $\times P_Y$ in plastic sections or elastic section modulus of critical section $\times P_Y$ for other sections.

2.2.5 Classification of Cellular Beams

The computation of the nominal moment strength M_p of a laterally supported beam necessitates first the classification of the cellular beam. The beam can be plastic, compact, non-compact or slender according to BS5950 provisions [14]. In compact sections, local buckling of the compression flange and the web does not occur before the plastic hinge develops in the cross section. On the other hand in non-compact sections, the local buckling of compression flange or web may occur after the first yield is reached at the outer fiber of the flanges. Classification of I-shaped sections is carried out according to Table 2.1 of BS5950 which is repeated below.

Type of Element	Plastic	Compact	Semi-compact
Outstand Element of Compression Flange	$\frac{b_f}{2t_f} \leq 8.5 \epsilon$	$\frac{b_f}{2t_f} \leq 9.5 \epsilon$	$\frac{b_f}{2t_f} \leq 15 \epsilon$
For web, with neutral axis at mid-depth	$\frac{H_s - 2t_f}{t_w} \leq 79 \epsilon$	$\frac{H_s - 2t_f}{t_w} \leq 98 \epsilon$	$\frac{H_s - 2t_f}{t_w} \leq 120 \epsilon$

Table 2.1 Limiting width to thickness ratios

$$M_{P(plastic)} = P_Y \times S_x \quad (2.17)$$

$$M_{p(elastic)} = P_Y \times Z_x \quad (2.18)$$

$$\varepsilon = \left(\frac{275}{P_Y} \right)^{1/2} \quad (2.19)$$

$$\lambda_F = \frac{b_F}{2t_F} \quad (2.20)$$

$$\lambda_w = \frac{H}{t_w} \quad (2.21)$$

$$H = d - 2t_F \quad (2.22)$$

The moment capacity of beams for plastic or compact sections and semi-compact sections is calculated respectively in 2.17 and 2.18. In these equations; P_y is the design strength of steel, S_x is the plastic modulus and Z_x is the elastic modulus of section about relevant axis. In equation 2.19, ε defines a constant in connection with limiting with to thickness ratios. λ_F given in equation 2.20 is slenderness ratio for I-shaped member flanges and the thickness in which b_F and t_F are the width and the thickness of the flange. Equation 2.21 describes, λ_w , slenderness ratio for beam web, in which H plus allowance for underrsize inside fillet at compression flange for rolled I-shaped sections shown in equation 2.22, where d is the overall depth of the section and t_w is the web thickness. H/t_w is readily available in *UB*-section properties table.

2.2.6 Deflection of Cellular Beams

The limiting values for deflection of a beam under applied load combinations are given in BS5950, Part 1. According to these limitations the maximum deflection of a cellular beam should not exceed span/360. The deflection of cellular beam is computed using the virtual work method which is explained in detail in [14]. Figure 2.7 shows points of inflection at sections i and $i+1$. Shear force under applied load combinations is distributed equally to upper and lower tees. The axial and horizontal forces in these tees are given by;

$$T_i = \frac{M_i}{h} \quad (2.23)$$

$$V_h = \frac{S(V_i + V_{i+1})}{2h} \quad (2.24)$$

Where; h is the distance between the centroids of upper and lower tees and S is distance between centrals of holes. The deflection at each point is found by applying a unit load at that point.

Internal forces under a unit load are given by

$$\frac{\overline{V}_i}{2}, \quad \overline{N}_i, \quad \overline{V}_h \quad (2.25)$$

Deflection due to bending moment in tee;

$$y_{mt} = \frac{0.091(D_0/2)^3}{3EI_T} (\overline{V}_i \overline{V}_i) \quad (2.26)$$

Deflection due to bending moment in web post of beam;

$$y_{wp} = \frac{13.15}{Et_w} \left[\log_e \left(\frac{S - 0.9(D_0/2)}{S - 2.0(D_0/2)} \right) + 2 \left(\frac{S - 2.0(D_0/2)}{S - 0.9(D_0/2)} \right) - \frac{1}{2} \left(\frac{S - 2.0(D_0/2)}{S - 0.9(D_0/2)} \right)^2 - \frac{3}{2} \right] V_h \bar{V}_h \quad (2.27)$$

Deflection due to axial force in tee;

$$y_{at} = \frac{2S}{EA_T} (T_i \bar{T}_i) \quad (2.28)$$

Deflection due to shear in tee;

$$y_t = \frac{0.45(D_0/2)}{GA_{TWEB}} (V_i \bar{V}_i) \quad (2.29)$$

Deflection due to shear in web post;

$$y_w = \frac{1.636}{Gt_w} X \log_e \left(\frac{S - 0.9(D_0/2)}{S - 2.0(D_0/2)} \right) V_h \bar{V}_h \quad (2.30)$$

Where E is the elasticity modulus of steel cellular beam, I_T is total moment of inertia of cell beam, G is shear modulus of steel and X is the web post form factor. The total deflection of a single opening under applied load conditions is obtained by summing the deflections computed above in Eq. 2.26-2.30.

$$y_T = y_{mt} + y_{wp} + y_{at} + y_t + y_w \quad (2.31)$$

On the other hand the deflection of the cellular beam is calculated by multiplying the deflection of each opening by the total number of openings in the beam as given in [14].

CHAPTER 3

THE DESIGN OPTIMIZATION OF CELLULAR BEAMS USING META-HEURISTIC SEARCH TECHNIQUES

3.1 Optimum Design Problem of Cellular Beams

The design of a cellular beam requires the choice of an original rolled beam from which the cellular beam is to be produced, circular opening diameter and the spacing between the centers of these circular holes or the total number of holes in the beam. Hence, the sequence number of the rolled beam sections in the standard steel section tables, hole diameter and the total number of holes are taken as design variables in the optimum design problem considered. For this purpose, a design pool is prepared consisting of list of standard rolled beam sections, a list of various diameter sizes and a list of integer number starting from 2 to 40 (this number can be increased or decreased according to length of span) for the total number of holes in a cellular beam. The optimum design problem formulated considering the design constraints explained in the previous sections yields the following mathematical model.

Find an integer design vector $\{I\} = \{I_1, I_2, I_3\}^T$ where I_1 is the sequence number for the rolled beam section in the standard steel sections list, I_2 is the sequence number for the hole diameter in the discrete set which contains various diameter values and I_3 is the total number of holes for the cellular

beam. Once I_1 is selected, then the rolled steel beam designation becomes known and all cross sectional properties of the beam become available for the design. The corresponding values to I_2 and I_3 in the design sets make the hole diameter and the total number of holes also available for the cellular beam.

Therefore, the design problem for the minimization of the weight of the cellular beam turns out to be:

$$W_{CB} = \rho_s A_{CB} L_{CB} - \rho \left(\pi \left(\frac{D_0}{2} \right)^2 N_{hole} \right) \quad (3.1)$$

Where; W_{CB} denotes the weight of the cellular beam, ρ_s is the density of steel. A_{CB} , L_{CB} , D_0 , and N_{hole} represent the total cross-sectional area of a steel profile, span of the cellular beam, diameter of the web holes and the total number of holes in the beam, respectively.

Design of a cellular beam requires the satisfaction of some geometrical and behavioral restrictions that are formulated through Eqns. (3.2-3.13). Depending on the values of diameter of holes, distance between the hole centers and the final depth of the beam determined, following geometrical constraints must be satisfied;

$$g_1 = 1.08 D_0 - S \leq 0 \quad (3.2)$$

$$g_2 = S - 1.60 D_0 \leq 0 \quad (3.3)$$

$$g_3 = 1.25 D_0 - H_s \leq 0 \quad (3.4)$$

$$g_4 = H_s - 1.75 D_0 \leq 0 \quad (3.5)$$

In Eqns. (3.2-3.5), S denotes the distance between centers of circular openings and H_s is the overall depth of cellular beam.

The maximum moment, M_U , under applied load combinations should not exceed the plastic moment capacity M_p of the cellular beam for a sufficient flexural capacity.

$$g_5 = M_U - M_p \leq 0 \quad (3.6)$$

It is also required that the shear stresses (V_{MAXSUP}) computed at the supports are smaller than allowable shear stresses (P_V), the ones at the web openings (V_{OMAX}) are smaller than allowable vertical shear stresses (P_{VY}) and finally, the horizontal shear stresses (V_{HMAX}) are smaller than the upper limit (P_{VH}) of the same; as formulated in Eqns. (3.7-3.9).

$$g_6 = V_{MAXSUP} - P_V \leq 0 \quad (3.7)$$

$$g_7 = V_{OMAX} - P_{VY} \leq 0 \quad (3.8)$$

$$g_8 = V_{HMAX} - P_{VH} \leq 0 \quad (3.9)$$

The web post flexural and buckling capacity of cellular beam is checked in the Eqn.3.10. In this expression, the maximum moment determined at A-A section (M_{A-AMAX}) should be smaller than the maximum allowable web post moment (M_{WMAX}).

$$g_9 = M_{A-MAX} - M_{W-MAX} \leq 0 \quad (3.10)$$

Eqns. 3.11 and 3.12 check the interaction between the secondary bending stress and the axial force for the critical section in the tee.

$$g_{10} = V_{TEE} - 0.5 P_{VY} \leq 0 \quad (3.11)$$

$$g_{11} = \frac{P_0}{P_U} - \frac{M}{M_P} - 1 \leq 0 \quad (3.12)$$

Where; V_{TEE} is referred to as the vertical shear on the tee at $\theta = 0$ of web opening, P_0 and M are the internal forces on the web section as shown in Fig 4. The deflection constraint is imposed such that the maximum displacement is restricted to $L/360$, where y_{MAX} denotes the maximum deflection.

$$g_{12} = y_{MAX} - \frac{L}{360} \leq 0 \quad (3.13)$$

3.2 Stochastic Search Techniques in Optimization

The solution of the optimum design problem described in previous section necessitates the selection of appropriate steel beam section from a standard list, an opening diameter and the total number of openings to be used in the cellular beam such that with these selected parameters, the response of the cellular beam remains within the limitations imposed in expressions (3.2)-(3.13) and its weight given in expression (3.1) is the minimum. This is clearly a discrete programming design problem. The solution methods available among the mathematical programming techniques to obtain solutions to discrete

programming problems are somewhat cumbersome and not very efficient for practical use. Fortunately, the emergence of stochastic search techniques that are based upon the simulation of paradigms found in nature has changed this situation altogether. The basic idea behind these search techniques is to simulate the natural phenomena, such as survival of the fittest in genetic algorithms, flock migration in swarm intelligence, shortest path to food source in ant colony optimization, best harmony of instruments in harmony search algorithm, the cooling process of molten metals through annealing into a numerical algorithm and staying alive of the fittest and most experienced in memetic algorithm [23-31]. These innovative stochastic search and optimization methods, simulated annealing [32], evolution strategies [33], particle swarm optimizer [34], tabu search method [35], ant colony optimization [36], harmony search method [37], genetic algorithms [38] and etc., are very suitable and effective in finding the solution of combinatorial optimization problems. They do not require the gradient information of the objective function and constraints and they use the probabilistic transition rules not the deterministic ones. The optimum structural design algorithms that are based on these techniques are robust and quite effective in finding the solution to discrete programming problems. There are large numbers of such metaheuristic techniques available in the literature nowadays. A detailed review of these algorithms as well as their applications in the optimum structural design is carried out in Saka [39] and Hasancebi et al [40].

In the present dissertation research, the solution of the discrete non-composite cellular beam design problem given by Eqns. (3.2-3.13) is investigated using two meta-heuristic search techniques; namely harmony search algorithm and particle swarm optimizer.

3.2.1 Harmony Search Method

One of the recent additions to the meta-heuristic search techniques of combinatorial optimization problems is the harmony search method initiated by Geem and Kim [37]. This presented stochastic technique is based on the musical performance process that takes place when a musician searches for a better state of harmony [41]. In the process of musical production, a musician chooses and brings together number of different notes from the whole notes and then plays these with a musical instrument to find out whether it gives a pleasing harmony. The musician then tunes some of these notes to achieve a better harmony. Similarly, a candidate solution is generated in the optimum design process by modifying some of the decision variables to find optimum solution. Structural designer in a design of a steel structure selects steel profiles for the members of a structure randomly or using her/his previous experience. This selection constitutes a potential design for the structure under consideration. The candidate solution obtained is then checked to see whether it improves the objective function or not, as it is in the case of finding out whether euphonic music is obtained or not. Like the other meta-heuristic techniques, harmony search algorithm uses stochastic random search instead of gradient search.

HS algorithm was used in structural optimization and computational structural mechanics immediately after its emergence. The recent applications have shown that this method is an efficient and robust numerical optimization technique that can be utilized in finding the optimum solution of structural optimization problems. Amongst these studies, Lee and Geem [37, 41] used the technique for optimum design of space truss structures. The minimum weight design of planar frames formulated according to both BS5950 [21] and LRFD-AISC [42] design codes were carried out using HS algorithm in [43] and [44], respectively. In Ref. [43], a harmony search based solution algorithm for

optimum design of geodesic domes was developed by Saka, where in addition to size variables; a single shape variable is used to modify the height of the dome under consideration. Then, the success of the method in optimum W-sections for the transverse and longitudinal beams of grillage systems was examined in Erdal and Saka [45-46]. Besides, in [40] harmony search method is used in the optimum design of real size trusses where the design problem is formulated according to ASD-AISC [47] and its performance is compared to other metaheuristic techniques. Finally, Hasançebi et al. developed an adaptive harmony search algorithm for the optimum design of structures. In adaptive harmony search method, unlike the standart application of the technique, algorithm parameters adjust automatically during the optimization process. The efficiency of the proposed algorithm is numerically investigated using two large-scale steel frames that are designed for minimum weight according to the provisions of ASD-AISC specification [48]. The solutions obtained from this proposed method are compared with those of the standard algorithm as well as of the other metaheuristic search techniques. In all these applications, it was concluded that harmony search was a very effective technique to obtain the optimum solution to various structural design problems.

The basic components of the harmony search algorithm can now be outlined in five steps as follows.

Step 1 Initialization of a Parameter Set: A harmony search optimization parameter sets are initialized first. These parameters consists of four entities called as a harmony memory size (hms), a harmony memory considering rate ($hmcr$), a pitch adjusting rate (par) and a maximum search number (N_{cyc}). It is worthwhile to mention that in the standard harmony search algorithm these parameters are treated as static quantities, suitable values are chosen within their recommended ranges of $hmcr \in (0.70 \sim 0.95)$ and $par \in (0.20 \sim 0.50)$ [37, 41]. It should be mentioned that the selection of these values are problem dependent and it requires number of trials to identify the appropriate ones.

Step 2 Initialization and Evaluation of Harmony Memory Matrix: A harmony memory matrix \mathbf{H} is generated and randomly initialized next. This matrix incorporates (hms) number of feasible solutions. Each solution (harmony vector, \mathbf{I}^i) consists of nv integer numbers between 1 to ns selected randomly each of which corresponds sequence number of design variables in the design pool, and is represented in a separate row of the matrix; consequently the size of \mathbf{H} is ($hms \times nv$).

$$\mathbf{H} = \begin{bmatrix} I_1^1 & I_2^1 & \dots & I_{nv}^1 \\ I_1^2 & I_2^2 & \dots & I_{nv}^2 \\ \dots & \dots & \dots & \dots \\ I_1^{hms} & I_2^{hms} & \dots & I_{nv}^{hms} \end{bmatrix} \begin{matrix} \phi(\mathbf{I}^1) \\ \phi(\mathbf{I}^2) \\ \dots \\ \phi(\mathbf{I}^{hms}) \end{matrix} \quad (3.14)$$

I_i^j is the sequence number of the i^{th} design variable in the j^{th} randomly selected feasible solution. (hms) solutions shown in Eqn. (3.14) are

then analyzed, and their objective function values are calculated. The solutions evaluated are sorted in the harmony memory matrix in the increasing order of objective function values, that is $\phi(\mathbf{I}^1) \leq \phi(\mathbf{I}^2) \leq \dots \leq \phi(\mathbf{I}^{hms})$.

Step 3 Generating a New Harmony: A new harmony solution vector $\mathbf{I}' = [I'_1, I'_2, \dots, I'_{nv}]$ is improvised by selecting each design variable from either harmony memory or the entire discrete set. The probability that a design variable is selected from the harmony memory is controlled by a parameter called harmony memory considering rate (*hmcr*). To execute this probability, a random number r_i is generated between 0 and 1 for each variable I_i . If r_i is smaller than or equal to *hmcr*, the variable is chosen from harmony memory in which case it is assigned any value from the i -th column of the \mathbf{H} , representing the value set of variable in *hms* solutions of the matrix (Eqn. 3.15). Otherwise (if $r_i > hmcr$), a random value is assigned to the variable from the entire discrete set.

$$I'_i = \begin{cases} I'_i \in \{I_i^1, I_i^2, \dots, I_i^{hms}\} & \text{if } r_i \leq hmcr \\ I'_i \in \{1, \dots, ns\} & \text{if } r_i > hmcr \end{cases} \quad (3.15)$$

If a design variable attains its value from harmony memory, it is checked whether this value should be pitch-adjusted or not. Pitch adjustment simply means sampling the variable's one of the neighboring values, obtained by adding or subtracting one from its current value. Similar to *hmcr* parameter, it is operated with a probability known as pitch adjustment rate (*par*), (Eqn. 3.16). If not activated by *par*; the value of the variable does not change.

$$I_i'' = \begin{cases} I_i' \pm 1 & \text{if } r_i \leq par \\ I_i' & \text{if } r_i > par \end{cases} \quad (3.16)$$

Constraint handling: The new harmony solution vector obtained using above-mentioned rules is checked whether it violates design constraints. If this vector is severely infeasible it is discarded and another harmony vector is sought. However, if it is slightly infeasible, it is included in the harmony matrix. In this way the slightly infeasible harmony vector is used as a base in the pitch adjustment operation to provide a new vector that may be feasible. This is achieved by using large error values initially for the acceptability of the new design vectors. The error value is then gradually reduced during the design cycles until it reaches to its final value. This value is then kept the same until the end of iterations. This adaptive error strategy is found quite effective in handling the design constraints in large design problems.

Step 4 Update of Harmony Matrix: After selecting new values generating the harmony solution vector, its objective function value is calculated. After selecting the new values for each design variable the objective function value is calculated for the newest harmony vector. If this value is better than the worst harmony vector in the harmony matrix, it is then included in the matrix while the worst one is taken out of the matrix. The harmony memory matrix is then sorted in descending order by the objective function value.

Step 5 Termination: The steps 3 and 4 are repeated until a pre-assigned maximum number of cycles N_{cyc} is reached. This number is selected large enough such that within this number no further improvement is possible in the objective function.

3.2.2 Particle Swarm Optimization Method

Particle swarm optimization (PSO) method is a population based stochastic search technique inspired by social behavior of bird flocking or fish schooling. This behaviour is concerned with grouping by social forces that depend on both the memory of each individual as well as the knowledge gained by the swarm [49-51]. As a meta-heuristic search and optimization technique, PSO algorithm has gained a worldwide popularity and found important applications in many disciplines of science and engineering. In the field of structural optimization, the method is successfully utilized to determine the optimum solutions of different design problems. Amongst recent studies, Perez and Behdinan [52] have extended the algorithm to cover the optimum design of space structures. They carried out the effect of different setting parameters and functionality on truss structures. He, Prempain and Wu [53] proposed an improved PSO algorithm to solve mechanical design problems involving problem-specific constraints and mixed variables. In Ref. [54], Fourie and Groenwold developed a particle swarm based solution algorithm for simultaneous optimum design of small scale pin-jointed structures, where optimum size and shape of a structure were sought concurrently to minimize its structural weight. Later, Hasançebi et al. [40] have compared the performance of PSO method with other six stochastic search techniques including harmony search algorithm in the optimum design of real size pin-jointed structures formulated according to ASD-AISC [47].

The particle swarm optimization procedure involves a number of particles which represents the swarm initialized randomly in the search space of an objective function. Each particle in the swarm represents a candidate solution of the optimum design problem. Originally particle swarm optimizer is developed for continuous design variables. To be able to use the method for discrete design variables, some adjustments are required.

The basic steps of the particle swarm optimization for a general discrete optimization problem can be outlined as follows.

Step 1 Swarm of particles is initialized randomly with sequence numbers I_0^i which corresponds positions I_0^i and initial velocities v_0^i that are randomly distributed throughout the design space. Here I_0^i represents the sequence number of values in the discrete set. These are obtained from the following expressions.

$$I_0^i = INT[I_{\min} + r(I_{\max} - I_{\min})] \quad (3.17)$$

$$v_0^i = [(I_{\min} + r(I_{\max} - I_{\min})) / \Delta t] \quad (3.18)$$

Where the term r represents a random number between 0 and 1, I_{\min} is equal to 1 and I_{\max} is the total number of values in the discrete set respectively. Once I_0^i is computed, the corresponding x_0^i value is taken from the discrete set.

Step 2 The objective function values $f(x_k^i)$ are evaluated using the design space positions x_k^i .

Step 3 The optimum particle position p_k^i at the current iteration k and the global optimum particle position p_k^g are updated by equating p_k^i to $f(x_k^i)$ and p_k^g to the best $f(x_k^i)$.

Step 4 The velocity vector of each particle is updated considering the particle's current velocity and position, the particle's best position and global best position, as follows:

$$v_{k+1}^i = wv_k^i + c_1r_1 \frac{(p_k^i - x_k^i)}{\Delta t} + c_2r_2 \frac{(p_k^g - x_k^i)}{\Delta t} \quad (3.19)$$

where r_1 and r_2 are random numbers between 0 and 1, p_k^i is the best position found by particle i so far, and p_k^g is the best position in the swarm at time k . w is the inertia of the particle which controls the exploration properties of the algorithm. c_1 and c_2 are trust parameters that indicate how much confidence the particle has in itself and in the swarm respectively.

Step 5 The sequence number for the position of each particle is updated from

$$I_{k+1}^i = INT(I_k^i + v_{k+1}^i \Delta t) \quad (3.20)$$

Where I_{k+1}^i is the sequence number in the discrete set for x_{k+1}^i which is the position of particle i at iteration $k+1$, v_{k+1}^i is the corresponding velocity vector and Δt is the time step value.

Step 6 Steps 2-5 are repeated until pre-determined maximum number of cycles is reached.

In the particle swarm method algorithm parameters are treated as static quantities, and hence they are assigned to suitable values selected within their recommended ranges of following values $w \in (0.05 \sim 0.50)$, $\mu \in (10 \sim 50)$, c_1 and $c_2 \in (1.0 \sim 2.0)$ and $\Delta t \in (1.0)$ [55-58].

3.2.3 The Comparison of HS and PSO Algorithms with An Example

Harmony search method and particle swarm based optimum design algorithm presented in the previous subsections are used to design a cellular beam to compare which method is better while finding the optimum solution. Due to unavailability of UB sections in Turkey, the tests are performed using NPI sections. However, UB sections are used in two comparative optimization analyses. This is because, availability of larger variety of UB sections to be selected leads to more precise results to be used for comparison of two methods. Among the steel sections list 64 UB sections starting from 254×102×28 UB to 914×419×388 UB are selected to constitute the discrete set of steel profiles from which the design algorithm selects the sectional designations for the cellular beams [59]. For the hole diameters discrete set that has 421 values ranging from 180 mm to 600 mm with the increment of 1mm is prepared. Another discrete set is arranged for the number of holes that contains numbers ranging from 2 to 40 with the increment of 1.

3.2.3.1 Cellular Beam with 4-m Span

A simply supported beam shown in Figure 3.1 is selected as first design example to demonstrate the steps of optimum design algorithms developed for cellular beams that are based on harmony search and particle swarm methods. The beam has a span of 4 m and is subjected to 5 kN/m dead load including its own weight. A concentrated live load of 50 kN also acts at mid-span of the beam as shown in the same figure.

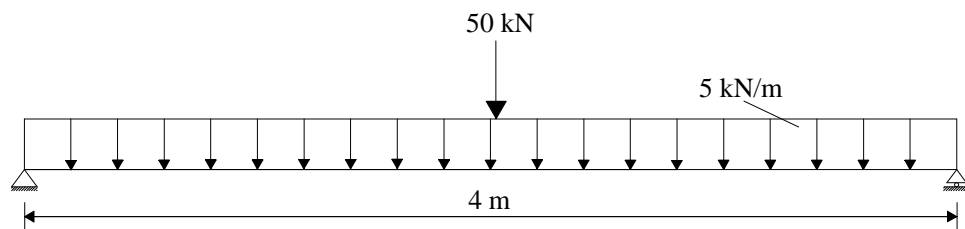


Figure 3.1 Loading of 4-m simply supported beam

The maximum displacement of the beam under these point and distributed loads is restricted to 12 mm while other design constraints are implemented from BS5950 as explained in Section 3.1. The modulus of elasticity is taken as 205 kN/mm^2 and Grade 50 steel is adopted for the beam which has the design strength of 355 MPa. The size of harmony memory matrix and number of particles (hms and μ) is taken as 10 and maximum number of generations is kept the same for both harmony search and particle swarm methods.

In the use of the harmony search method, the other parameters *hmcr* and *par* are taken as 0.8 and 0.35 respectively. It took 17 cycles for the harmony search method to fill the harmony memory matrix. This matrix is given in Table 3.1

Table 3.1 The initial feasible designs selected by PSO and HS algorithms

PSO Algorithm (Initial)					HS Algorithm (After 17 iterations)				
Particle No	Section (UB)	Number of Holes	Hole Dia. (mm)	Weight (kg)	Row Number	Section (UB)	Number of Holes	Hole Dia. (mm)	Weight (kg)
1	356x127x33	8	386	120,53	1	356x127x39	10	316	144,80
2	406x140x39	8	429	137,71	2	406x178x60	6	412	231,48
3	406x140x39	7	366	148,20	3	406x178x74	7	538	255,95
4	305x102x33	8	342	124,06	4	406x178x74	7	396	284,50
5	406x178x74	8	380	280,79	5	457x191x74	7	352	287,56
6	356x171x57	10	291	217,60	6	457x191x98	5	581	371,18
7	305x127x37	9	371	132,54	7	533x210x109	6	558	398,71
8	356x171x45	8	324	172,20	8	533x210x122	5	560	464,99
9	406x178x67	8	365	255,68	9	610x229x125	6	499	476,21
10	305x127x37	8	349	139,32	10	686x254x140	4	590	543,51

Table 3.2 Feasible designs obtained after 32 iterations by PSO and HS algorithms

PSO Algorithm					HS Algorithm				
Particle No	Section (UB)	Number of Holes	Hole Dia. (mm)	Weight (kg)	Memory No	Section (UB)	Number of Holes	Hole Dia. (mm)	Weight (kg)
1	305x165x54	9	387	195,79	1	356x127x39	10	316	144,80
2	406x140x39	8	429	137,71	2	356x171x45	9	359	163,44
3	356x171x67	9	391	243,97	3	406x178x60	6	412	231,48
4	305x102x33	8	342	124,06	4	406x178x74	7	538	255,95
5	406x140x46	9	386	166,00	5	406x178x74	7	396	284,50
6	356x171x57	10	291	217,60	6	457x191x74	7	352	287,56
7	356x171x45	9	374	163,44	7	457x191x98	5	581	371,18
8	356x127x33	9	359	119,66	8	533x210x109	6	558	398,71
9	305x165x54	9	389	195,39	9	533x210x122	5	560	464,99
10	305x127x37	8	349	139,32	10	610x229x125	6	499	476,21

The first row of this matrix has the least weight and corresponds to 356×127×39 UB section which is selected from the 64 UB-sections list. The cellular beam should be produced such that it should have 10 circular holes each having 402mm diameter in this cycle. HS algorithm can not find better sections between 18th and 31th cycles than the ones shown in Table 3.1. However, 32th cycle gives a better harmony memory matrix as shown in Table 3.2.

The new objective function value 163.44 kg is better than the worst harmony in the memory matrix 543.51 kg. Hence this new design is placed in the 2th row of

the harmony memory matrix and the worst design with the largest objective function value is discarded from the harmony memory matrix. The new design does not affect the first row of the harmony memory matrix in this search. However later, when the harmony search algorithm continues to seek better designs another vector that is obtained in later cycles changes the harmony memory matrix.

Table 3.3 Feasible designs obtained after 780 iterations by PSO and HS algorithms

PSO Algorithm					HS Algorithm				
Particle No	Section (UB)	Number of Holes	Hole Dia. (mm)	Weight (kg)	Memory No	Section No (UB)	Number of Holes	Hole Dia. (mm)	Weight (kg)
1	305×102x25	9	374	86,27	1	305x102x25	9	402	82,19
2	305x102x25	10	365	83,19	2	305x102x25	10	345	82,50
3	254x146x43	10	336	157,78	3	305x102x25	10	342	82,80
4	305x102x25	9	351	89,10	4	305x102x25	10	315	82,90
5	305x102x25	10	348	85,81	5	305x102x25	10	312	83,11
6	305x102x25	11	334	84,15	6	305x102x25	9	335	83,52
7	305x102x25	11	330	84,80	7	305x102x25	10	305	83,72
8	254x146x37	12	303	133,65	8	305x102x25	9	328	83,82
9	305x102x25	11	333	84,32	9	305x102x25	9	313	84,33
10	305x102x25	10	368	82,71	10	305x102x25	9	310	84,43

The optimum result presented in Table 3.3 is obtained after 780 iterations. It is noticed that this design vector remained the same even though the design cycles are continued to reach 5000 which was the pre-selected maximum number of iterations.

Table 3.4 Comparison of optimum designs for 4-m simply supported beam

Search Method	Optimum Section Designations (UB)	Diameter of Hole (mm)	Total Number of Holes	Minimum Weight (kg)
HS Algorithm	305×102×25	402	9	82.19
PSO Algorithm	305×102×25	368	10	82.71

It is apparent from the Table 3.4 that the optimum design has the minimum weight of 82.19 kg. In the optimum design the harmony search algorithm selects 305×102×25 UB section for the root beam. Furthermore it decides that the cellular beam should have 9 circular holes each having 402mm diameter.

Similar to harmony search algorithm the particle swarm optimizer also starts initializing the parameters. The values c_1 and c_2 are selected as 1, 2 is adopted for w and the values of Δt and V_{\max} are chosen as 2. The total number of particles is selected as 10. At the initial runs the particle swarm algorithm generates ten feasible design vectors each of which is assigned to each particle and the search for the optimum solution starts with this set of particles. The initial set of feasible designs assigned to each particle is listed in Table 3.1. In this table, the first particle has the feasible design with minimum weight. This design has the minimum weight of 120.53 kg where the universal beam section of 356×127×33 UB is selected for the root beam. The beam should be produced such that it should have 8 circular holes each having 386mm diameter at this weight. Design cycles are started with these values of the particles and the positions and the objective function values of particles keep on changing iteration after iterations. The best among these positions is kept as

the optimum design attained in the current iteration. If this one is better than the global one then it is assumed as the optimum design obtained up to the present iteration. After 32 iterations the designs obtained are listed in Table 3.2. It is apparent from the table that 8th particle has a design with the least weight of 119.66. Table 3.3 contains the designs obtained after 430 iterations. It is noticed that the optimum design obtained in this table does not improve even though the iterations are continued until 5000. Comparing to harmony search method, the optimum design is obtained after 430 iterations in particle swarm algorithm. It is apparent from Table 3.4 that the optimum design has the minimum weight of 82.71 kg which selects 305×102×25 UB section for the root beam, total of 10 holes in the beam each having 368mm diameter. In addition, the design history curve for both techniques is shown in Figure 3.2.

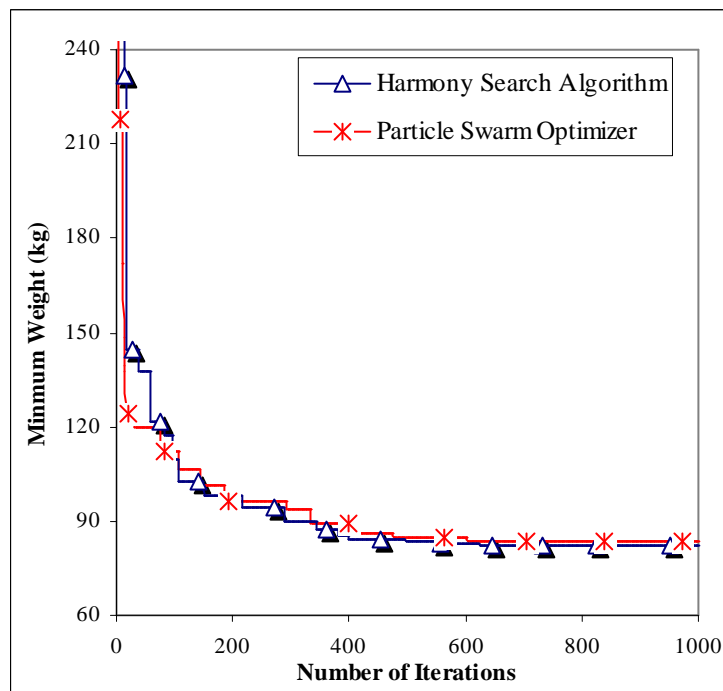


Figure 3.2 The design history graph for 4-m cellular beam

In this particular problem, these results demonstrate that while both the strength and geometric constraints are dominant in HS algorithm, in PSO algorithm, only the strength constraints are severe. To sum up, the optimum result of harmony search technique is compared with particle swarm optimization method to show accuracy and performance of methods on cellular beams. Although the algorithms of HS and PSO are mathematically quite simple, they are quite robust in finding the solutions of combinatorial optimum design problems as it is demonstrated in the example considered. Comparison of the optimum designs attained by particle swarm optimizer and harmony search algorithm clearly demonstrates that the harmony search algorithm yields better solution than the particle swarm optimizer for this design example at the same number of structural analyses. This result also demonstrates that harmony search algorithm is a very rapid and effective method for optimum design of small-scale problems that consist of a small number of decision variables. Consequently, the technique is recommended for its application to optimization of the three different cellular beam problems, presented in the next subsection, which in fact led to its adoption in our experimental study. The ultimate load capacities of these optimally designed cellular beams are tested under the action of same concentrated loadings in experimental work.

3.3 Design Examples

HS method based design algorithm presented in the previous sections is used to design of three different cellular beams. The selected method, harmony search algorithm, will now be applied for optimization of cellular NPI beams, on which the tests are performed. Among the steel sections list 24 NPI sections starting from NPI-80 to NPI-600 to constitute the discrete set steel sections from which the design algorithm selects the sectional designations for the cellular beams [58]. There are 431 hole diameter of cellular beams which

varies between 70 and 500mm with increment of 1mm. The discrete set for the number of holes starts with 2 and goes up to 40 with increment of 1.

3.3.1 Cellular Beam with NPI-240 Section

Simply supported cellular beams with a span of 3 m are subjected to a concentrated load; live load of 260 kN, as shown in Figure 3.3. The allowable displacement of the beam space under live-load is limited to 9 mm. The modulus of elasticity is taken as 205 kN/mm² and the design strength for Grade 50 of steel is 355 kN/mm². For this simply supported beam, harmony memory matrix size (*hms*) is taken as 20. Harmony memory considering rate (*hmcr*) is selected as 0.7 while pitch-adjusting rate (*par*) is considered as 0.3 on the basis of the empirical findings by Geem and Lee [37, 41]. The maximum number of searches was set to 10,000 for this example.

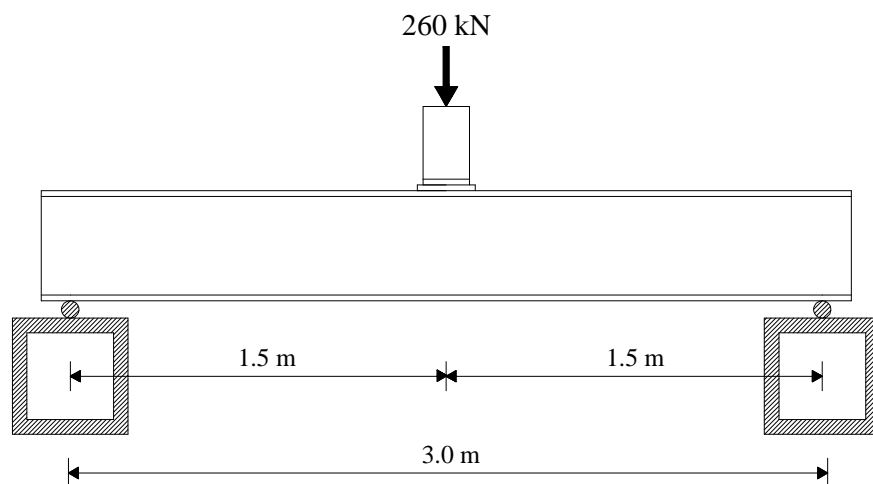


Figure 3.3 Typical cross section of beam with 3-m for NPI-240

The feasible designs presented in Table 3.5 are obtained after 650 iterations. It is noticed that this design vector remained the same even though the design cycles are continued to reach 10,000 which was the pre-selected maximum number of iterations. The optimum design of the cellular beam is carried out by the algorithm presented and the optimum results obtained are given in Table 3.6. This design is determined after 10,000 cycles and the minimum weight of the cellular beam is 99.46 kg. Harmony search algorithm selects NPI-240 profile, 8 circular holes and 251mm for the hole diameter. Design history graph obtained with harmony search algorithm in the optimum design of NPI_240 cellular beam is shown in Figure 3.4. The optimum shape of the cellular beam for the loading considered is shown in Figure 3.5.

Table 3.5 Feasible designs obtained after 650 iterations by HS algorithms

<i>hms</i>	SSQ (kN)	Section Des.	Diameter (cm)	N. of Holes
1	0.98	9	251	8
2	1.22	11	331	7
3	1.26	11	306	7
4	1.26	11	329	6
5	1.28	11	246	9
6	1.31	11	244	7
7	1.31	11	239	7
8	1.31	11	230	8
9	1.44	12	298	5
10	1.45	12	315	5
11	1.45	12	247	9
12	1.48	12	248	7
13	1.48	12	233	7
14	1.50	12	205	9
15	1.58	13	359	6
16	1.59	13	352	4
17	1.60	13	381	5
18	1.68	13	216	9
19	1.68	13	212	8
20	1.79	14	387	4

Table 3.6 Optimum Design of NPI_240 Cellular beam with 3-m span

Optimum NPI-Section Designations	Hole Diameter (mm)	Total Number of Holes	Maximum Strength Related Ratio	Minimum Weight (kg)
NPI-240	251	8	0.98	99.46

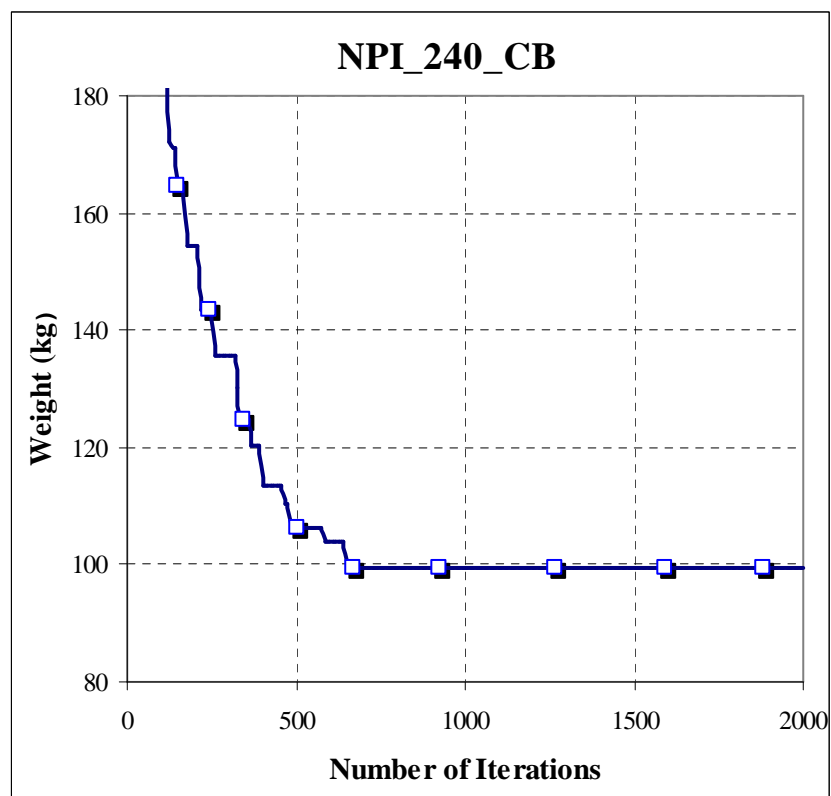


Figure 3.4 The design history graph for NPI_240 cellular beam

NPI 240 Cellular Beam

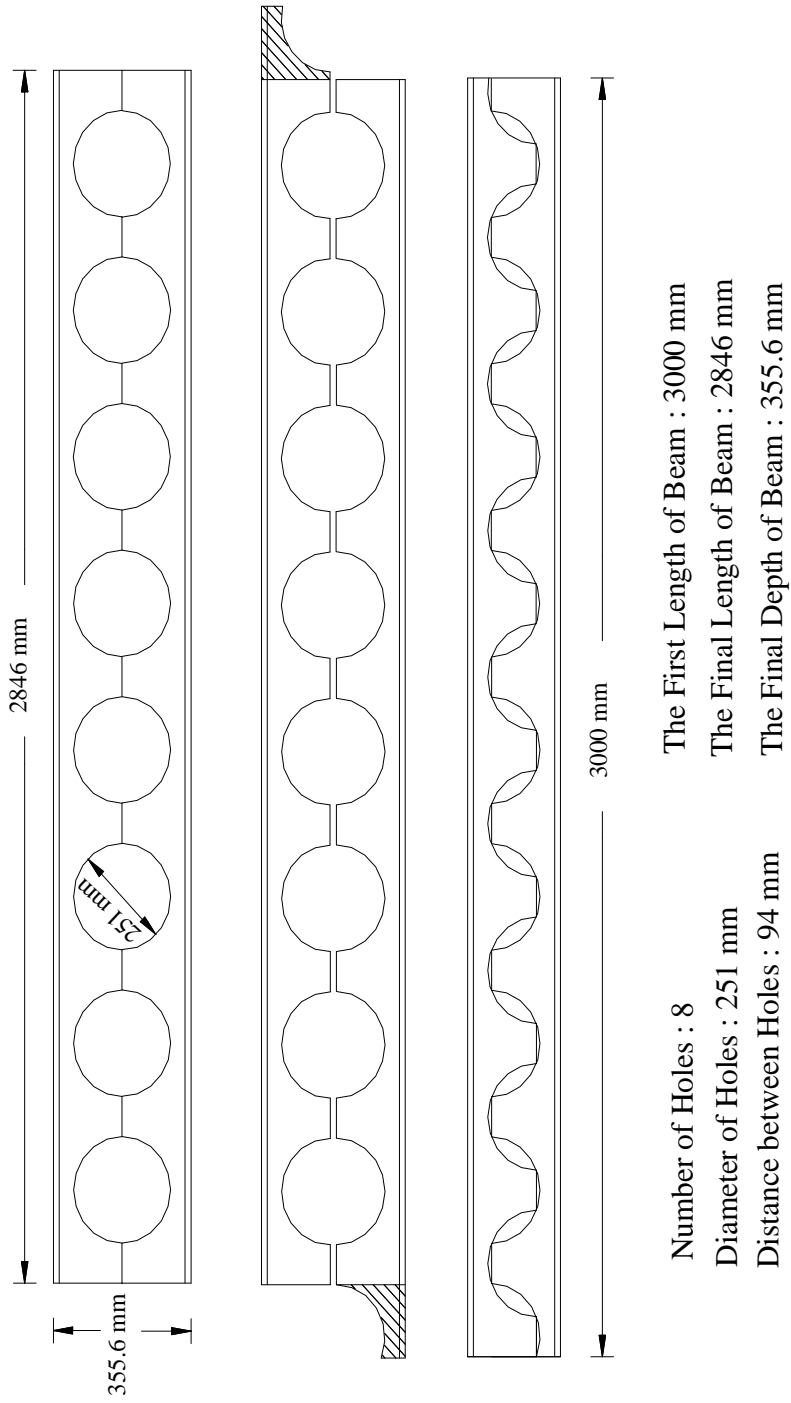


Figure 3.5 Optimum Shape of NPI-240 after 10,000 Iterations

3.3.2 Cellular Beam with NPI-260 Section

Simply supported cellular beams with a span of 3 m are subjected to a concentrated load; live load of 200 kN, as shown in Figure 3.6. The allowable displacement of the beam space under live-load is limited to 9 mm. The modulus of elasticity is taken as 205 kN/mm^2 and the design strength for Grade 50 of steel is 355 kN/mm^2 . For this simply supported beam, harmony memory matrix size (hms) is taken as 30. Harmony memory considering rate ($hmcr$) is selected as 0.9 while pitch-adjusting rate (par) is considered as 0.1 on the basis of the empirical findings by Geem and Lee [37, 41]. The maximum number of searches was set to 10,000 for this example.

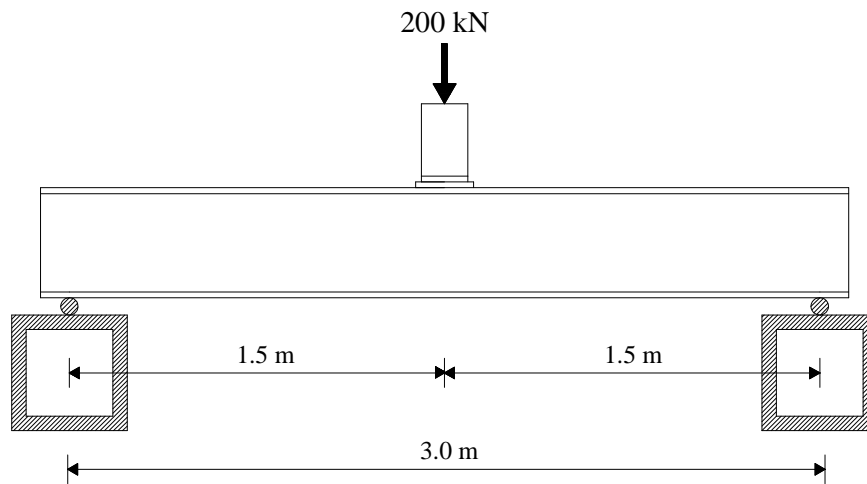


Figure 3.6 Typical cross section of beam with 3-m for NPI-260

The feasible designs presented in Table 3.7 are obtained after 900 iterations. It is noticed that this design vector remained the same even though the design cycles are continued to reach 10,000 which was the pre-selected maximum number of iterations. The optimum design of the cellular beam is carried out by the algorithm presented and the optimum results obtained are given in Table

3.8. This design is determined after 10,000 cycles and the minimum weight of the cellular beam is 113.95 kg. Harmony search algorithm selects NPI-260 profile, 7 circular holes and 286mm for the hole diameter. Figure 3.7 demonstrates the design history graph obtained with harmony search algorithm in the optimum design of NPI_240. The optimum shape of the cellular beam for the loading considered is shown in Figure 3.8.

Table 3.7 Feasible designs obtained after 900 iterations by HS algorithms

<i>hms</i>	SSQ (kN)	Section Des.	Diameter (cm)	N. of Holes
1	1.12	10	286	7
2	1.24	11	321	7
3	1.29	11	289	6
4	1.44	12	276	8
5	1.46	12	293	6
6	1.47	12	255	8
7	1.49	12	221	8
8	1.60	13	381	5
9	1.84	14	280	7
10	1.87	14	213	10
11	2.01	15	315	7
12	2.01	15	398	4
13	2.03	15	353	5
14	2.04	15	329	5
15	2.08	15	220	10
16	2.20	16	323	7
17	2.21	16	349	6
18	2.25	16	259	9
19	2.30	16	219	10
20	2.51	17	233	10
21	2.52	17	229	10
22	2.67	18	380	6
23	2.79	18	328	5
24	2.80	18	313	6
25	3.11	19	322	5
26	3.28	20	390	6
27	3.36	20	331	7
28	3.38	20	300	8
29	3.45	20	325	5
30	4.45	22	372	5

Table 3.8 Optimum Design of NPI_260 Cellular beam with 3-m span

Optimum NPI-Section Designations	Hole Diameter (mm)	Total Number of Holes	Maximum Strength Related Ratio	Minimum Weight (kg)
NPI-260	286	7	0.95	113.95

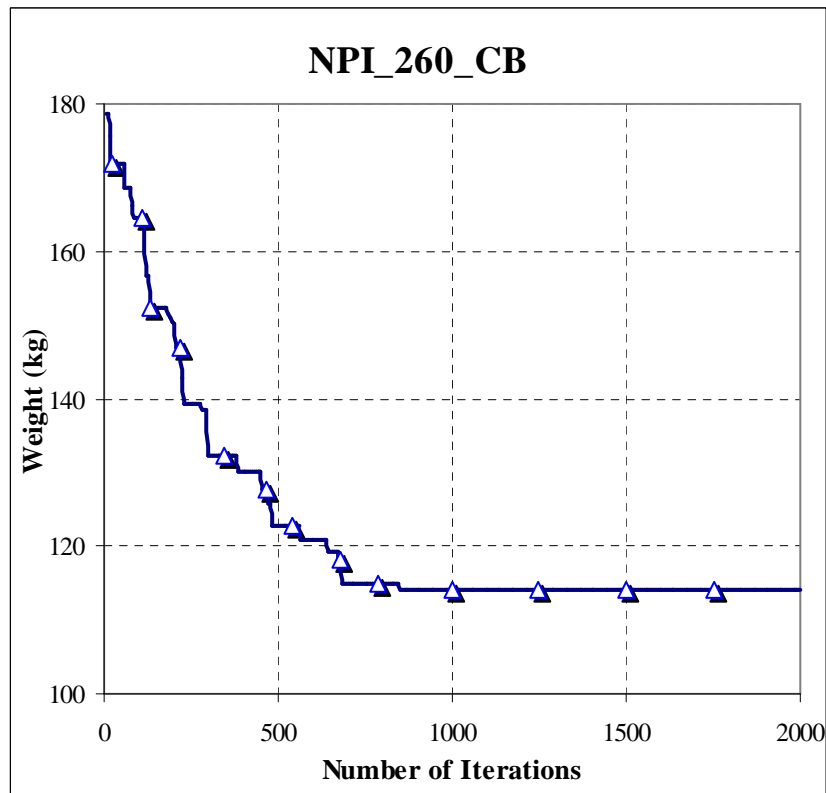


Figure 3.7 The design history graph for NPI_260 cellular beam

NPI 260 Cellular Beam

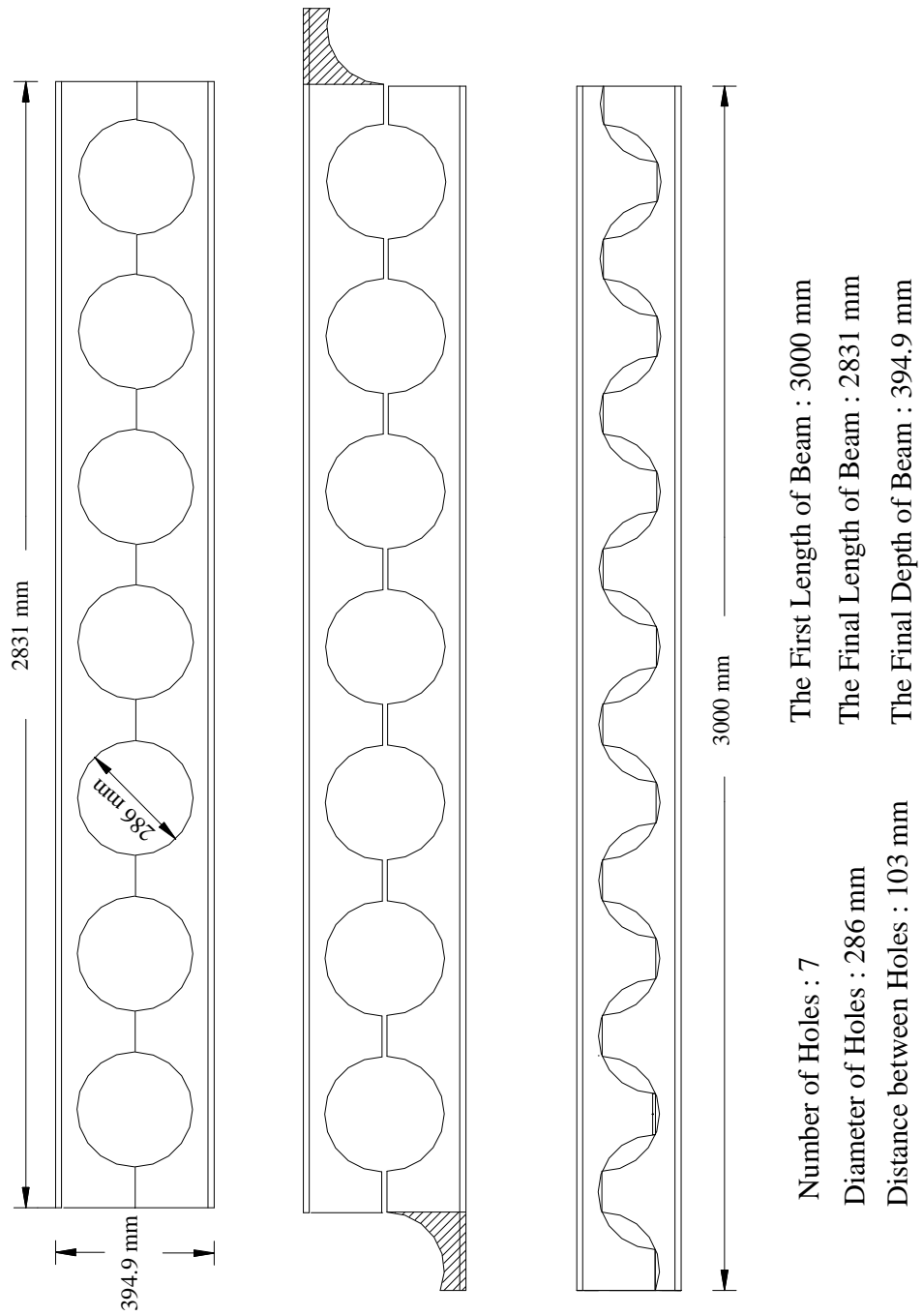


Figure 3.8 Optimum Shape of NPI-260 after 10,000 Iterations

3.3.3 Cellular Beam with NPI-280

Simply supported cellular beams with a span of 3 m are subjected to a concentrated load; live load of 340 kN, as shown in Figure 3.9. The allowable displacement of the beam space under live-load is limited to 9 mm. The modulus of elasticity is taken as 205 kN/mm^2 and the design strength for Grade 50 of steel is 355 kN/mm^2 . For this simply supported beam, harmony memory matrix size (hms) is taken as 40. Harmony memory considering rate ($hmcr$) is selected as 0.9 while pitch-adjusting rate (par) is considered as 0.3 on the basis of the empirical findings by Geem and Lee [37, 41]. The maximum number of searches was set to 10,000 for this example.

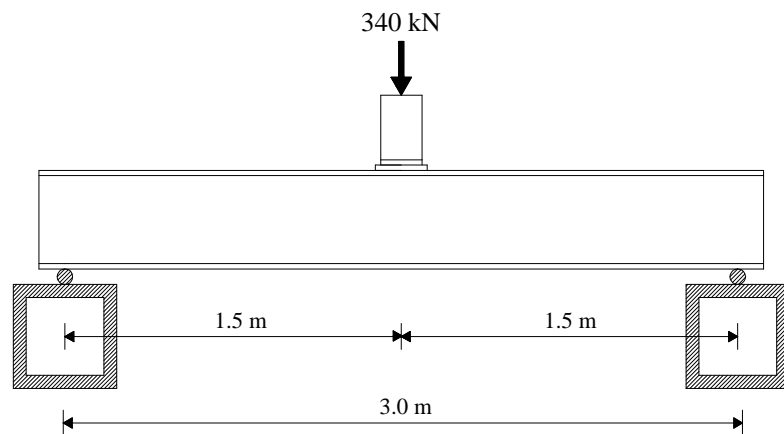


Figure 3.9 Typical cross section of beam with 3-m for NPI-280 .

The feasible designs presented in Table 3.9 are obtained after 1200 iterations. It is noticed that this design vector remained the same even though the design cycles are continued to reach 10,000 which was the pre-selected maximum number of iterations. The optimum design of the cellular beam is carried out by the algorithm presented and the optimum results obtained are given in Table 3.10. This design is determined after 10,000 cycles and the minimum weight of the cellular beam is 132.11 kg. HS algorithm selects NPI-280 profile, 6 circular

holes and 251mm for the hole diameter. Design history graph obtained with harmony search algorithm in the optimum design of NPI_240 cellular beam and optimum shape of the cellular beam for the loading considered is respectively shown in Figure 3.10 and Figure 3.11.

Table 3.9 Feasible designs obtained after 1200 iterations by HS algorithms

HMS	SSQ (kN)	Section Des.	Diameter (cm)	N. of Holes
1	1.30	11	277	6
2	1.48	12	250	7
3	1.48	12	248	7
4	1.60	13	346	6
5	1.60	13	343	6
6	1.61	13	306	7
7	1.64	13	302	6
8	1.79	14	342	6
9	1.80	14	335	6
10	1.82	14	319	6
11	1.84	14	297	6
12	1.84	14	280	7
13	1.88	14	226	8
14	2.01	15	398	4
15	2.07	15	271	6
16	2.10	16	399	6
17	2.10	15	209	10
18	2.13	16	385	6
19	2.17	16	368	6
20	2.22	16	400	4
21	2.22	16	393	4
22	2.43	17	324	7
23	2.44	17	344	6
24	2.47	17	356	5
25	2.47	17	329	6
26	2.51	17	246	9
27	2.53	17	247	8
28	2.65	18	389	6
29	2.78	18	349	5
30	3.03	19	395	5
31	3.05	19	323	7
32	3.11	19	314	5
33	3.11	19	318	6
34	3.24	20	400	6
35	3.71	21	361	6
36	3.73	21	301	8
37	3.74	21	383	4
38	3.74	21	349	6
39	3.75	21	372	5
40	4.30	22	393	6

Table 3.10 Optimum Design of NPI_280 Cellular beam with 3-m span

Optimum NPI-Section Designations	Hole Diameter (mm)	Total Number of Holes	Maximum Strength Related Ratio	Minimum Weight (kg)
NPI-280	277	6	0.97	132.11

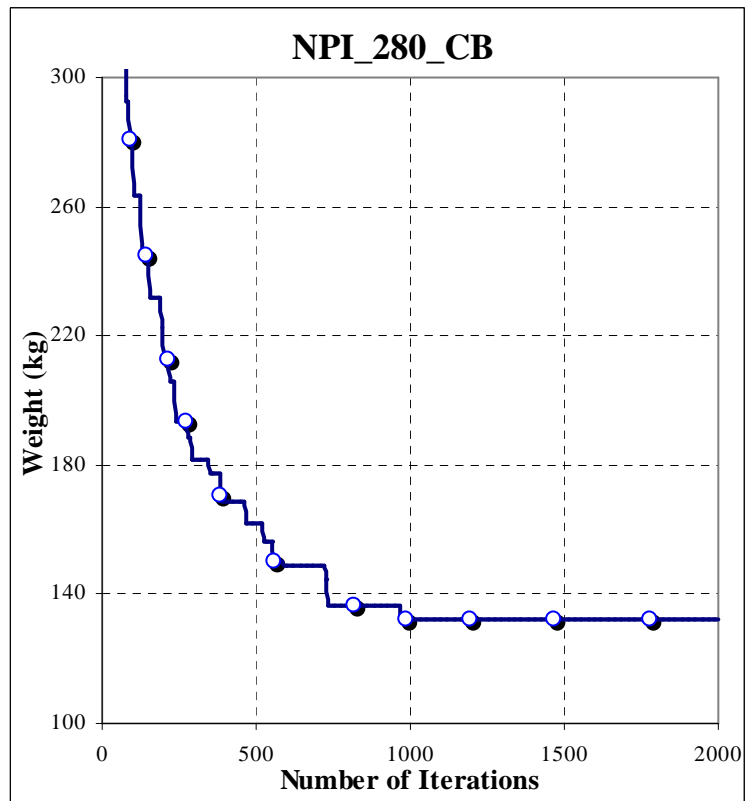


Figure 3.10 The design history graph for NPI_280 cellular beam

NPI 280 Cellular Beam

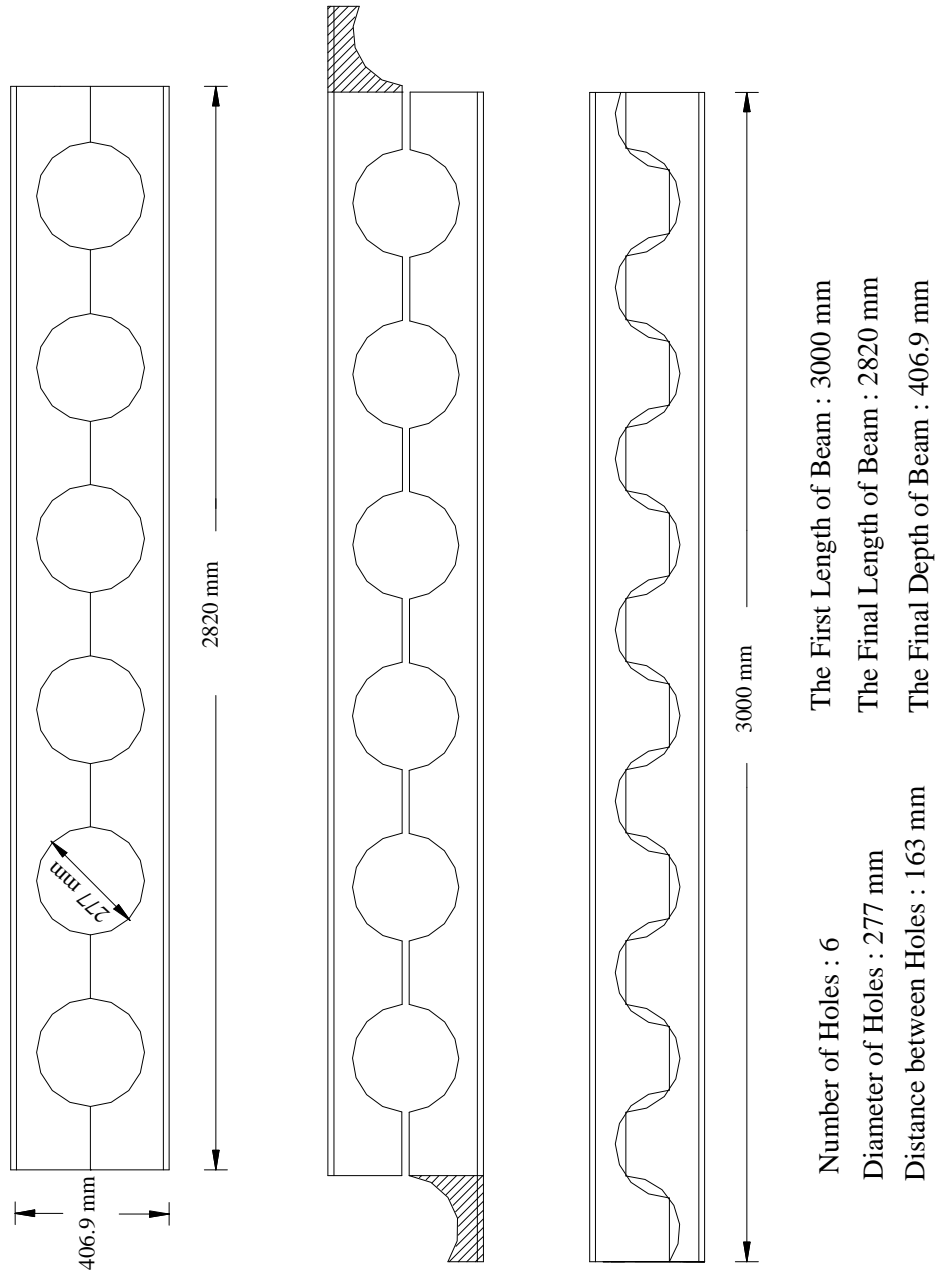


Figure 3.11 Optimum Shape of NPI-280 after 10,000 Iterations

CHAPTER 4

EXPERIMENTAL TESTS ON OPTIMALLY DESIGNED STEEL CELLULAR BEAMS

4.1 Experimental Studies on Steel Cellular Beams

In the experimental part of this dissertation, the ultimate load carrying capacities of optimally designed steel cellular beams are tested in a self reacting frame. The tested cellular beam specimens are designed by using harmony search optimization method as explained in the previous chapter. The tests have been carried out on twelve full-scale non-composite cellular steel beams. There are three different types of **NPI_CB_240**, **NPI_CB_260** and **NPI_CB_280** I-section beams, and four tests have been conducted for each specimen. These optimally designed beams which have preliminary span lengths of 3000 mm are subjected to point load acting at the mid-span.

An illustration of test set up and one of these specimen cellular beams is given in Figure 4.1. Finite element models of each tested specimens are then generated in ANSYS program to perform elastic buckling analysis, predict critical loads and compare FEM results with experimental test results for each tested cellular beam.



Figure 4.1 Cellular Beam in Test Frame

- (a) **Symmetrical non-composite NPI_CB_240 cellular beams:** This cellular beam has been produced on the basis of original NPI_240 beam as a top tee and bottom tee section. Final depth and span of the beam has been established as 355.6 mm and 2846 mm after optimization, respectively.
- (b) **Symmetrical non-composite NPI_CB_260 cellular beams:** This beam has been produced on the basis of hot rolled NPI_260 steel beam as an upper and lower tee section. Final depth and span of beam has been established as 394.9 mm and 2831 mm after optimization, respectively.
- (c) **Symmetrical non-composite NPI_CB_280 cellular beams:** This beam has been produced on the basis of NPI_280 steel beam as a top tee and bottom tee section. Final depth and span of beam has been established as 406.9 mm and 2820 mm after optimization process, respectively.

All steel cellular beam specimens are placed on simple supports at both ends. A pair of lateral supports is provided at the end of each beam end for preventing lateral torsional buckling. The consequence of lateral stability for web expanded beams is defined by Chen and Lui in 1987 [60] as “...if sufficient lateral bracing is not provided to the compression flange, out of plane bending and twisting of the cross section will occur when the applied loads reach a certain limit.”

The simply supported steel cellular beams are tested under the action of a concentrated load. The load is provided by hydraulic jack reacting on the laboratory floor and aligned equally on each side of the beam. The canister type load cell used for the experiments is calibrated before testing procedure took place. To record overall displacements of the cellular beams, three transducers are mounted. Figure 4.2 is a picture showing the test setup and the equipment used to record the experimental data for the flexural loading of steel cellular beams.

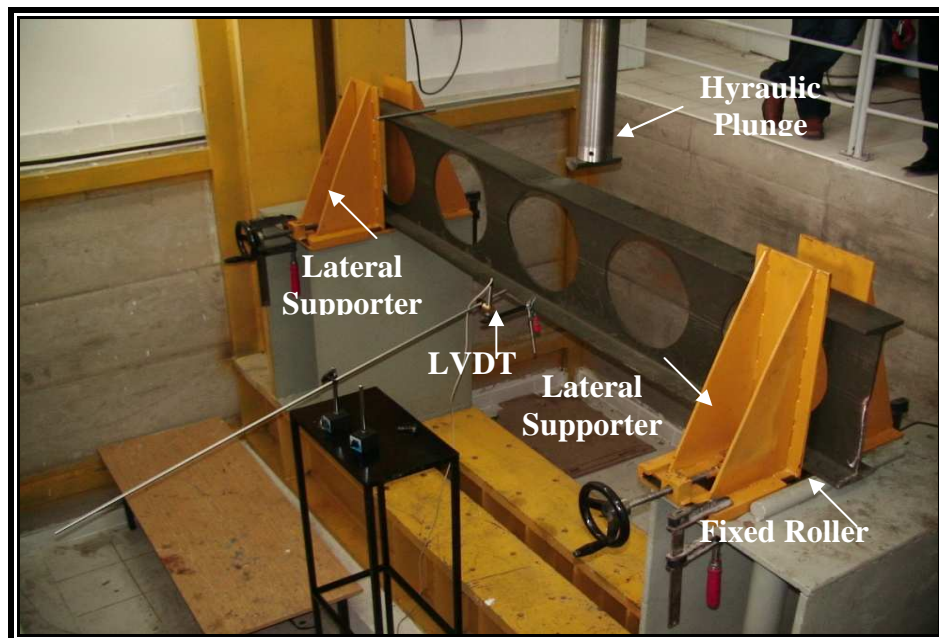


Figure 4.2 Experimental set up and load introduction

4.2 Fabrication of Optimally Designed Cellular Test Beams

Using web-expanded beams together with cellular beams is founded on special use of original hot rolled I-section beams. These web-expanded beams are formed by double cutting two semi-circular sections along their centerline in the web of steel I-beam section along the length of the span. The first cut of the original beam shown in Figure 4.4 generates the top circle of the cell and the second one shown in Figure 4.5 creates the opposite of the top circle. When the cutting processes are completed, two parts of original solid I-beam are then separated, shifted and welded together to obtain a beam of greater depth with halves of circular holes in the steel section. These circular web holes made up of the original rolled I-section beam raise the overall beam depth, moment of inertia and section modulus.

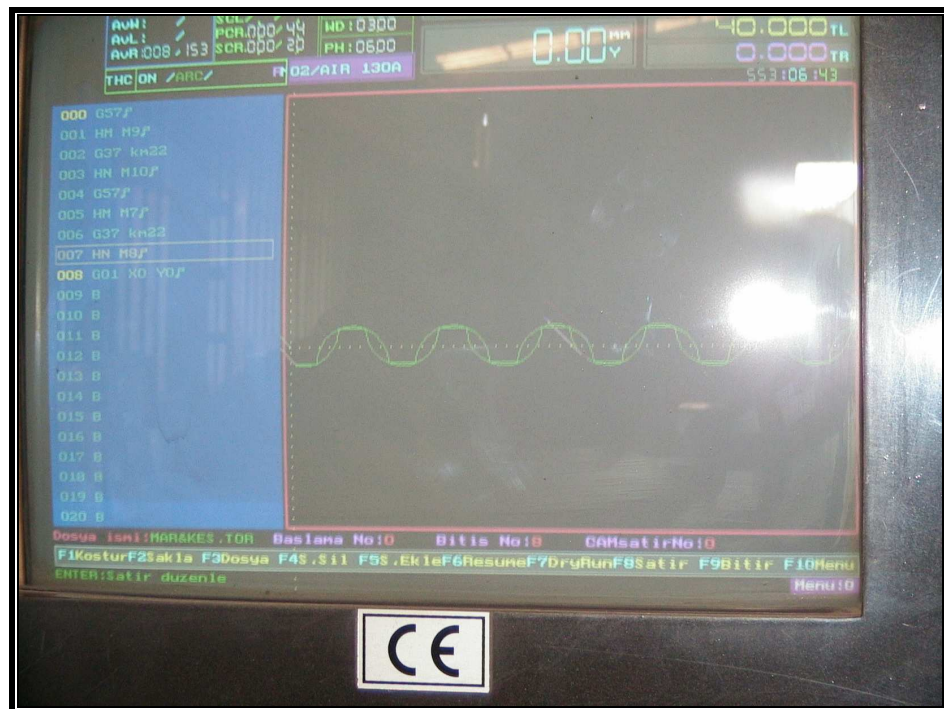


Figure 4.3 The appearance of the computer drawing of the cellular beam

The cutting process is done with CNC (Computer Numerical Control) plasma method to obtain smooth and perfect matching of the holes, shown in Figure 4.3. Figure 4.4 and Figure 4.5 show the first and second flame cutting process of beams, respectively.

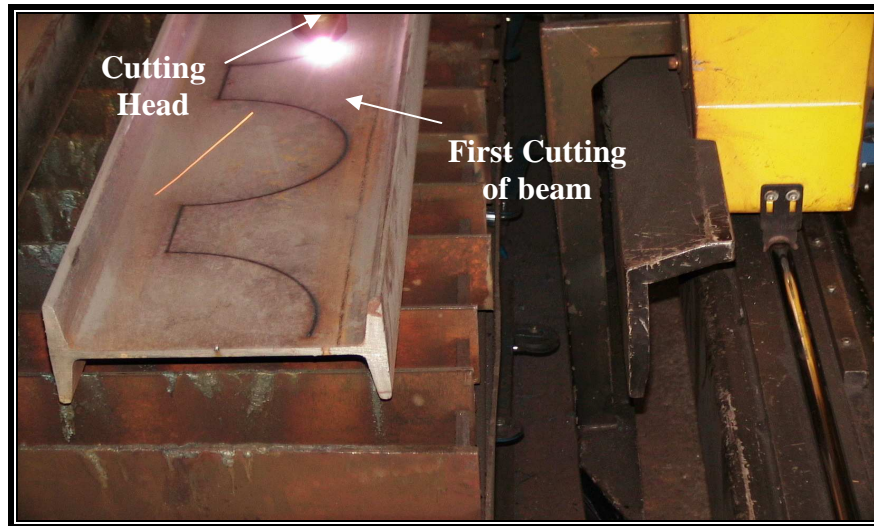


Figure 4.4 The first flame cutting process of original I-section beam

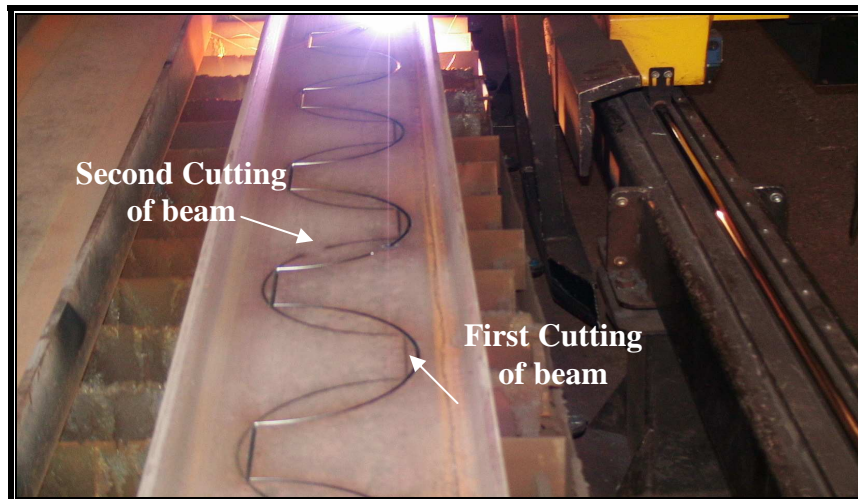


Figure 4.5 The second flame cutting process of original I-section beam

After flame cutting process, the top and bottom tee sections are then separated and welded back together to increase the height of the beam. The separation and assembling of the upper and lower sections are respectively shown in Figure 4.6 and Figure 4.7.

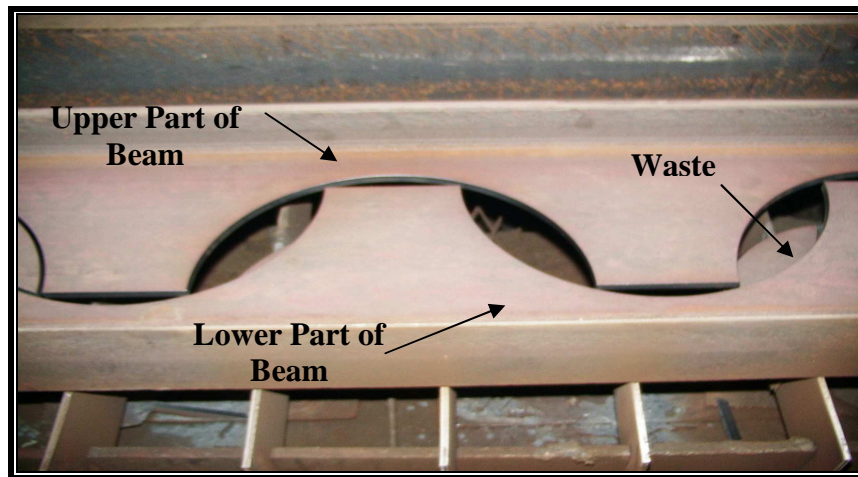


Figure 4.6 The separation of tee sections of the beam



Figure 4.7 The assembling of the tee sections

It can clearly be seen from the Figure 4.7 and Figure 4.8 that the weld line of the cellular beam is limited and weld seams of beam are inspected visually.

During the welding process, to prevent bending of the cellular beam as shown in Figure 4.7 the upper and lower portions are attached to each other. Under the applied load conditions, the cellular beam consists of areas to be welded, as shown below to prevent the break with both the front and the back of the welding operation in the location of the junction



Figure 4.8 The welding of upper and lower tees of the cellular beam

After cutting, separating and re-welding processes, the resulting cellular beam shown in Figure 4.9 becomes much deeper which has larger moment of inertia and sectional modulus than the original I-beam.



Figure 4.9 The appearance of cellular beam after cutting and re-weld process

4.3 Load Cell Calibration

Load cells convert applied force into a recordable signal that comes out of an electronic system as a strain gage based transducer. They are calibrated before starting the testing procedure. On the basis of generated output signal type, load cell designs can be separated to the way they sense weight such as shear, bending, tension and compression. In this study, canister type load cells shown in Figure 4.10 are used for single and multi-weighting applications.



Figure 4.10 Canister Load Cell for heavy duty design

Load cells offer accuracies from within 0.03% to 0.6% full scale and are suitable for almost all industrial applications. Canister type load cell design is ideal for axial compression applications. NT-501A shown in Figure 4.11 is used for the experiments was calibrated in seven steps from *CAL1* to *CAL7* in order before the testing procedure took place [61].



Figure 4.11 NT-501A Indicator for calibration

Calibration Menu:

CAL 1 : Maximum Capacity Set (range : 1-99.999)

(Maximum capacity means maximum weight that the scale can be measured)

CAL 2 : Minimum Division Set (range : 0.001-500)

(The minimum division means the value of one division)

CAL 3 : Setting Weight in Span Calibration

(The setting weight must be within %10 to %100 of maximum weight)

CAL 4 : Zero Calibration

(If zero calibration is done without any error, Success message is displayed)

CAL 5 : Span Calibration

(If span calibration is done without any error, Success message is displayed)

CAL 6 : Check if the calibration is done properly

(If the displayed weight is equal to the setting weight you entered in ***CAL3***)

CAL 7 : Input weight constant calibration after selecting national code

If the minimum division is taken as 100, the variation of setting weight is shown in Table 4.1 and Figure 4.12.

Table 4.1 The variation of setting weight with minimum division set 100

Calibration Number	Applying Load (kg)	Setting Weight (kg)	Accuracies within (%)
1	5000	5000	0,0
2	10000	10000	0,0
3	15000	15100	0,6
4	20000	20100	0,5
5	25000	25100	0,4

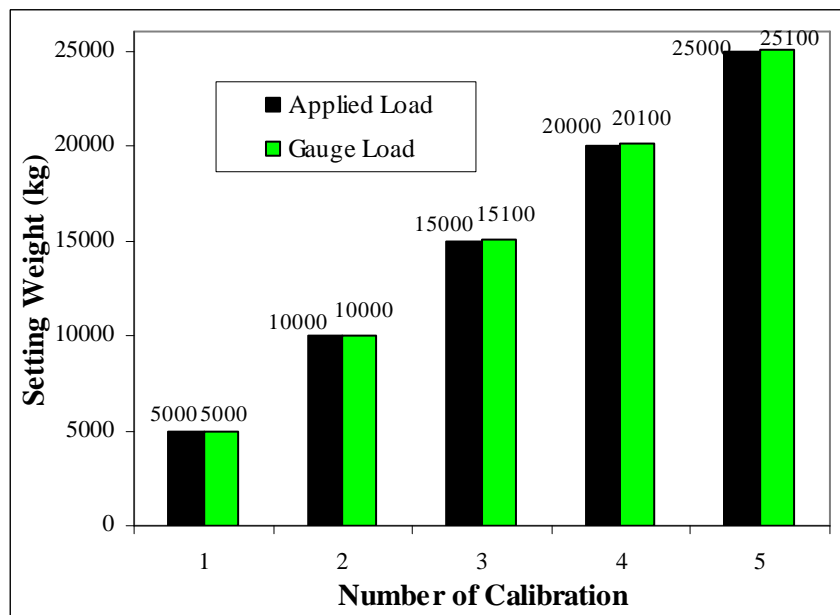


Figure 4.12 The variation of setting weight for minimum division set 100

If the minimum division value is taken as 50, the variation of setting weight is shown in Table 4.2 and Figure 4.13.

Table 4.2 The variation of setting weight with minimum division set 50

Calibration Number	Applying Load (kg)	Setting Weight (kg)	Accuracies within (%)
1	5000	5000	0.0
2	10000	10050	0.5
3	15000	15050	0.3
4	20000	20050	0.2
5	25000	25100	0.4

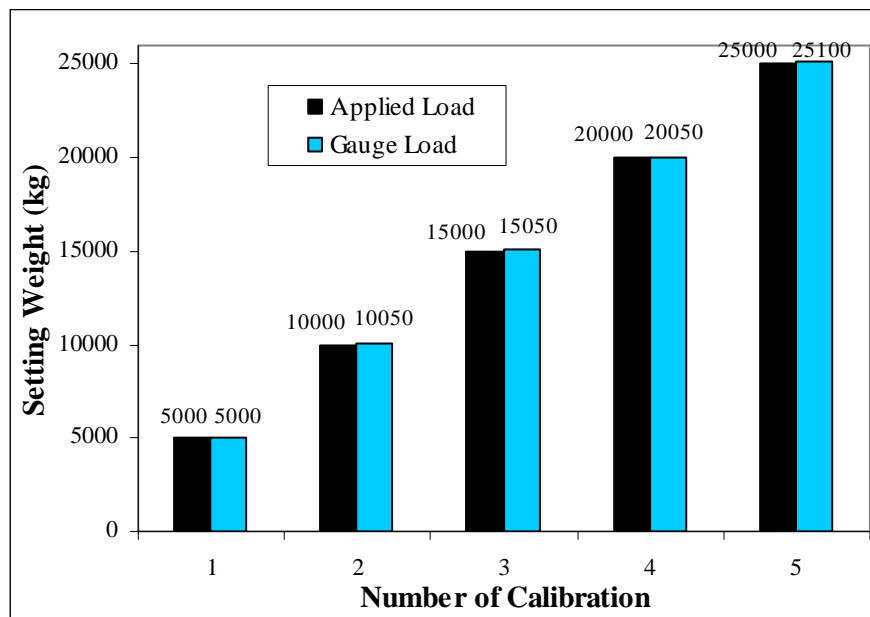


Figure 4.13 The variation of setting weight for minimum division set 50

If the minimum division value is taken as 20, the variation of setting weight is shown in Table 4.3 and Figure 4.14. Table 4.3 also shows that accuracies of load cell is sufficient for this division value and the difference between applied load and setting weight is acceptable to justify for these experimental studies.

Table 4.3 The variation of setting weight with minimum division set 20

Calibration Number	Applied Load (kg)	Setting Weight (kg)	Accuracies within
1	5000	5000	0.0
2	10000	10040	0.4
3	15000	15060	0.4
4	20000	20060	0.3
5	25000	25080	0.3

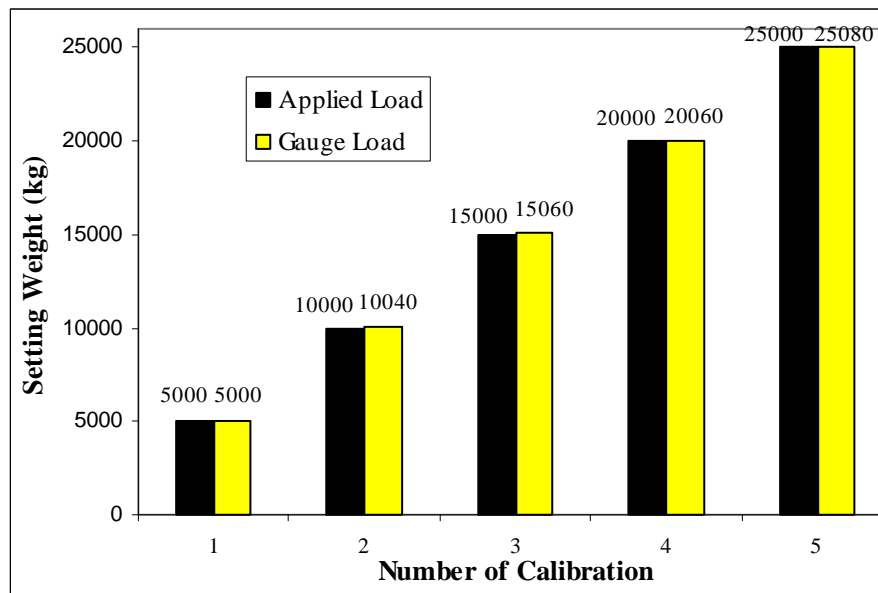
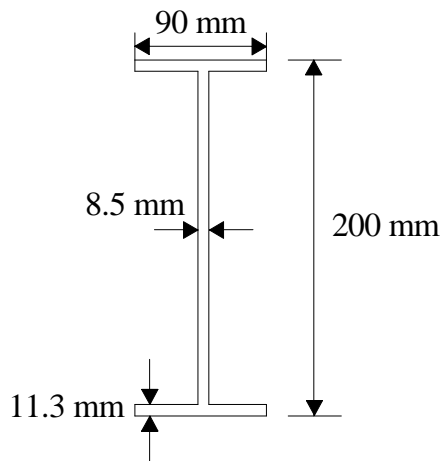


Figure 4.14 The variation of setting weight for minimum division set 20

4.4 Flexural Bending Testing with Hydraulic Power Unit

Before initiating the experimental studies on cellular beams, the simply supported NPI-200 steel beam whose cross sectional properties are given below was tested under the action of a point load in a self-reacting frame in order to verify the accuracies of load and displacement values detected by compression cylinder and transducers.



$$b_f = 90 \text{ mm}, t_w = 7.5 \text{ mm},$$

$$I_x = 2140 \times 10^4 \text{ mm}^4$$

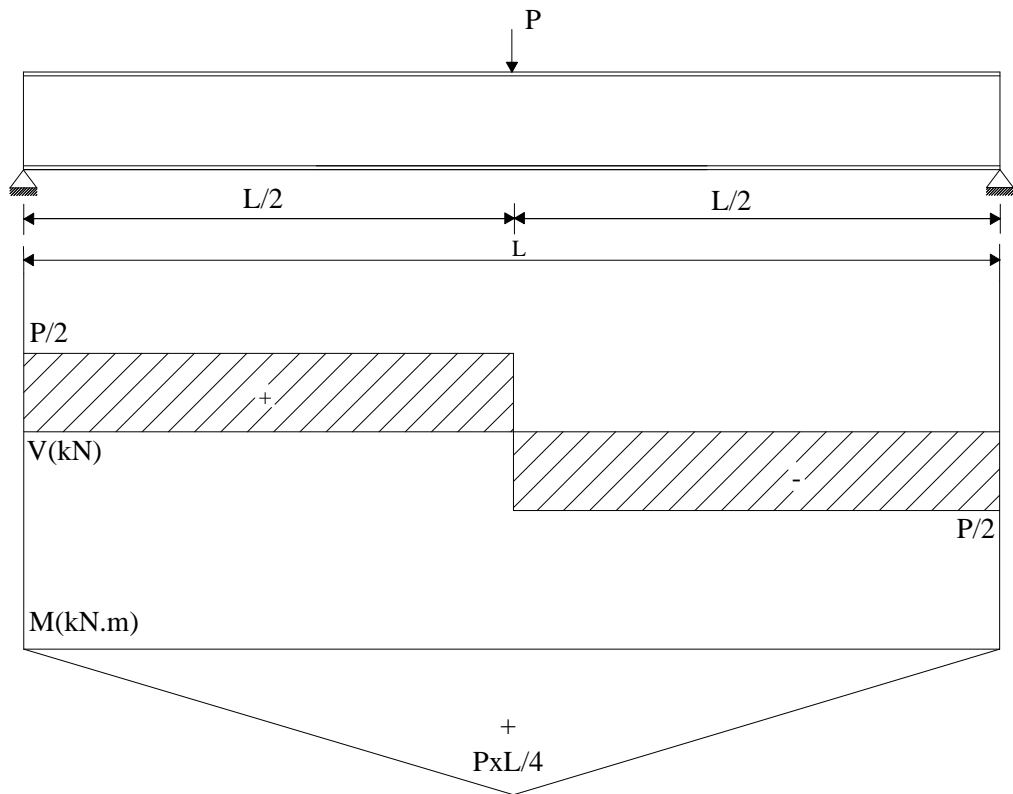
$$Z_x = 214 \times 10^3 \text{ mm}^3$$

$$\text{Unit Weight} = 26.2 \text{ kg/m},$$

$$l = 1700 \text{ mm}, E = 205000 \text{ N/mm}^2$$

$$h = 200 \text{ mm}, t_f = 11.3 \text{ mm},$$

The load is provided by hydraulic pump at least a rate of approximately 1 kN/sec. The capacity of compression cylinder is 1000 kN. Load, vertical displacement and strain values are measured by transducers for each beam in the experimental studies which are transferred to computer automatically. Transducers offer accuracies from within $\pm 0.15\%$ full scale axial loading. The details of NPI-200 steel beam section are given in below.



$$M = \frac{P \times l}{4}, \quad \delta_c = \frac{P \times l^3}{48EI} \quad \text{and} \quad \sigma_y = \frac{P \times l}{4} \times \frac{1}{Z_x}$$

$$P_{cr} = \frac{355 \times 125,000 \times 4}{1700} = 125,882 \text{ N} = 125.882 \text{ kN}$$

$$\delta_c = \frac{P \times l^3}{48EI} = \frac{125,882 \times 1700^3}{48 \times 205000 \times 2140 \times 10^4} = 2.937 \text{ mm} = 0.2937 \text{ cm}$$

Figure 4.15 shows applying concentrated load to NPI-200 beam with a span of 1700 mm. When the 125.882 kN concentrated load was applied this beam, transducer recorded a 2.821mm deflection at mid-span of the beam.



Figure 4.15 NPI-200 beams under point loading in the self-reaction frame

$$\text{Relative error} = \frac{|\delta_{\text{theory}} - \delta_{\text{experimental}}|}{\delta_{\text{theory}}} \times 100 = \frac{|2.937 - 2.821|}{2.937} \times 100 = \%3.94$$

If we compare the theoretical displacement with the experimental result; relative error has been found as %3.94. This error is an acceptable interval for starting the real tests.

4.5 Experimental Test Program of Optimally Designed Cellular Beams

The experimental tests are carried out in the Mechanics Laboratory of Engineering Sciences Department at Middle East Technical University (METU). Three different beam sections are tested under point loading to investigate buckling of web posts and their flexural behaviour. All cellular beams are fabricated by Karatepe Metal Products from NPI sections produced

by Kardemir Steel Company. The dimensions used in manufacturing steel cellular beams are based upon optimization results of the first part of the thesis study.

4.5.1 Test Specimens

The details of the steel cellular beams used from specimen 1 till to specimen 12 are given following subsections. The dimensions of test beams are also demonstrated in the same figures. The main parameters worked in each test are summarized in Table 4.4, Table 4.6 and Table 4.8. All beams used in the tests are fabricated from NPI (N-normal, P-parallel flanges, I-section) beam sections NPI_240, NPI_260 and NPI_280.

4.5.2 Test Arrangement

All cellular beams are provided with simple supports. Lateral supports are provided at the end of each beam to prevent lateral torsional buckling of beams. The simply supported steel cellular beams are to be tested under the action of a concentrated loading. The load is provided by hydraulic jack reacting on the laboratory floor. The load cells used for the experiments are calibrated before the testing procedure took place. To record displacements of the cellular beams, three transducers are mounted to test specimens.

4.5.3 Instrumentation of Tests

Instrumentation consisted of linear variable displacement transducers (LVDT) and load cell. Applied load values are recorded on an AI8B data acquisition

system. The linear variable displacement transducers are manufactured by Tokyo Sokki Kenkyujo Co. The locations of these transducers are demonstrated in Figure 4.16.

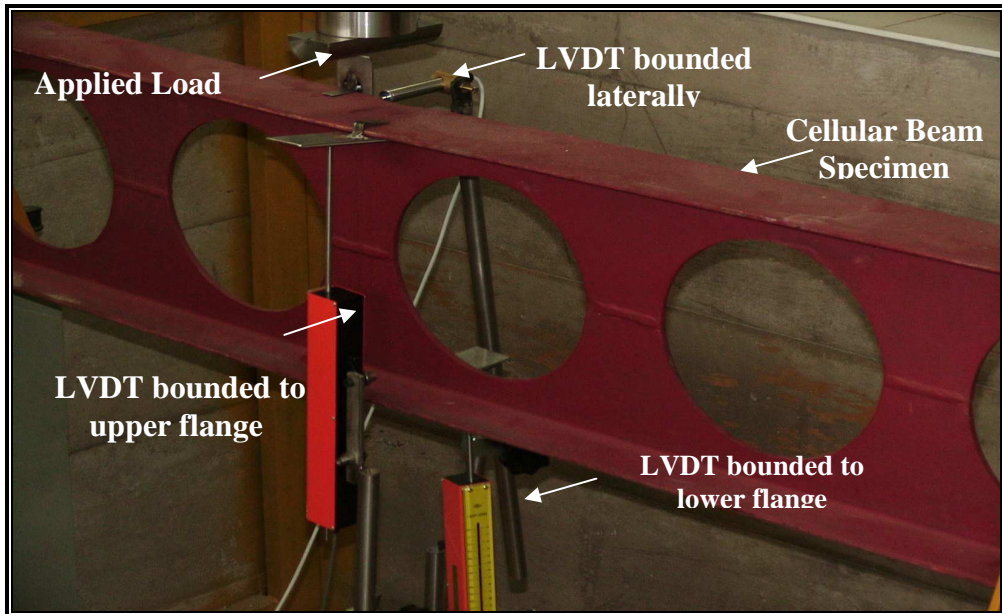


Figure 4.16 Demonstration of transducers on beam

The linear displacement transducers are placed vertically on upper flange and bottom flange of middle of the beams. Besides, one more transducer is placed laterally at upper flange of middle of the beams.

4.5.4 Test Procedure

For each cellular beam, the adjustment of loading rod positions has been applied carefully. The purpose of this action is to prevent the eccentric loading. In all tests, load is applied in order until the beam failed. Increments of load are used initially.

4.5.5 Material Properties of Specimens

All steel beams are fabricated from sections from the same heat. A short length of the NPI section profile is provided for material tensile testing. Three tension test coupons from web of the every NPI beams are tested. Results of the tensile testing are given in Chapter 5 with more detail. The steel material conformed to average yield stress for NPI_240 is 390 MPa, for NPI_260 is 290 MPa, for NPI_280 is 295 MPa.

4.5.6 Flexural Bending Tests of Cellular Beams

The main focus of the experiment is to investigate ultimate carrying load capacity of cellular beams and to observe what type of failure would take place after compression tests on the cellular beams. In the following step, experimental results are compared with numerical calculations.

4.5.6.1 NPI_240 Section Cellular Beam

Four optimally designed cellular beams with eight openings fabricated from NPI_240 sections are tested to find out ultimate load carrying capacities of such beams. These four simply supported test beams which have the same dimensions are subjected to central single concentrated loading shown in the Figure 4.17 below.



Figure 4.17 NPI-240 Cellular Beams with Eight Openings

Dimensional properties of NPI_240 section expanded steel cellular beams and test loads, which are the ultimate carrying loads obtained during experiments, were reported in Table 4.4.

Table 4.4 Dimensional Properties an Ultimate Load of NPI_240

Beam	NPI-240 TEST1	NPI-240 TEST2	NPI-240 TEST3	NPI-240 TEST4
d_g	355.6 mm	355.6 mm	355.6 mm	355.6 mm
b_f	106 mm	106 mm	106 mm	106 mm
t_f	13.1 mm	13.1 mm	13.1 mm	13.1 mm
t_w	8.7 mm	8.7 mm	8.7 mm	8.7 mm
D_0	251 mm	251 mm	251 mm	251 mm
S	94 mm	94 mm	94 mm	94 mm
L	2846 mm	2846 mm	2846 mm	2846 mm
F_u	270.5 kN	273.7 kN	284.1 kN	286.2 kN



Figure 4.18 Lateral torsional buckling on NPI-240_TEST1

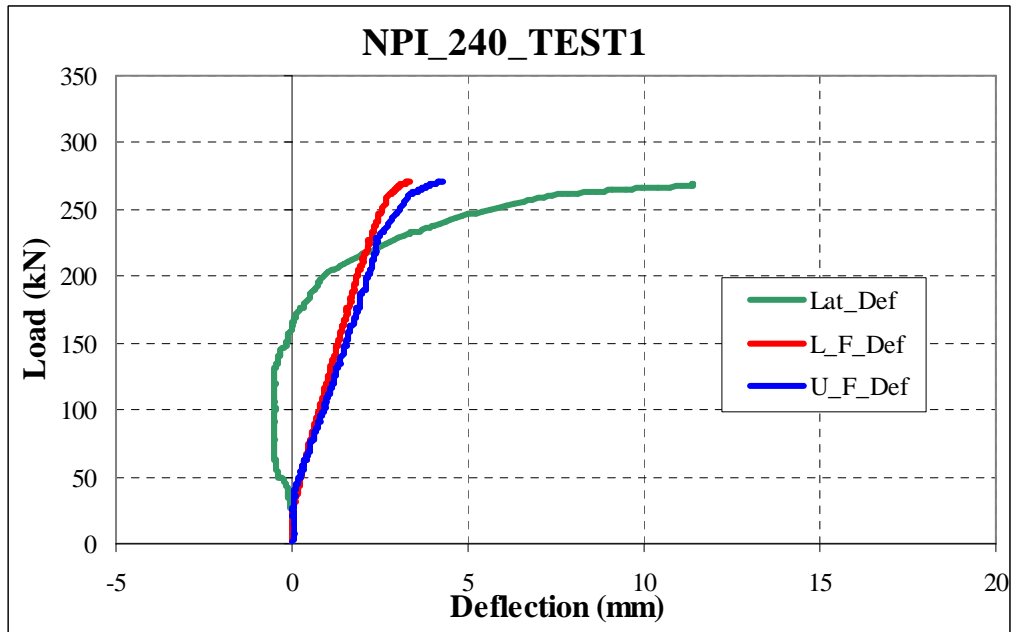


Figure 4.19 Load-Deflection Graphic for NPI-240_TEST1

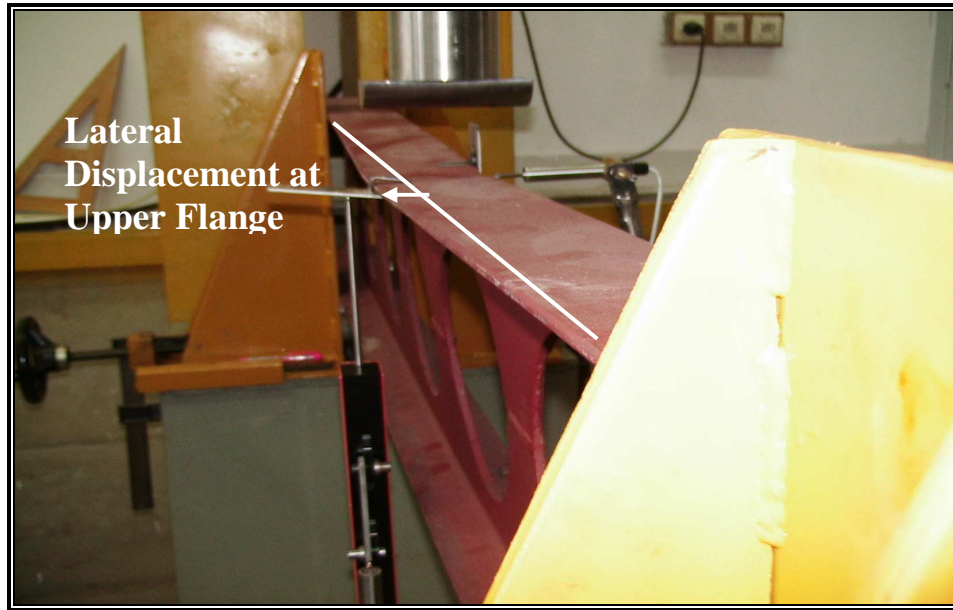


Figure 4.20 Laterally torsional buckling on NPI-240_TEST2

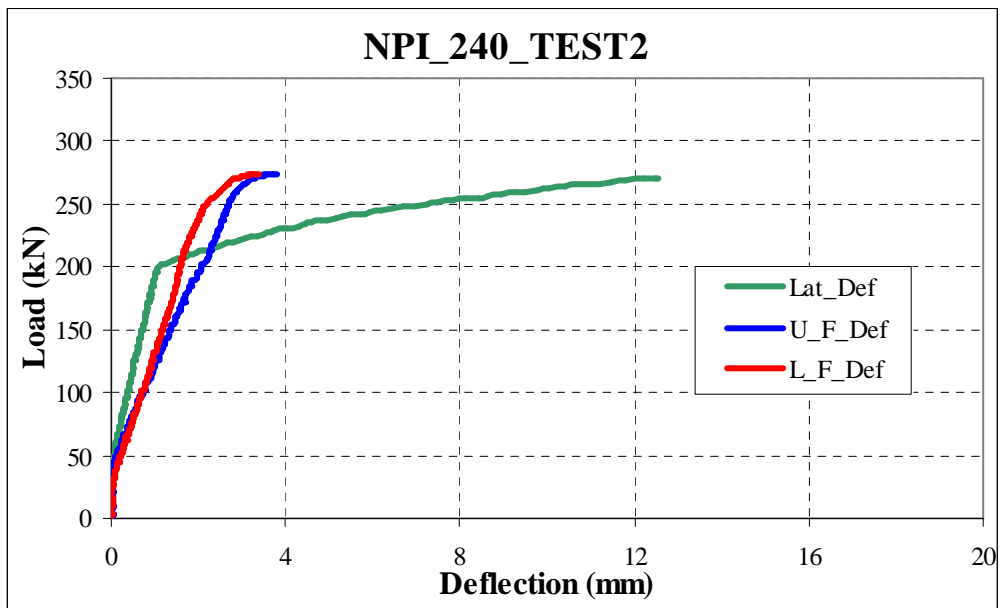


Figure 4.21 Load-Deflection Graphic for NPI-240_TEST2

The results obtained from experimental tests on NPI_240 section beams demonstrate that the first two beams failed from lateral torsional buckling due to a lack of lateral support. These results are illustrated in Figure 4.18 and Figure 4.20. Figure 4.19 and Figure 4.21 evidently show that lateral movements on the middle part of the upper flange of beams are very high in comparison with the vertical displacements on the beams. In Figure 4.19, the vertical deflections for the lower and upper flanges were measured 3.358 mm and 4.286 mm respectively. The horizontally mounted LVDT measured the lateral deflection as 11.375 mm for the first test beam. In Figure 4.21, On the other hand, the vertical deflections for the lower and upper flanges were measured 3.787 mm and 3.386 mm respectively. The horizontally mounted LVDT measured the lateral deflection as 12.512 mm for the second test beam. These results occurred owing to lateral instability of cellular test beams. It was also observed that these two laterally torsional buckled beams have failed respectively under the applied values of 270.5 kN and 273.7 kN. During the optimization process of steel cellular beams according to BS5950 specifications, lateral movement is completely assumed to be blocked. For this purpose, lateral bracing is integrated to the middle part of the test beams to prevent lateral movement along the span on these beams in an experimental study (shown in Figure 4.22).

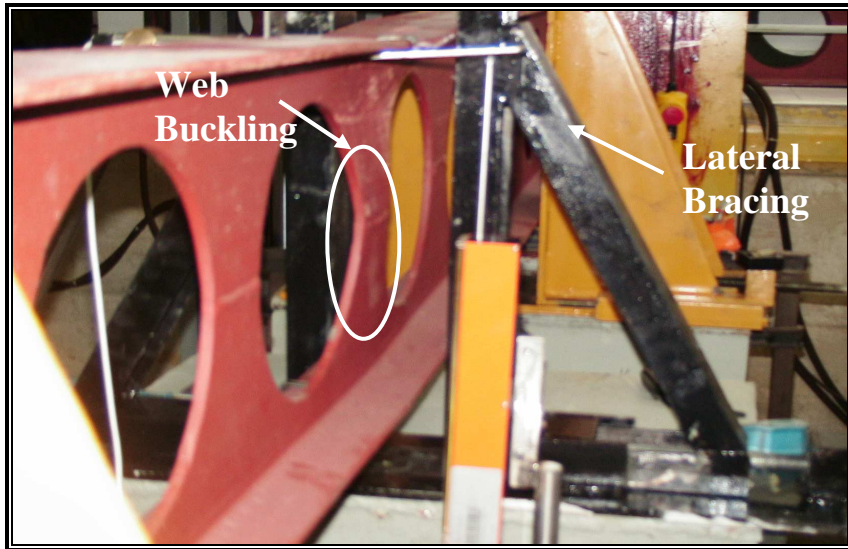


Figure 4.22 Web-post buckling on NPI-240_TEST3

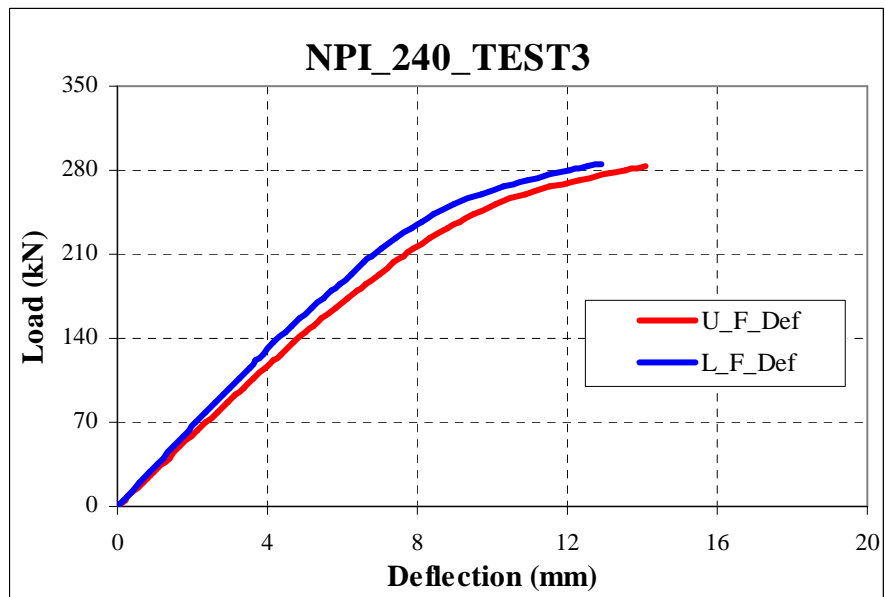


Figure 4.23 Load-Deflection Graphic for NPI-240_TEST3



Figure 4.24 Web-post buckling on NPI-240_TEST4

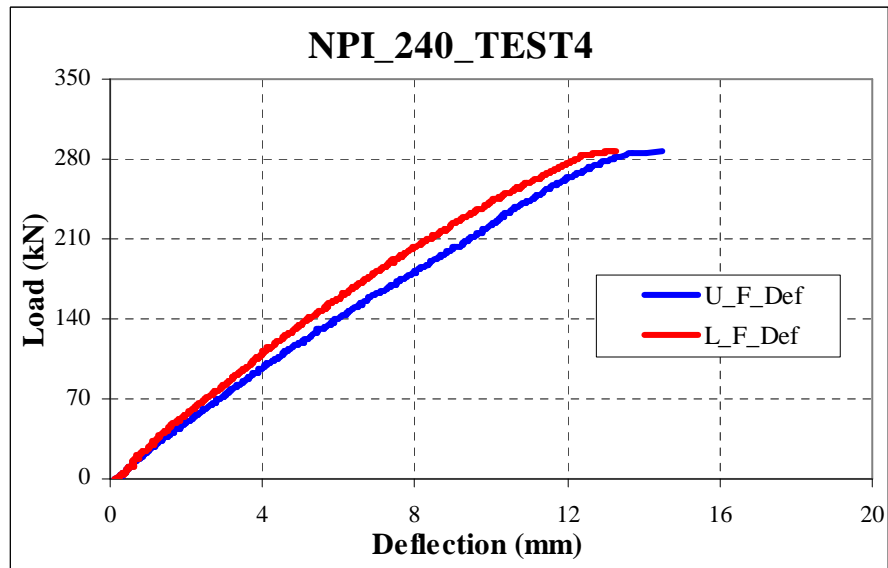


Figure 4.25 Load-Deflection Graphic for NPI-240_TEST4

The results obtained from experimental tests on NPI_240 section beams demonstrate that NPI-240_ TEST3 and NPI-240_ TEST4 beams failed from web buckling. This is illustrated in Figure 4.22 and Figure 4.24. When the beam was laterally supported in the middle with a system, ultimate load capacity has been increased. Vertical displacements on the middle part of the upper and lower flange of beams are respectively shown in Figure 4.23 and Figure 4.25. Upper and lower deflection values of cellular beams are shown in Table 4.5 with more detail. Lateral displacement is not shown in the load-deflection graph for the reason that lateral movement values can be neglected as they are very small. The reason for web buckling is web thickness, the ratio of pitch opening and hole diameter. These two web buckled beams have failed respectively with 284.1 kN and 286.2 kN applied load values shown in Table 4.5. These results demonstrate that the strength of cellular beams increase approximately of 13-14 kN after the lateral supports are placed in the middle part of the beams.

Table 4.5 Ultimate Load Capacities and Failure Modes of NPI_240 Sections

SPECIMENS	NPI-240 TEST1	NPI-240 TEST2	NPI-240 TEST3	NPI-240 TEST4
Ultimate Loads	270.5 kN	273.7 kN	284.1 kN	286.2 kN
Upper Flange Deflection (U_F_Def)	4.286 mm	3.787 mm	13.892 mm	14.146 mm
Lower Flange Deflection (L_F_Def)	3.358 mm	3.386 mm	12.986 mm	13.195 mm
Lateral Deflection (Lat_Def)	11.375 mm	12.512 mm	2.468 mm	2.131 mm
Failure Type	Lateral Torsional Buckling	Lateral Torsional Buckling	Web-Post Buckling	Web-Post Buckling

4.5.6.2 NPI_260 Section Cellular Beams

In the second experimental tests of this section, four cellular beams with seven openings fabricated from NPI_260 beam sections were tested to determine their ultimate load carrying capacity. Simple supports and a central single point load were used for all four specimens. Dimensional properties of NPI_260 profile sections and the ultimate loads at which beams lost their load carrying ability during experiments are illustrated in Table 4.6.

Table 4.6 Dimensional Properties and Ultimate Load of NPI_260

Beam	NPI-260 TEST1	NPI-260 TEST2	NPI-260 TEST3	NPI-260 TEST4
d_g	394.5 mm	394.5 mm	394.5 mm	394.5 mm
b_f	113 mm	113 mm	113 mm	113 mm
t_f	14.1 mm	14.1 mm	14.1 mm	14.1 mm
t_w	9.4 mm	9.4 mm	9.4 mm	9.4 mm
D₀	286 mm	286 mm	286 mm	286 mm
S	103 mm	103 mm	103 mm	103 mm
L	2831 mm	2831 mm	2831 mm	2831 mm
F_u	216.9 kN	214.9 kN	211.7 kN	224.4 kN

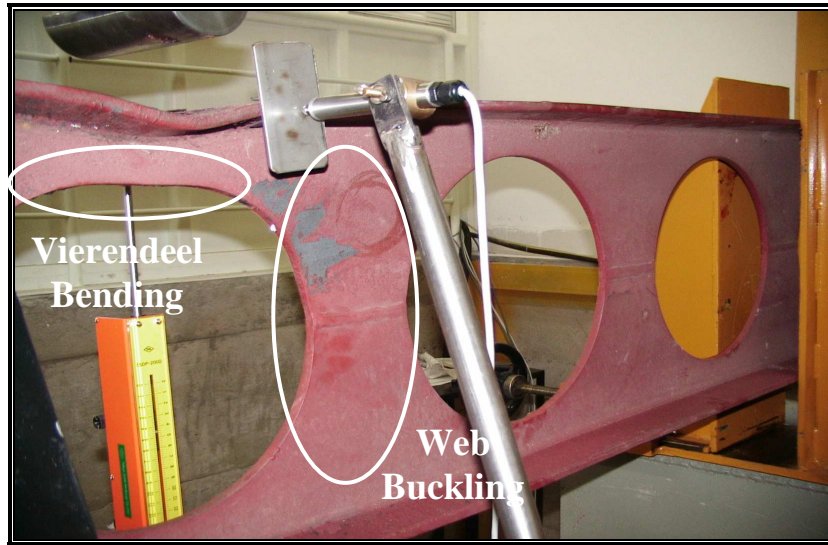


Figure 4.26 Vierendeel Bending and Web Buckling on NPI-260_TEST1

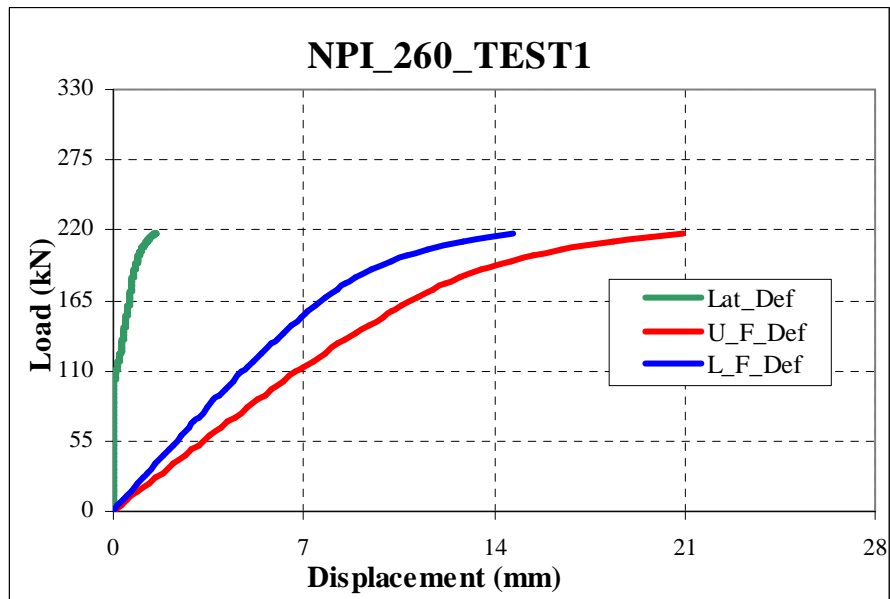


Figure 4.27 Load-Deflection Diagrams for NPI-260_TEST1

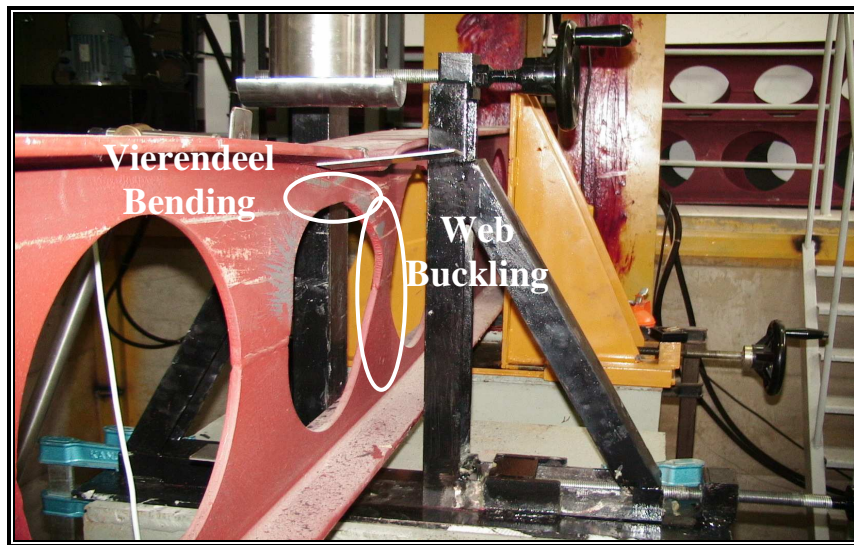


Figure 4.28 Vierendeel Bending and Web Buckling on NPI-260_ TEST2

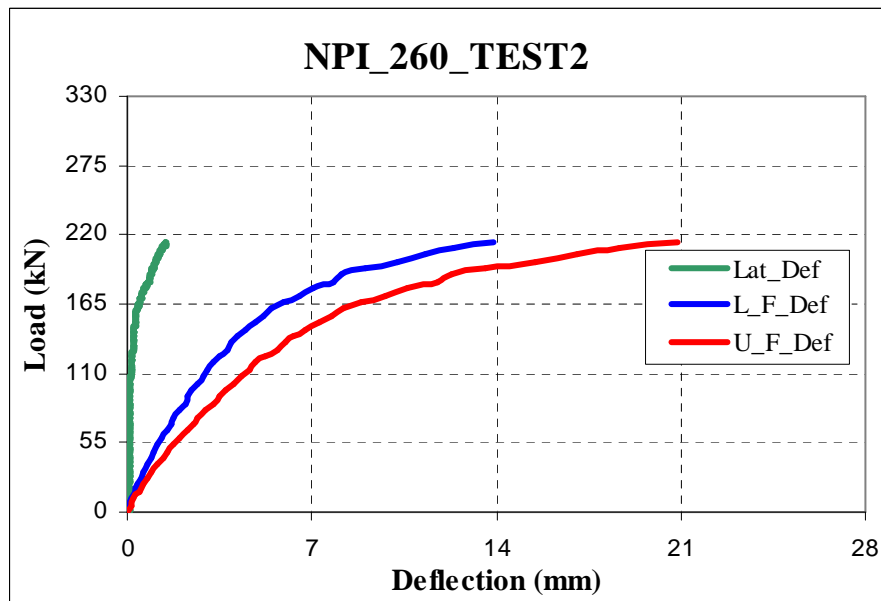


Figure 4.29 Load-Deflection Diagrams for NPI-260_ TEST2

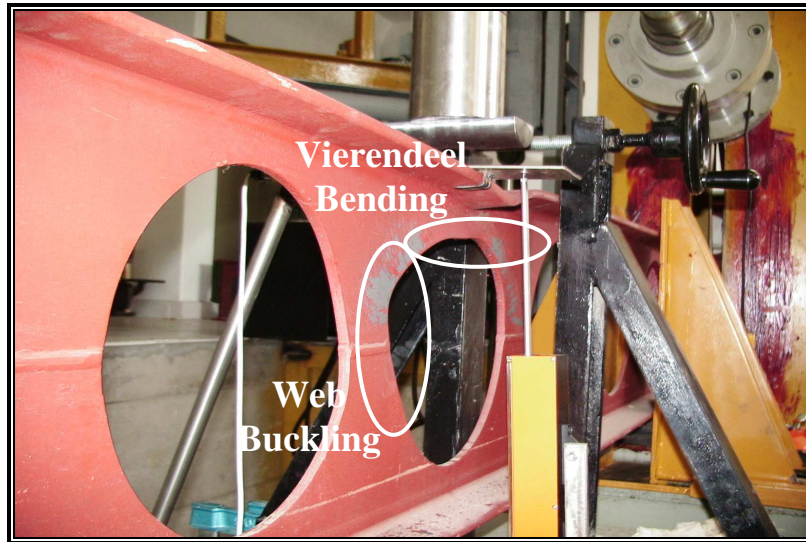


Figure 4.30 Vierendeel Bending and Web Buckling on NPI-260_TEST3

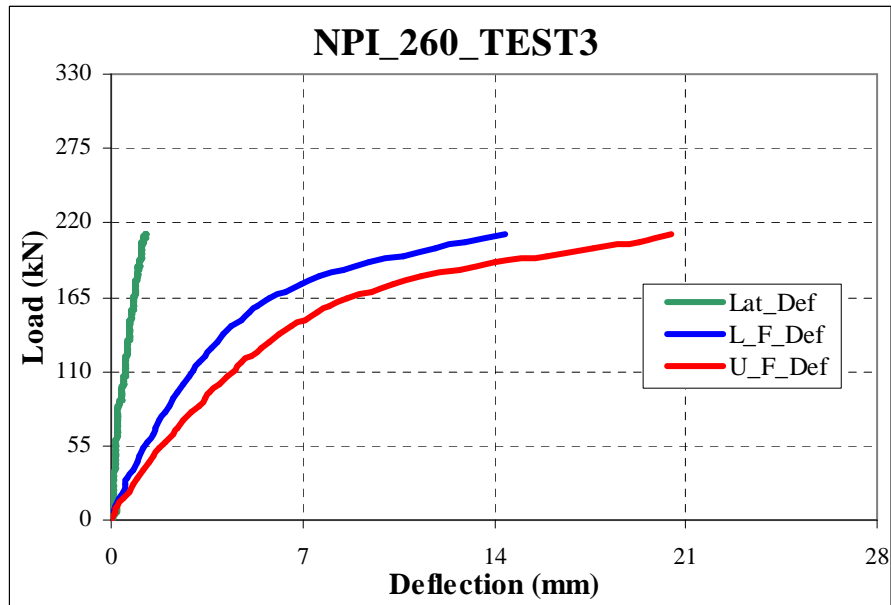


Figure 4.31 Load-Deflection Diagrams for NPI-260_TEST3

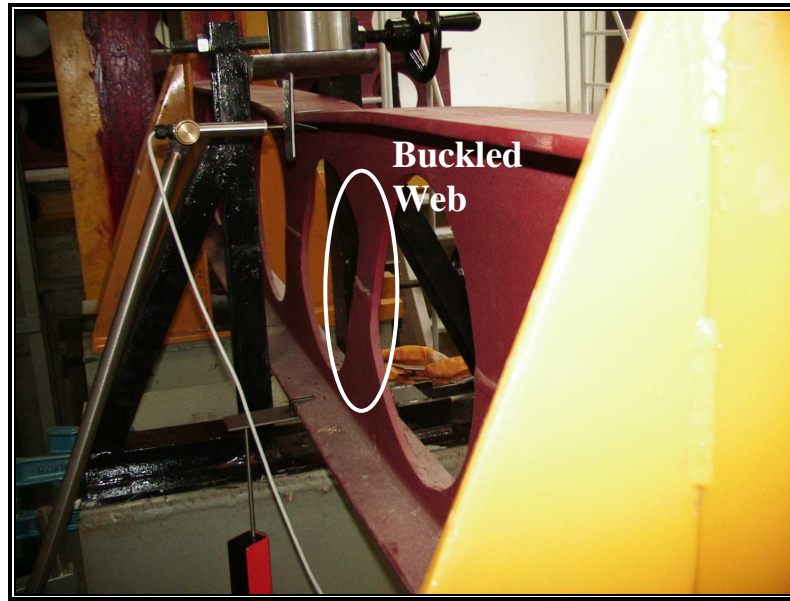


Figure 4.32 Vierendeel Bending and Web Buckling on NPI-26 0_TEST4

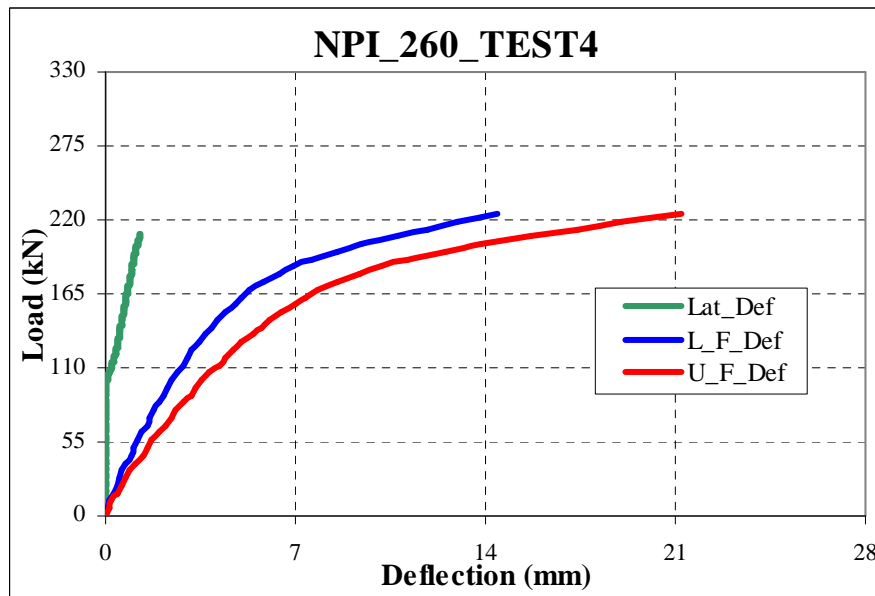


Figure 4.33 Load-Deflection Diagrams for NPI-260_TEST4

The results obtained from experimental tests on NPI_260 section beams demonstrate that all of the beams failed from web buckling and Vierendeel bending as revealed in Figures 4.26, 4.28, 4.30 and 4.32. The flexural capacity of the upper and lower tees under bending is critical. Because the load applies above the holes similar to this NPI_260 beams case, Vierendeel bending has occurred on the beams in addition to web buckling. Vertical displacements in the middle part of the upper and lower flange of beams and lateral movements are respectively shown in Figures 4.27, 4.29, 4.31 and 4.33. It was also observed that these four buckled steel cellular beams have failed respectively under the applied values 216.1 kN, 214.9 kN, 211.7 kN and 224.4 kN. Besides the measured ultimate loads, deflection values and failure types are illustrated in Table 4.7.

Table 4.7 Ultimate Load Capacities and Failure Modes of NPI_260 Sections

SPECIMENS	NPI-260 TEST1	NPI-260 TEST2	NPI-260 TEST3	NPI-260 TEST4
Ultimate Loads	216.9 kN	214.9 kN	211.7 kN	224.4 kN
Upper Flange Deflection (U_F_Def)	20.976 mm	20.863 mm	20.494 mm	21.238 mm
Lower Flange Deflection (L_F_Def)	14.181 mm	13.846 mm	13.663 mm	14.429 mm
Lateral Deflection (Lat_Def)	1.576 mm	1.405 mm	1.223 mm	1.281 mm
Failure Type	Vierendeel Bending and Web buckling	Vierendeel Bending and Web buckling	Vierendeel Bending and Web buckling	Vierendeel Bending and Web buckling

4.5.6.3 NPI_280 Section Cellular Beams

In the last part of the experimental study, four cellular beams with six openings fabricated from NPI_280 sections were tested to detect ultimate load carrying capacity of these beams. Simple supports and a central single point load were used for all four specimens as with other tests. Dimensional properties and values of NPI_280 profile section beams and ultimate test loads were reported as the ultimate loads obtained during experiments demonstrated in Table 4.8.

Table 4.8 Dimensional Properties an Ultimate Load of NPI_280

Beam	NPI-280_A	NPI-280_B	NPI-280_C	NPI-280_D
d_g	406.9 mm	406.9 mm	406.9 mm	406.9 mm
b_f	119 mm	119 mm	119 mm	119 mm
t_f	15.2 mm	15.2 mm	15.2 mm	15.2 mm
t_w	10.1 mm	10.1 mm	10.1 mm	10.1 mm
D₀	271 mm	271 mm	271 mm	271 mm
S	163 mm	163 mm	163 mm	163 mm
L	2820 mm	2820 mm	2820 mm	2820 mm
F_u	377.6 kN	384.2 kN	372.4 kN	368.9 kN

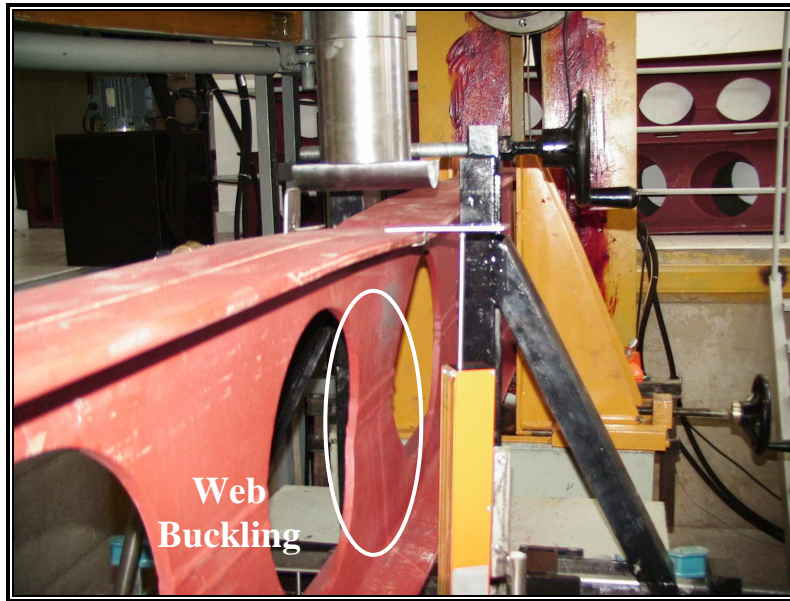


Figure 4.34 Web buckling on NPI-280_TEST1

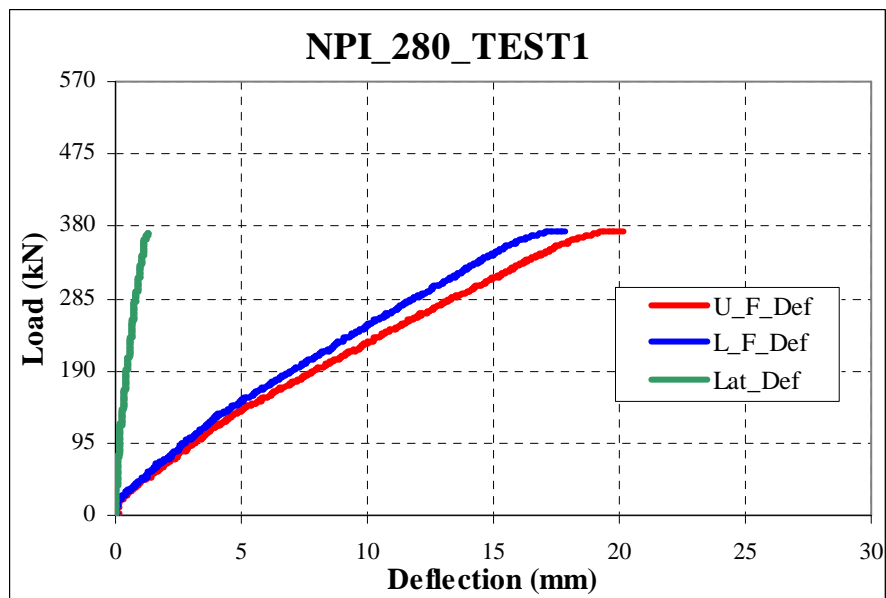


Figure 4.35 Load-Deflection Graphs for NPI-280_TEST1

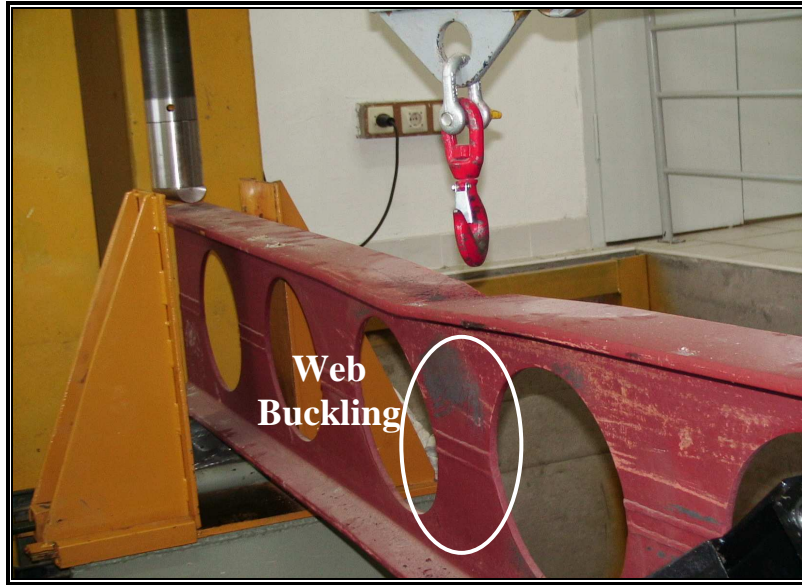


Figure 4.36 Web buckling on NPI-280_TEST2

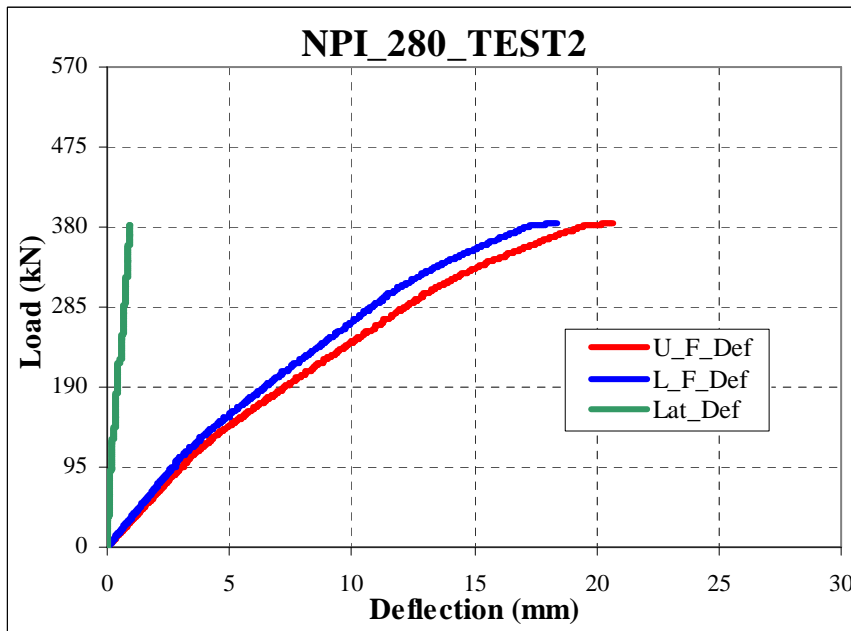


Figure 4.37 Load-Deflection Graphs for NPI-280_TEST2

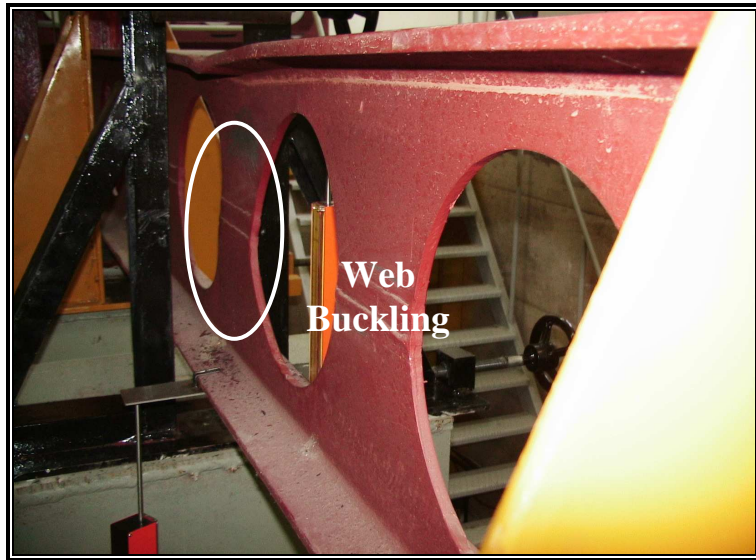


Figure 4.38 Web buckling on NPI-280_TEST3

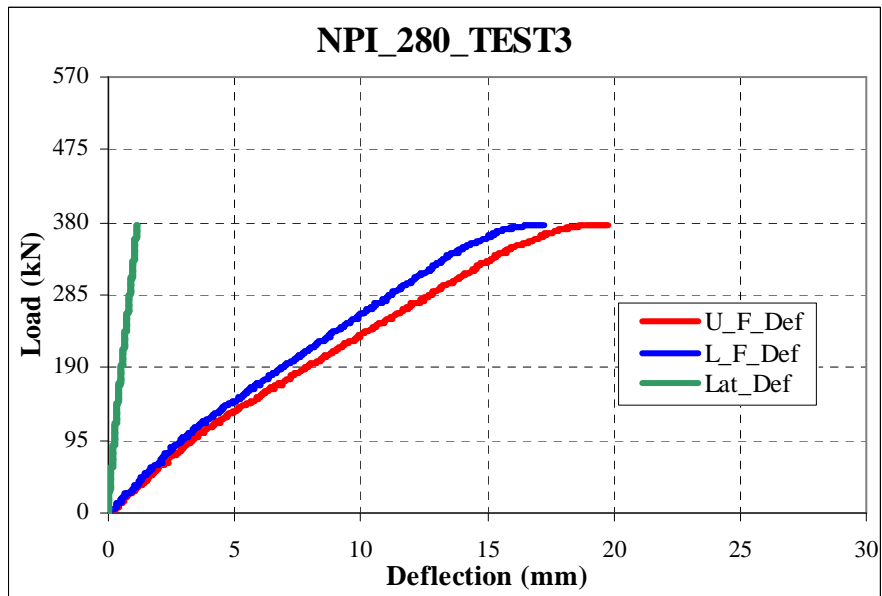


Figure 4.39 Load-Deflection Graphs for NPI-280_TEST3

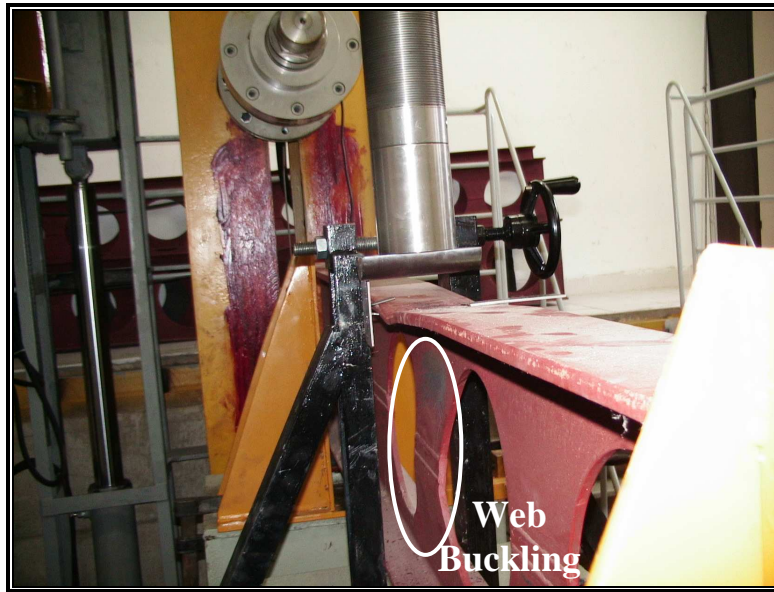


Figure 4.40 Web buckling on NPI-280_TEST4

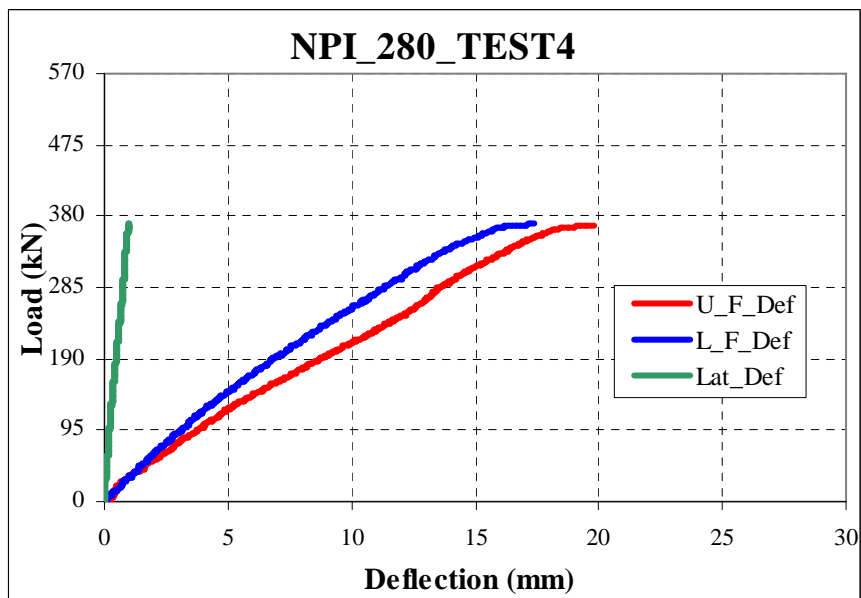


Figure 4.41 Load-Deflection Graphs for NPI-280_TEST4

The results obtained from experimental tests on NPI_280 section beams demonstrate that all of the beams failed from web-post buckling as exposed in Figures 4.34, 4.36, 4.38 and 4.40. The failure of these NPI_280 steel cellular beams under directly applied concentrated loading over a web-post is defined as web-post buckling. One of the reasons for this type of failure to happen is web geometries of these expanded beams. Another reason of web buckling is horizontal shear in the web-post of these tested beams due to double curvature bending over the depth of the web-post. The first inclined edge of the opening is stressed in tension and the other edge of the hole in compression, all of which results in a twisting effect of the web post along their depth. Vertical displacements on the middle part of the upper and lower flange of beams and lateral movements are respectively shown in Figures 4.35, 4.37, 4.39 and 4.41. Ultimate loads and measured deflection values under these loads are respectively shown in Table 4.9.

Table 4.9 Ultimate Load Capacities and Failure Modes of NPI_280 Sections

SPECIMENS	NPI-280 TEST1	NPI-280 TEST2	NPI-280 TEST3	NPI-280 TEST4
Ultimate Loads	377.6 kN	384.2 kN	372.4 kN	368.9 kN
Upper Flange Deflection (U_F_Def)	20.181 mm	20.694 mm	19.805 mm	19.891 mm
Lower Flange Deflection (L_F_Def)	17.878 mm	18.363 mm	17.384 mm	17.105 mm
Lateral Deflection (Lat_Def)	1.308 mm	0.903 mm	1.129 mm	0.997 mm
Failure Type	Web-post buckling	Web-post buckling	Web-post buckling	Web-post buckling

CHAPTER 5

TENSILE TESTS ON OPTIMALLY DESIGNED STEEL CELLULAR BEAM SPECIMENS

Tensile tests were performed to define the material characteristics of steel profiles from which cellular beam are produced. The material characteristics cover the yield strength, ultimate strength and modulus of elasticity of the steel. For this purpose coupons are cut from steel beam sections and tensile test are applied these coupons in the testing machine to find their strength values and the amount of elongation. Although all mechanical properties of beam specimens can be defined from tensile coupon tests, the main purpose of this device is to find out the relationship between the average normal stress and strain values.

5.1 Sample Requirements

Tensile tests on steel sections are conducted on standard shaped test specimens. These specially prepared beam coupons can be cut both in the form of cylinder or flat samples. In order to produce repeatable results and observe with standard test method requirements, steel beam coupons cut from cellular beams should have a specific ratio of length to width or diameter in the test area.

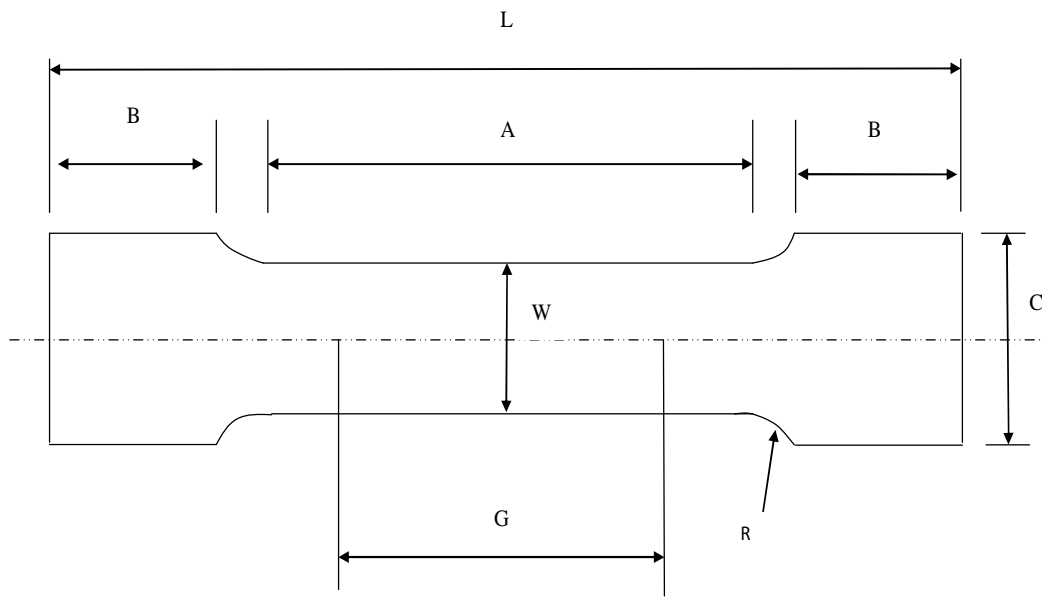


Figure 5.1 Standard dimensions for tensile test specimen

American Society for Testing and Materials (ASTM) E 8M-04 is applied in the standard tensile test of rectangular test specimen [62]. This process is called “*Standard Test Methods for Tension Testing of Metallic Materials*”. The notations for rectangular specimens and their dimensions are demonstrated respectively in Figure 5.1 and Table 5.1.

According to ASTM standard; recommended dimensions for rectangular test specimens are presented in the table next page. In some cases, specified in the NOTE-5 of *ASTM standard*, there should be a parallelism between the sections in terms of width. That is to say, the width of the reduced section should not be smaller than the width of tested material. If the width of the standard or sub size coupon specimens (W) is less than values given in the Table 5.1, the sides can be taken as parallel throughout the length of the specimen.

Table 5.1 Dimensions for standart tension test specimens

	Standard Specimens		Sub Size Specimen	
	Plate Type, 40-mm Wide			
	200-mm Gauge Length	50-mm Gauge Length	12.5-mm Wide	6-mm Wide
“G” Gauge Length	200±0.25	50±0.10	-	-
“W” Width	40+3	40+3	12.5±0.25	6.25±0.05
“R” Radius of fillet	13	13	13	6
“L” Overall length	450	200	200	100
“A” Length of reduced section	225	60	60	32
“B” Length of grip section	75	50	50	32
“C” Width of grip section	50	50	20	10

In this dissertation study, test specimens are cut from NPI-240, NPI-260 and NPI-280 steel cellular beams. Due to web geometry of these profiles, rectangular test specimens have taken according to ASTM international standards organization *NOTE-5*.

Rectangular test specimens cut from within the NPI profiles using computer numerical control method (CNC). This method is usually used for complex and intricately shaped part fabrication can be performed with greater accuracy and faster turnover rates. Cutting process of test specimens from cellular beams using CNC method are shown in Figure 5.2.

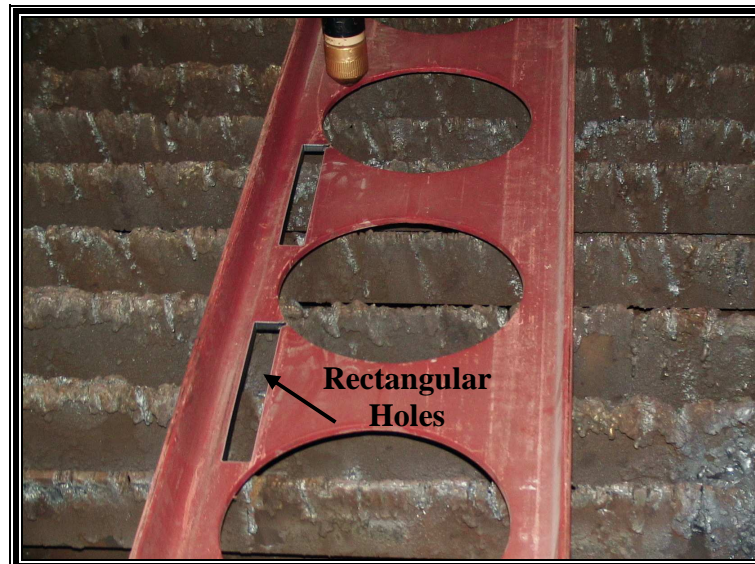
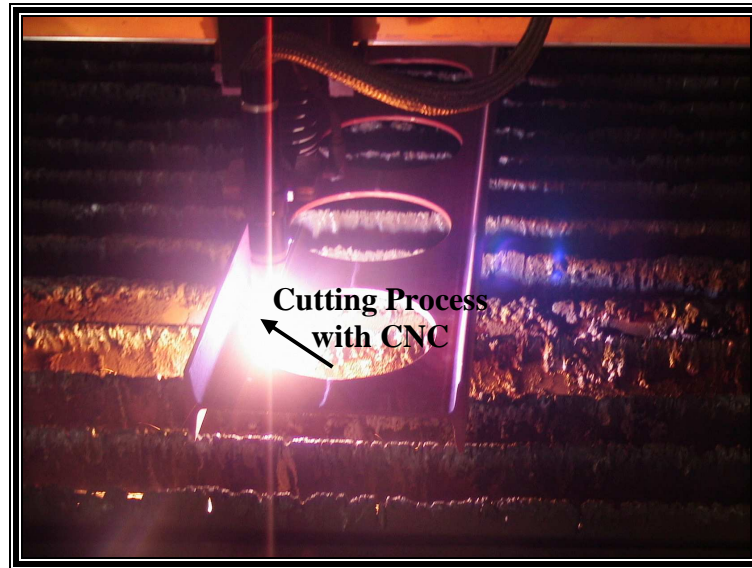


Figure 5.2 Cutting process of standart test specimen with CNC method

Test specimens shown in Figure 5.3 are rectangular sections of 200 mm total length, 20 mm width and a gage length of 100 mm of steel profiles.

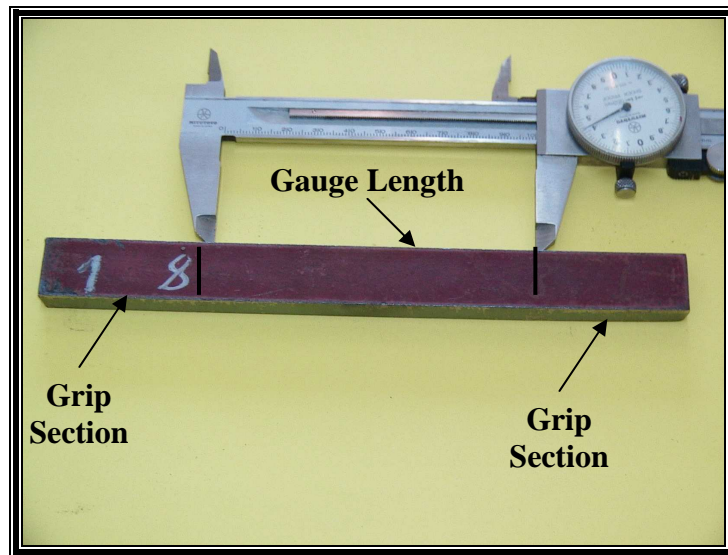


Figure 5.3 Standart tension test specimen from NPI profiles

The notations for rectangular specimens and their dimensions are demonstrated respectively in Figure 5.4.

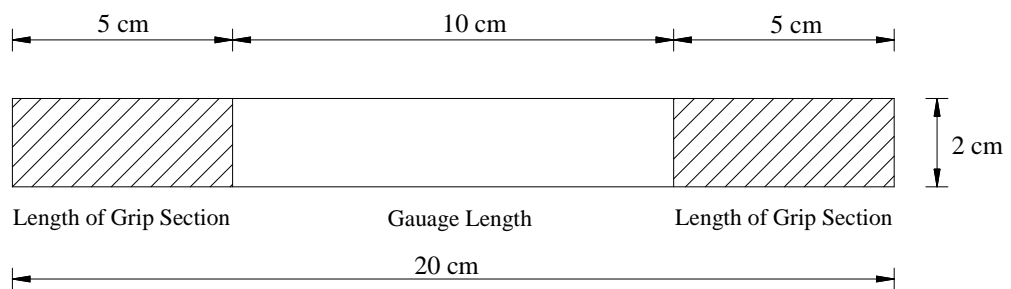


Figure 5.4 Dimensions for rectangular coupon cut from cellular beam specimen

5.2 Test Setup and Equipment

The universal hydraulic servo-controlled machine shown in Figure 2.4 is used to test the tension capacities of coupons. This machine can also perform compression and bending tests as well as tension to examine steel specimen in all mechanical properties. TF-H1000 test frame with computerized control system, shown in the Figure 5.5 below, which has a testing capacity of 1000 kN, a crosshead speed range of 5 to 40 mm/min with an accuracy of 0.1%, is used for tension tests.



Figure 5.5 Universal testing machine

5.3 The Objective of Tension Test

The objective of this tensile experiment is to determine the following properties of three different steel profiles (NPI-240, NPI-260, and NPI-280) from standard test specimen. The properties to be investigated include;

- Yield stress
- Ultimate stress
- Modulus of elasticity
- Ductility
- Proportional limit

5.4 The Procedure of Tensile Testing

The tensile test procedure of cellular beam coupons is carried on as following in accordance with ASTM E 8M-04 as shown in Figure 5.6 and Figure 5.7.

- The dimensions and properties for each beam specimen were defined.
- 10-cm gage length on each test specimen was marked off.
- The initial dimensions of each specimen were determined.
- The specimen was fixed in the tensile testing machine using standard mechanical pneumatic clamps, then attaching the linear extensometer, Novotechnik-LWH300, recorded applied load and resulting deflection and load values at failure.
- The speed of test was set to a constant speed of 5 mm/min. and then the tension test was started.
- Load, stress and strain data for each test was recorded to plot of the stress-strain curve.

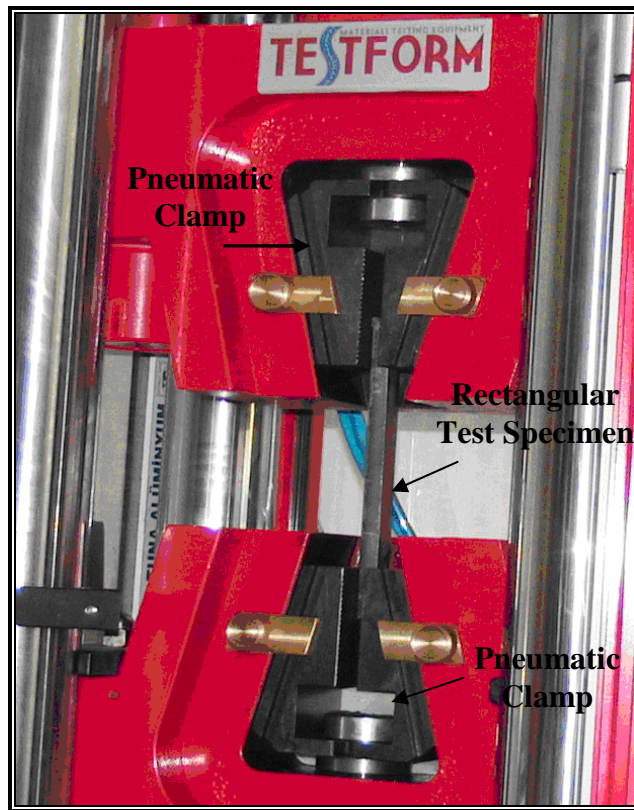


Figure 5.6 Rectangular test specimens under tension

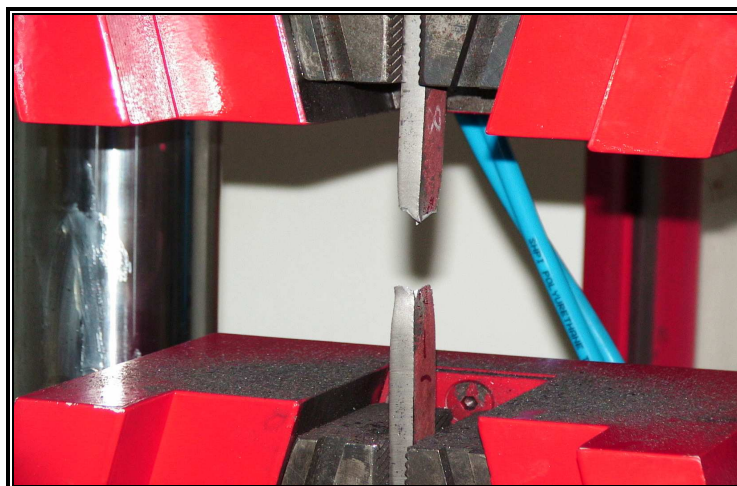


Figure 5.7 View of test specimens after rupture

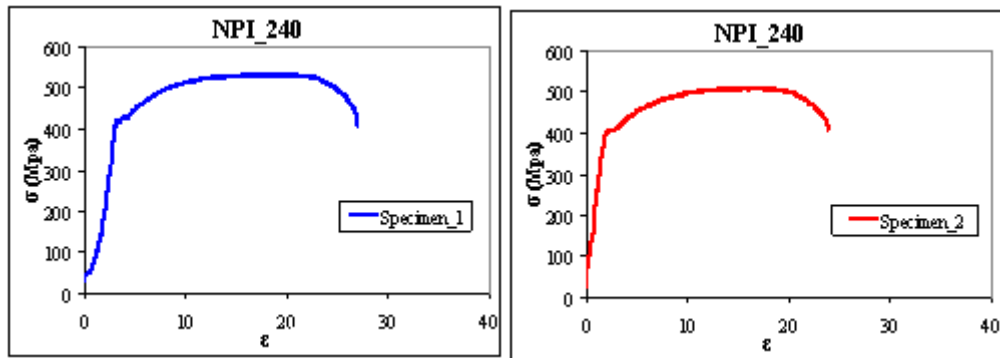
5.5 Test Results

The load and strain data are taken until the failure of the steel beam specimens. After failure of these test specimens, it was measured final length of the specimens, final gage lengths and was observed the character of the fracture. Figure 5.8 illustrates the geometric configurations of broken piece specimen at the end of the tension test.



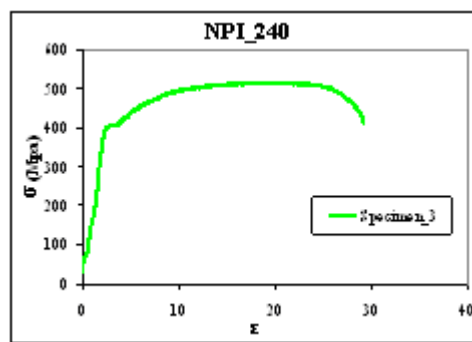
Figure 5.8 One of test specimens after tension test

Observed data from tensile tests were used to calculate the ultimate tensile strength of the specimens, and at the same time, converted and plotted a stress-strain curve for each specimen and determine the values indicated above and to compare test results with published values for these materials. These stress-strain graphs are then used in determination of the modulus of elasticity of the specimens. For this purpose, the slope of the elastic region of these curves is determined by fitting a straight line, with the least-square method. Stress-strain graphs for each specimen (NPI-240, NPI-260, and NPI-280) plotted in MS Excel Software are demonstrated respectively in Figure 5.9-5.11.

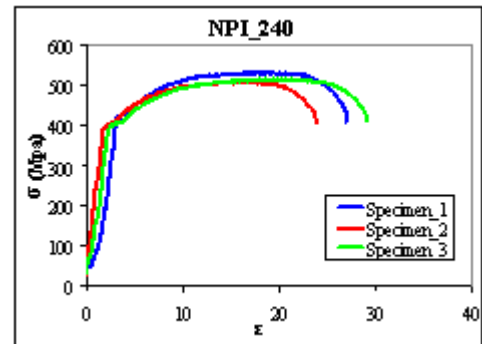


a) NPI_240, Specimen-1

b) NPI_240, Specimen-2



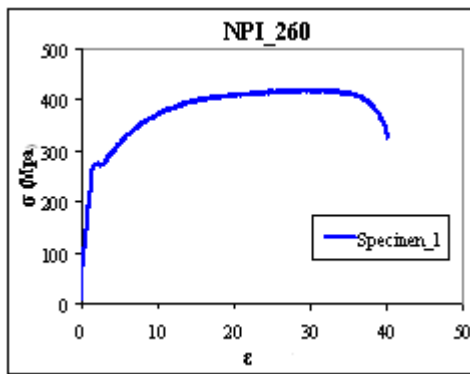
c) NPI_240, Specimen-3



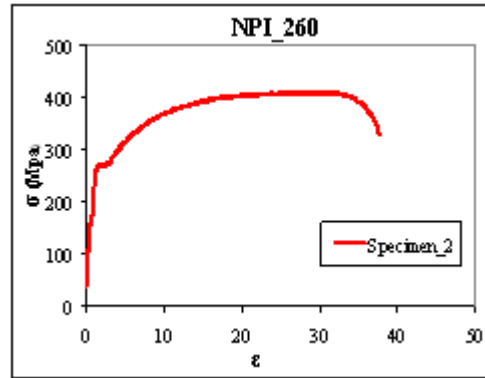
d) NPI_240, All Specimens

Figure 5.9 Stress-Strain graph of tensile test of NPI_240 profiles

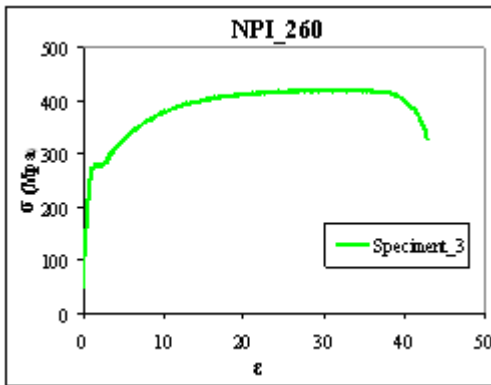
Using the stress-strain graphs in Figure 5.9, in this study, average values of elasticity modulus and elongation are determined 1.9×10^5 Mpa and 25.65%. After tension tests, the average values of tensile yield strength and ultimate strength are respectively determined 390 MPa and 495 MPa for NPI_240 steel beam profile sections.



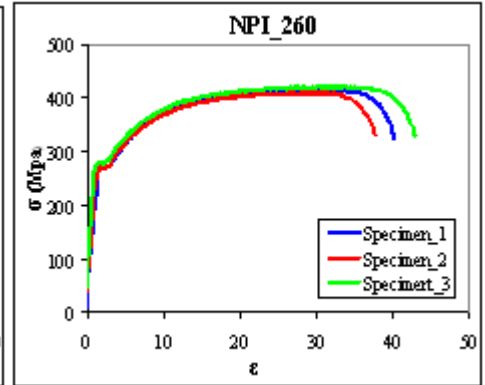
a) NPI_260, Specimen-1



b) NPI_260, Specimen-2



c) NPI_260, Specimen-3



d) NPI_260, All Specimens

Figure 5.10 Stress-Strain graph of tensile test of NPI_260 profiles

Using the stress-strain graphs in Figure 5.10, average values of elasticity modulus and elongation are determined 1.95×10^5 MPa and 39.21%. After tension tests, the average values of tensile yield strength and ultimate strength are respectively determined 285 MPa and 400 MPa for NPI_260 steel beam profile section.

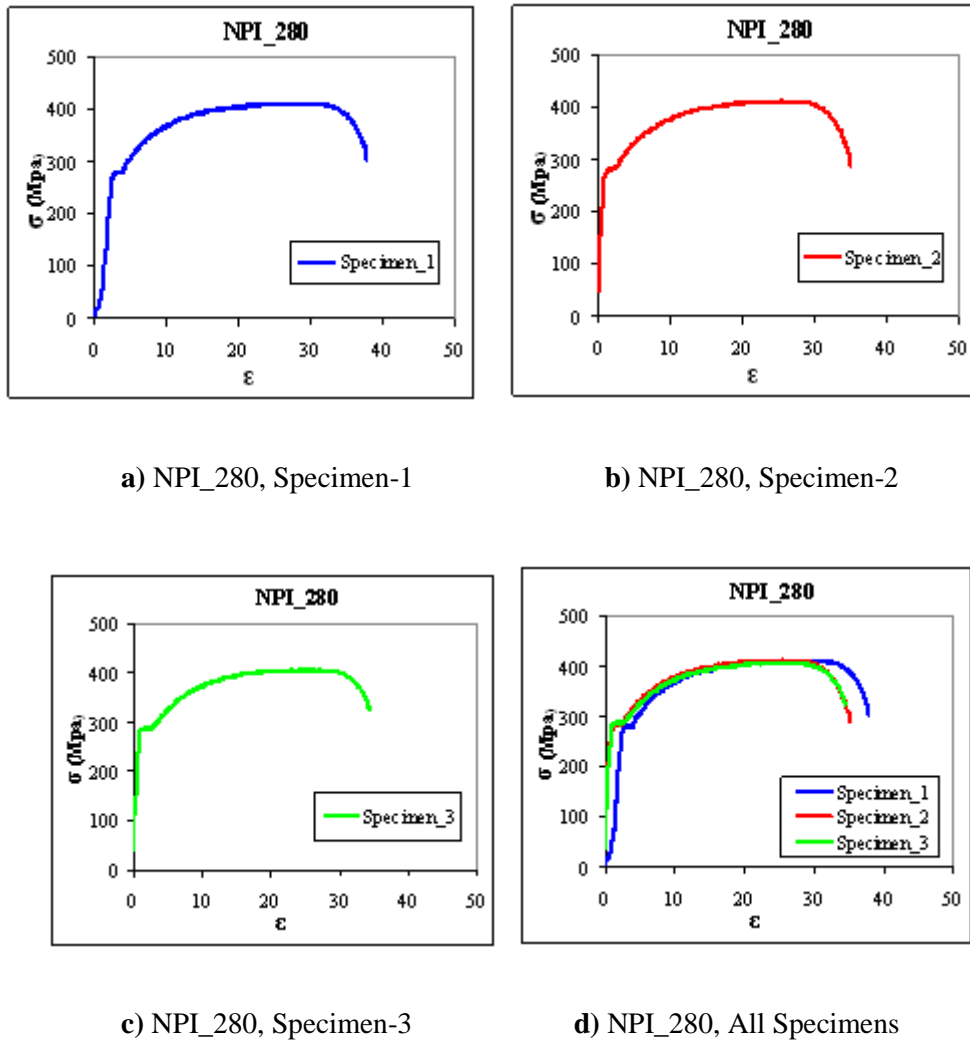


Figure 5.11 Stress-Strain graph of tensile test of NPI_280 profiles

Using the stress-strain graphs in Figure 5.11, average values of elasticity modulus and elongation are determined 1.85×10^5 MPa and 36.82%. After tension tests, the average values of tensile yield strength and ultimate strength are respectively determined 290 Mpa and 405 Mpa for NPI_280 steel profile section. In addition to these values, poisson ratio is taken as 0.3 for each NPI steel sections. Modulus of elasticity, poisson ratio, yield strength and ultimate strength values found at tensile test section are used in finite element analysis of cellular beams at the next chapter.

CHAPTER 6

NONLINEAR FINITE ELEMENT ANALYSIS OF OPTIMALLY DESIGNED STEEL CELLULAR BEAMS

6.1 Introduction to Finite Element Modeling

The objective of this chapter is to carry out non-linear finite element analysis of the cellular beams that were considered in the experimental study in order to determine their ultimate load capacity for comparison. The finite element method has been used to predict their entire response to increasing values of external loading until they lose their load carrying capacity. Finite element model of each specimen that is utilized in the experimental studies is carried out as illustrated in Figure 6.1.

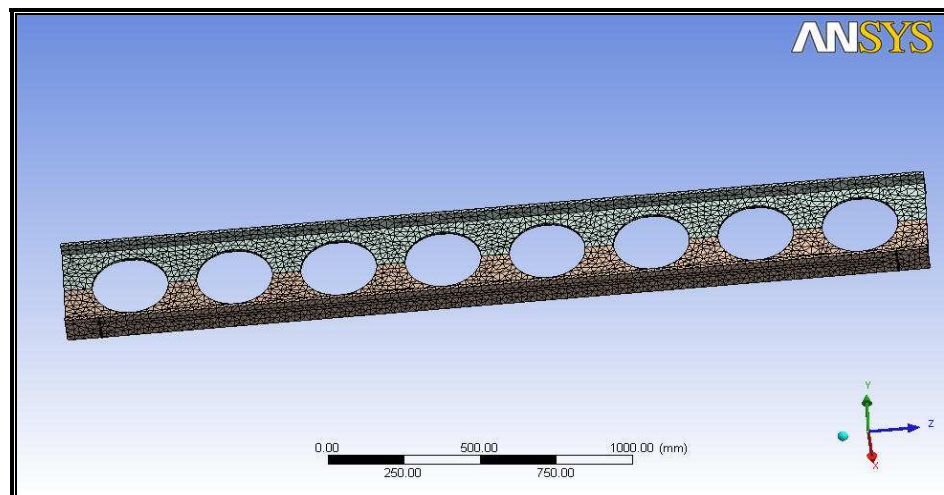


Figure 6.1 Finite element model of non-composite cellular beam

These finite element models are used to simulate the experimental work in order to verify of test results and to investigate the non-linear behaviour of failure modes such as web-post buckling, shear buckling and vierendeel bending of NPI_240, NPI_260 and NPI_280 section steel cellular beams.

ANSYS-workbench finite element modeling program is used to develop a three dimensional finite element beam model in this study. Nonlinear finite element models of these NPI steel cellular beam specimens are built to determine maximum values and locations of stress, strain and displacement concentrations under point loading. The non-linear analyses results of NPI profile steel cellular beams have been compared with results obtained from experimental studies.

6.2 Finite Element Modeling on Cellular Beams

Before starting the process of analysis, geometric dimensions of cellular beams are drawn with *SOLIDWORKS* program shown in Figure 5.2 below.

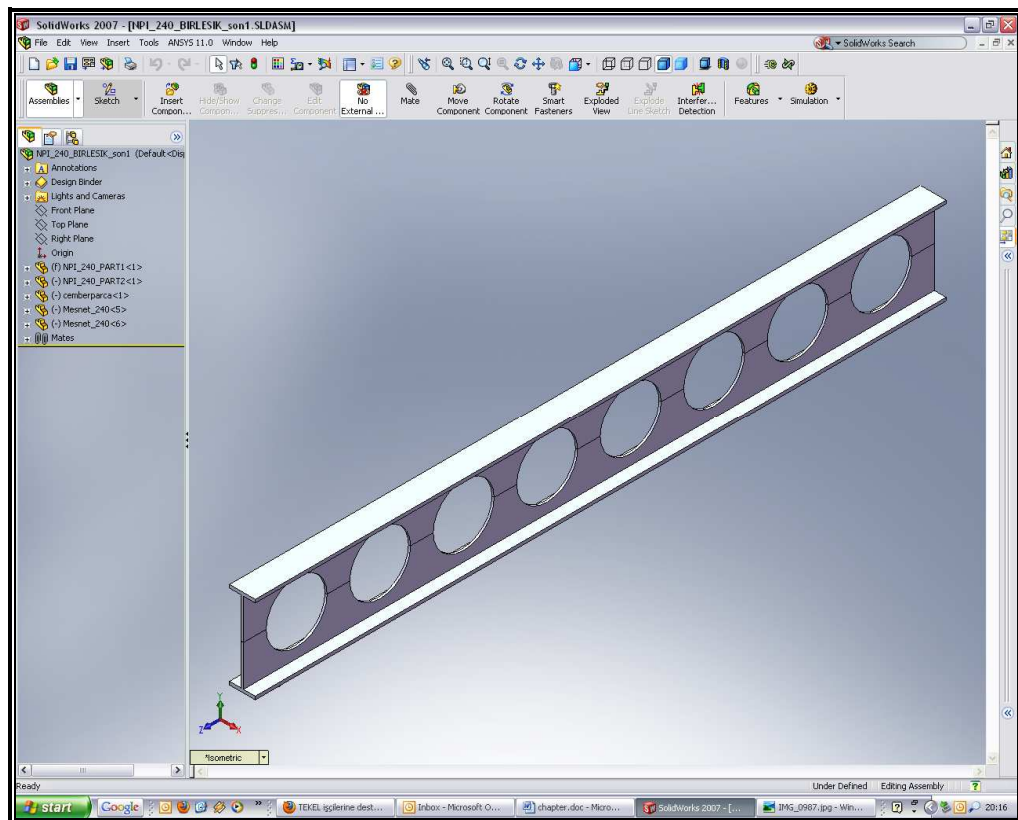


Figure 6.2 The geometry of Cellular Beam with *SOLIDWORKS*

After applying inputs related with prepared models of steel cellular beams, analysis process is initiated by using the software ANSYS. Material properties of steel cellular beams are extracted from material library; the library which covers standard concrete, steel and has the ability to create user defined custom materials for non-standard applications.

Nonlinear elastic material model is used for NPI_240, NPI_260 and NPI_280 steel NPI sections with Young's modulus of 1.9×10^5 , 1.95×10^5 and 1.85×10^5 MPa with average values found from tension tests and Poisson's ratio taken as 0.3 and the density of steel taken as 7.85×10^{-6} kg/mm. Tensile yield stress values obtained are respectively 390, 285 and 290 MPa for NPI_240, NPI_260 and NPI_280 steel profiles according to tensile testing results. In the same way, tensile ultimate stress values obtained are respectively 495, 400 and 405 MPa for NPI_240, NPI_260 and NPI_280 steel beam profiles. The material properties and their values for NPI_240 steel profile are shown in figure 6.3 below.

[-] Structural		Add/Remove Properties
<input type="checkbox"/> Young's Modulus	1.9e+005 MPa	
<input type="checkbox"/> Poisson's Ratio	0.3	
<input type="checkbox"/> Density	7.85e-006 kg/mm	
<input type="checkbox"/> Thermal Expansion	1.2e-005 1/°C	
<input type="checkbox"/> Alternating Stress		
<input type="checkbox"/> Strain-Life Parameters		
<input type="checkbox"/> Tensile Yield Strength	390. MPa	
<input type="checkbox"/> Compressive Yield Strength	390. MPa	
<input type="checkbox"/> Tensile Ultimate Strength	495. MPa	
<input type="checkbox"/> Compressive Ultimate Strength	495. MPa	
<input type="checkbox"/> Bilinear Isotropic Hardening		
[-] Thermal		Add/Remove Properties
<input type="checkbox"/> Thermal Conductivity	6.05e-002 W/mm·°C	
<input type="checkbox"/> Specific Heat	434. J/kg·°C	
[-] Electromagnetics		Add/Remove Properties
<input type="checkbox"/> Relative Permeability	10000	
<input type="checkbox"/> Resistivity	1.7e-004 Ohm·mm	

Figure 6.3 Structural properties of NPI_240 steel beam

The alternating stress curve and strain-life parameter graphics for NPI_240 steel profile according to structural definition values of steel beam are demonstrated respectively in Figures 6.4 and 6.5.

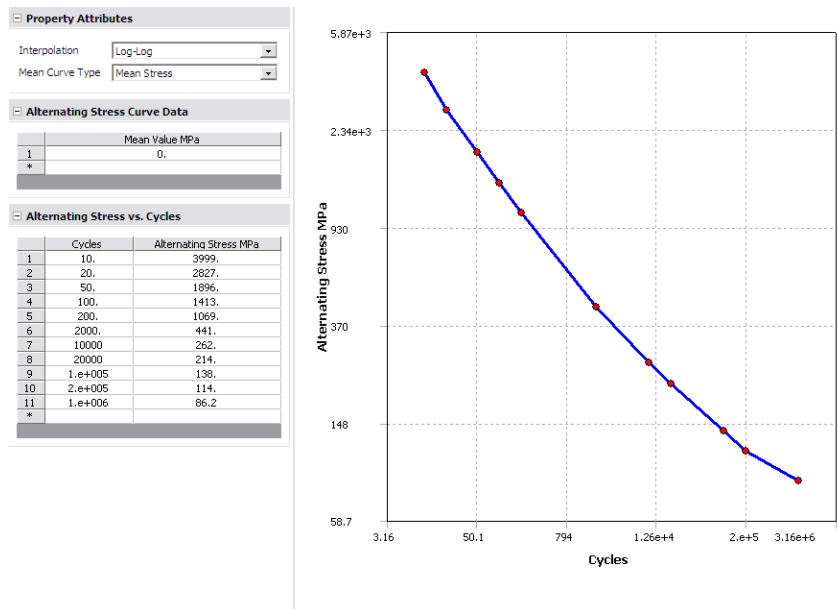


Figure 6.4 – Alternating stress curve of NPI_240 steel beam

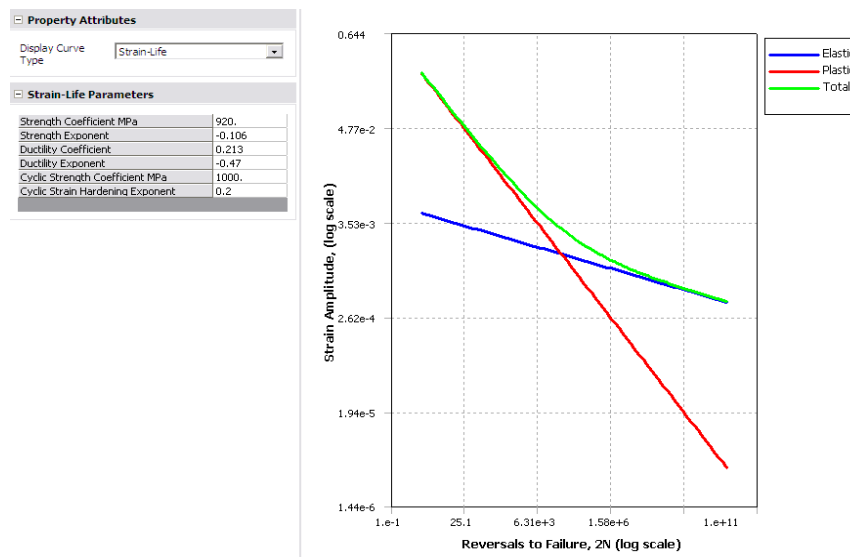


Figure 6.5 Strain-life parameter graph of NPI_240 steel beam

6.2.1 Element and Material Modeling on ANSYS Program

During FEA process, structure is divided into small and simple elements to calculate individual deformation easily. Tetrahedron volume finite elements are selected in the modeling of cellular beams. These elements are composed of 4-node or 10-node high-order element types and every node of this volume has three degrees of freedom. Tetrahedron volume elements with 4-node or 10-node patterns are shown in Figure 6.6. In this study, 10-node high-order which is known as *SOLID-187* has been selected as this element has a quadratic displacement behavior and is well suited to model irregular meshes comparing with other types.

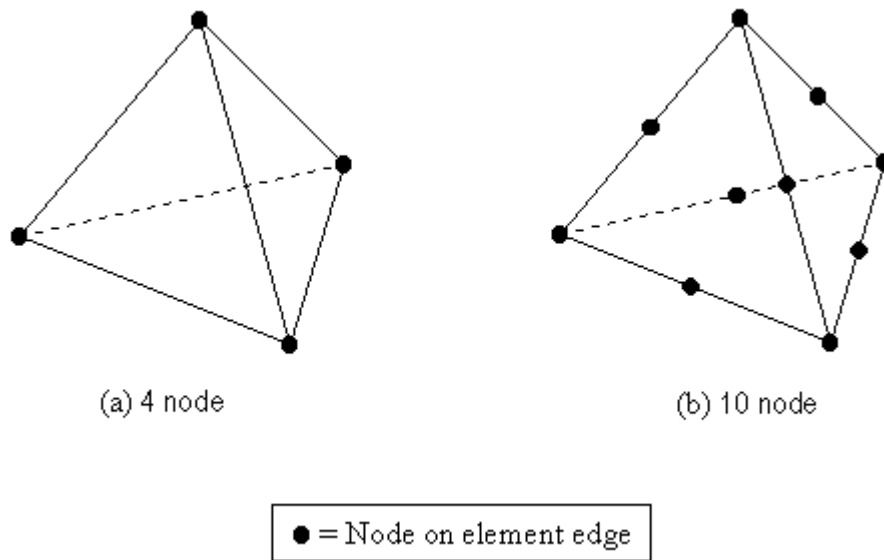


Figure 6.6 Tetrahedron volume element node patterns

For 3-D analysis of beams, the contact surface elements *CONTA-173* and *CONTA-174*, can be associated with the 3-D target segment elements. In this study, *CONTA-174* is selected to represent contact and sliding between 3-D

target surfaces and a deformable surface given that it is defined as a higher-order element. The element is applicable to 3-D structural and coupled field contact analyses. This element is defined by eight nodes and is located on the surfaces of 3-D solid or shell elements with midside of nodes.

It has the same geometric characteristic and node locations as the solid or shell element face to which it is connected as shown in Figure 6.7. When the element surface penetrates one of the target segment elements on a specific target surface, contact is easily completed.

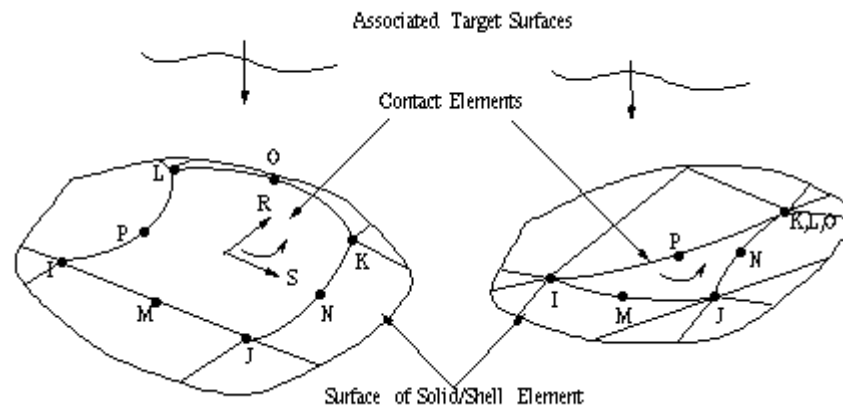


Figure 6.7 3-D Contact Element Geometry

For the target segment, *TARGE-170* is selected to represent various 3-D target surfaces for the *CONTA-174* contact surface elements shown in Figure 6.8. The contact elements which are potentially in contact with the target surface overlay the solid or shell elements with the boundary of a deformable body. This target surface is discretized by a set of target segment elements and is paired with its linked contact surface by the use of shared real constant set.

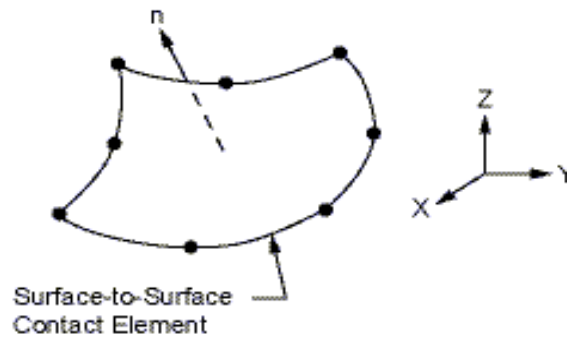


Figure 6.8 TARGE -170 element geometry

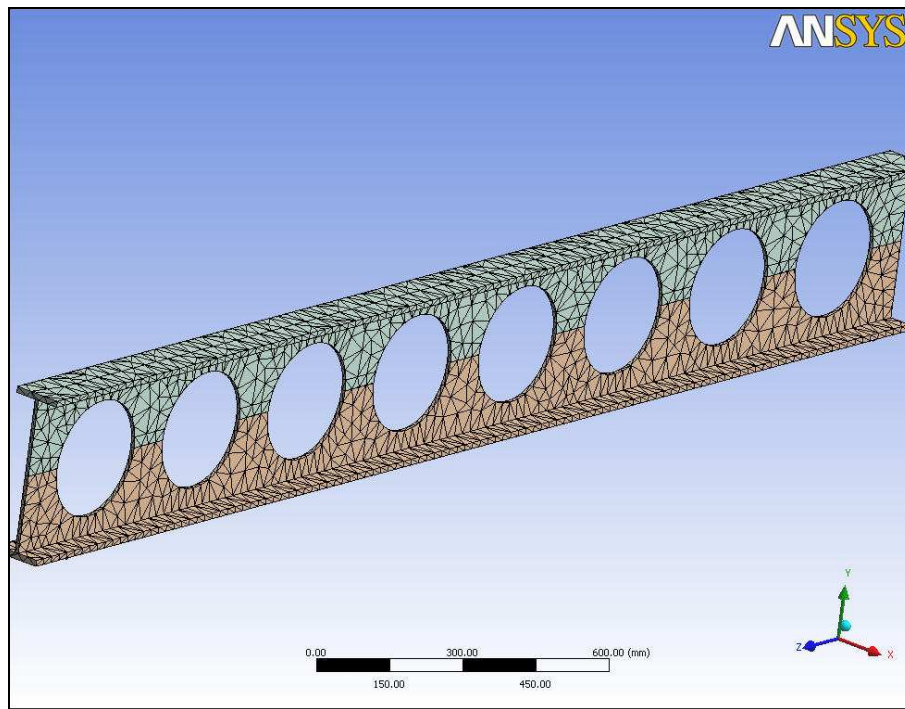
6.2.2 Mesh Generations on Cellular Beams with ANSYS Program

There are four types of meshing generations in ANSYS program. These methods are called Sweep, Automatically Generated, Tetrahedrons and Hex-Dominant. Since non-sweepable bodies force sweep method controlling, cellular beams can not be swept. Other meshing generation types, automatically generated, tetrahedrons and hex-dominant, are tested for finite element model of cellular beams to compare their created nodes and elements for the same mesh sizing. In this purpose, NPI_240 cellular beam is used to mesh with these generation types. Mesh size is taken as 100 mm for each method.

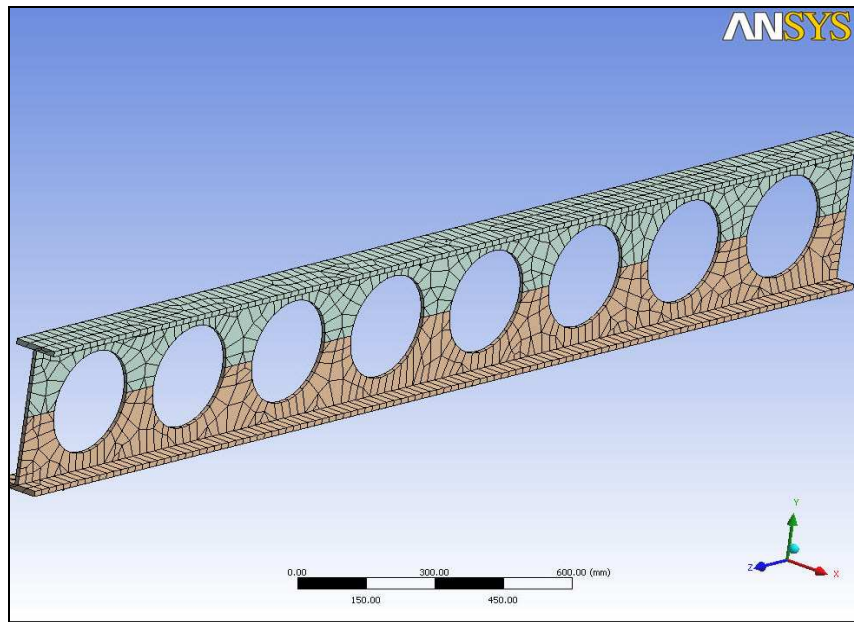
Table 6.1 Numbers of Nodes and Elements for Mesh Types

Mesh Type	Number of Nodes	Number of Elements
Automatically Generated	8847	3724
Hex – Dominant	6968	1877
Tetrahedrons	9413	4019

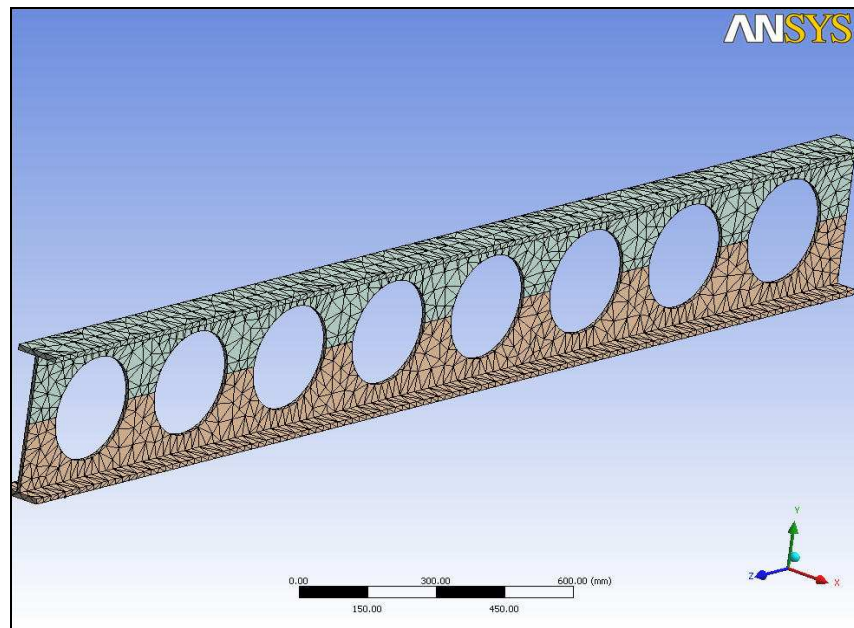
It is observed from Table 6.1 that when automatically generated, tetrahedrons and hex-dominant meshing methods give different values for nodes and elements. When the mesh type is taken as hex-dominant for 100 m mesh size, beam consists of 1877 elements and 6968 nodes. For the same mesh size, automatically-generated mesh consists of 3724 elements and 8847 nodes. In comparison with other mesh types, tetrahedron meshing provides better size distribution for the beam across the model with 4019 elements and 9413 nodes. Therefore, tetrahedron meshing option is selected for solving the cellular beam model. Consequently, an accurate simulation of the nonlinear behavior is obtained. Figure 6.9 illustrates different types of meshing for NPI_240 cellular beam.



(a) Automatically Generated Meshing



(b) Hex-Dominant Meshing



(c) Tetrahedron Meshing

Figure 6.9 Different Types Mesh Generations

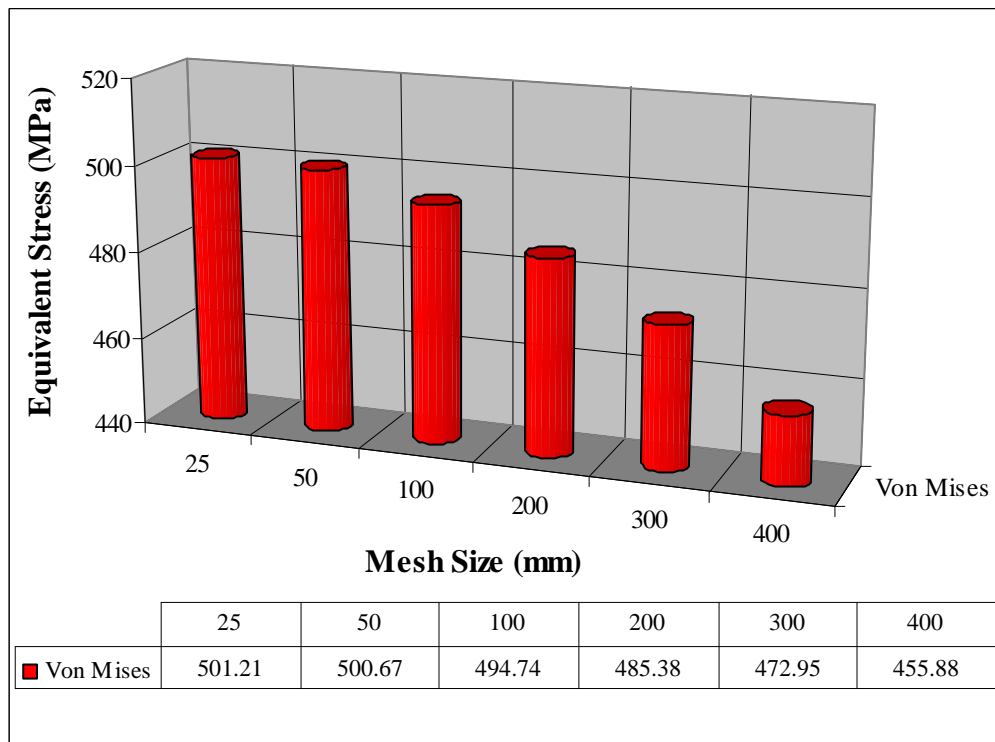


Figure 6.10 Different Mesh Sizes and Stress Values

Mesh sizing is important for accurate stress and displacement values. For this purpose, selected meshing type, the tetrahedron mesh divides various sizing mesh starting with 400 mm. When the stress and displacement values are stable, this mesh sizing can be applicable for FEM analysis. Figure 6.10 above illustrates that mesh sizing is important to find exact stress values. Figure 6.10 also demonstrates that maximum stress values (respectively 501.27 MPa and 500.67 MPa) on the steel cellular beam are nearly the same as the taken mesh sizes of 50 mm and 25 mm. It means 25 mm mesh size can be used for FEM analysis of these beams shown in Figure 6.11.

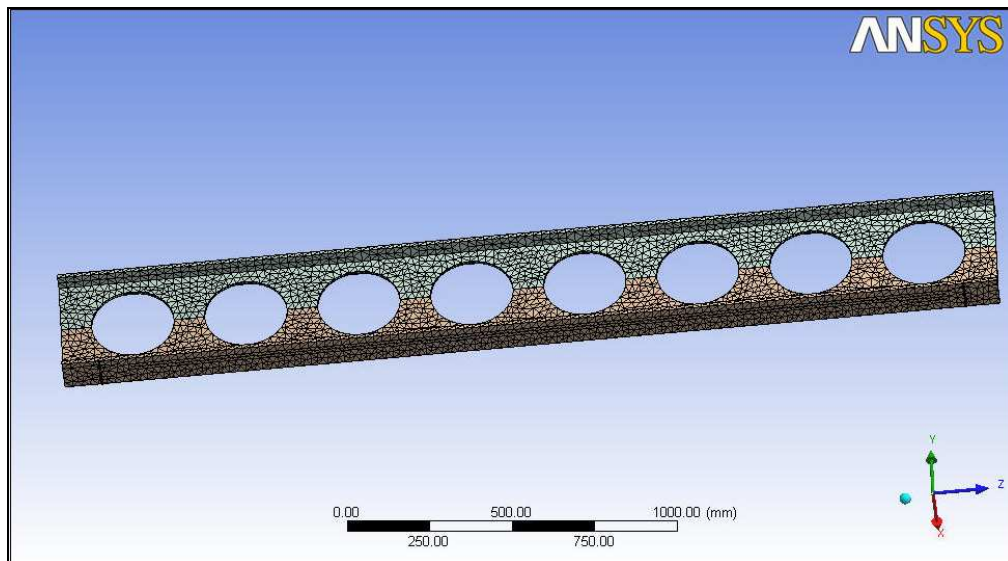


Figure 6.11 Tetrahedron Mesh Model with 25-mm Size

6.2.3 Setting Contact Analysis Parameters

Contact surfaces in ANSYS program allow representing a wide range of different types of interaction between components in a finite element model. In the present cellular beam model, there exists contact between NPI steel section and connection plates attached to beam as supports. Therefore, it is important to investigate the nature of interaction between NPI profile section and supporting connection plates. In this part of the research, numerical solution of the contact problem of cellular beams is presented with the help of ANSYS program.

6.2.4 Identification of Contact and Target Surface

The type of contact between the NPI steel cellular beams and the supporting connection plates represents one from contact surface to target surface. This

contact type is established when a surface of one body comes in contact with the surface of another body. This specific type of contact is commonly used for arbitrary bodies that have large contact areas. In addition, it is very efficient for bodies that experience large amounts of relative sliding with friction. The selected contact and target surfaces are shown in Figure 6.12.

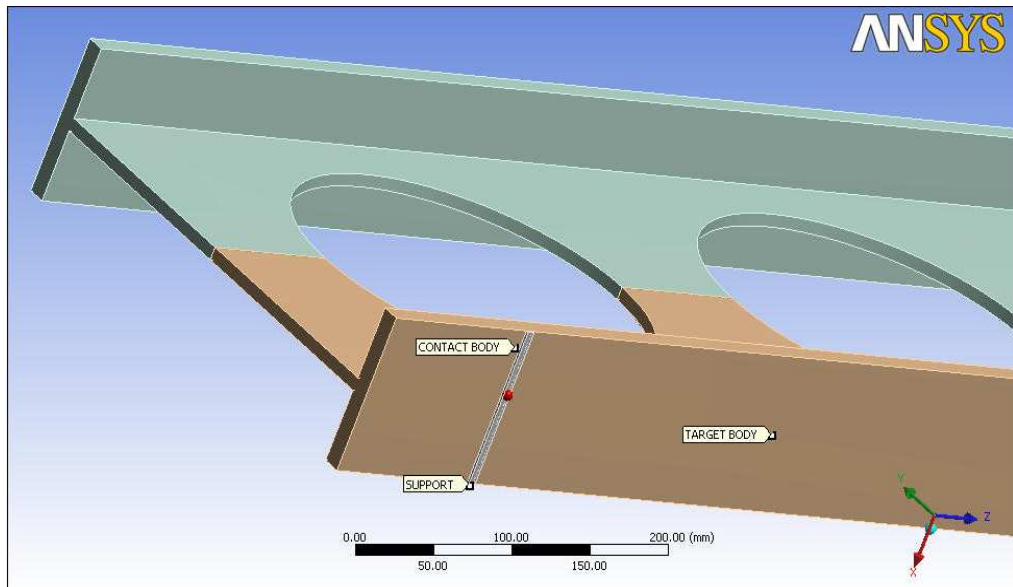


Figure 6.12 Contacts and Target Surface

6.2.4.1 Types of Contact

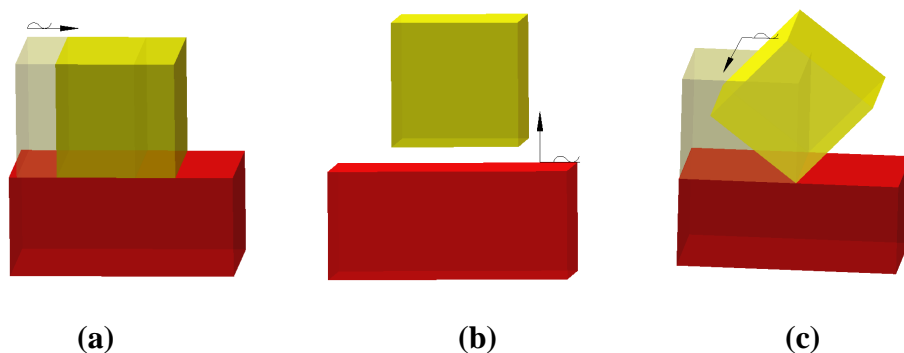


Figure 6.13 Contact Types

Contact surface has different types of behavior according to different characteristics of contact and there are several kinds of contact used in ANSYS program: frictional, frictionless, rough, contact without separation and bonded.

6.2.4.1.1 Frictional Contact

Two contacting faces can carry shear stresses up to a certain magnitude across their interface before they start sliding relative to each other as shown in Figure 6.13 (a).

6.2.4.1.2 Frictionless Contact

This type contact is a standard unilateral contact (shown in Figure 6.13 (c)); that is, normal pressure equals zero if separation occurs. So depending on the loading, gaps between bodies can emerge. This solution is nonlinear because the area of the contact may change when the load is applied. A zero coefficient of friction is assumed, thus allowing free sliding.

6.2.4.1.3 Rough contact

Similar to the frictionless contact type, as shown in Figure 6.13 (c), this contact type is perfectly rough frictional contact where there is no sliding. By default, no automatic closing of gaps is performed.

6.2.4.1.4 Contact without separation

This contact type is similar to bonded case. It only applies to regions of faces. Separation of faces in contact is not allowed, but small amounts of frictionless sliding can occur along contact faces, which means (a) is possible but (b) is not possible in Figure 6.13.

6.2.4.1.5 Bonded contact

In bonded type contact, no sliding or separation between faces or edges is allowed. In Figure 6.13, neither (a) nor (b) can occur. This type of contact allows for a nonlinear solution since the contact length/area does not change during the application of load. In this study, bonded contact is chosen between the NPI profile section parts and supporting connection plates.

6.2.4.2 Behavior of Contact

Several types of contact behavior are available in ANSYS program. These are symmetric, asymmetric and auto-asymmetric. Symmetric contact exists when there are both contact and target elements on the same surface. In asymmetric contact one face is chosen as contact and the other face as target, creating a contact pair. However, asymmetric contact is usually the most efficient way to model face-to-face contact for solid bodies. Lastly, auto asymmetric contact option allows the program to automatically identify and generate an asymmetric contact pair. When auto-asymmetric option is selected, during the solution phase the solver automatically chooses the more appropriate contact

face designation. In this study, symmetric contact is chosen between two contact surfaces of the steel cellular beam model.

6.2.4.3 Contact Analysis Algorithm

Major analysis algorithms available in ANSYS program are: Penalty Method, Multipoint Constraint, Pure Lagrangian and Augmented Lagrangian. Characteristics of each algorithm are presented below.

6.2.4.3.1 Penalty method

The penalty method uses a contact “spring” to establish a relationship between the two contact surfaces. The penalty method has short computation time and is the fastest among all the algorithms. Furthermore, large penetration may be produced.

6.2.4.3.2 Multipoint Constraint Method

Multipoint constraint algorithm is used in conjunction with bonded contact and contact without separation to model several types of contact assemblies and kinematic constraints.

6.2.4.3.3 Pure Lagrangian Method

The Pure Lagrangian Method does not require contact stiffness. Instead, it requires penetration control factor and maximum allowable tensile contact pressure. However, this method has long computational time.

6.2.4.3.4 Augmented Lagrangian Method

The Augmented Lagrangian Method is an iterative series of penalty methods. Compared to the Penalty method, the augmented lagrangian method usually leads to better conditioning and is less sensitive to the magnitude of contact stiffness. Yet, the augmented lagrangian method needs additional iterations when mesh becomes too distorted. In this study, the augmented-lagrangian method is used because it is possible to specify the maximum penetration tolerance.

6.3 Nonlinear Finite Element Model of Cellular Beams

The main objective of the nonlinear finite element analyses is to determine stress, strain and displacements in the NPI profile sections and to compare experimental results with the results of observed nonlinear analyses. Nonlinear static analyses produce more accurate stress results than linear static analyses for models where the loading results in concentrated stress values beyond the material yield point and also nonlinear analyze give more real behavior when compared with the linear ones. Based on these analyses, proper locations for the installment of transducers in the NPI beam sections are determined.

6.3.1 Definition of Static Structural Analysis Settings

Before proceeding to the solution, analysis options should be defined including boundary conditions, analysis type and stepping controls. Analysis setting is about the load to be applied to the structure, including load steps, load magnitude and load direction. For a static structure analysis, there can be one or several load steps. Furthermore, for each load step, several sub steps might be required to make the solution converge better and to obtain more accurate

results. Figure 6.14 illustrates the details of analysis settings for one sample in ANSYS-workbench program.

Details of "Analysis Settings"	
Step Controls	
Number Of Steps	10.
Current Step Number	1.
Step End Time	1. s
Auto Time Stepping	Program Controlled
Solver Controls	
Solver Type	Program Controlled
Weak Springs	Program Controlled
Large Deflection	Off
Inertia Relief	Off
Nonlinear Controls	
Force Convergence	Program Controlled
Moment Convergence	Program Controlled
Displacement Convergence	Program Controlled
Rotation Convergence	Program Controlled
Line Search	Program Controlled
Output Controls	
Calculate Stress	Yes
Calculate Strain	Yes
Calculate Results At	All Time Points
Analysis Data Management	
Solver Files Directory	C:\Documents and Settings\Administ...
Future Analysis	None
Save ANSYS db	No
Delete Unneeded Files	Yes
Nonlinear Solution	Yes
Visibility	
[A] Pressure	Display

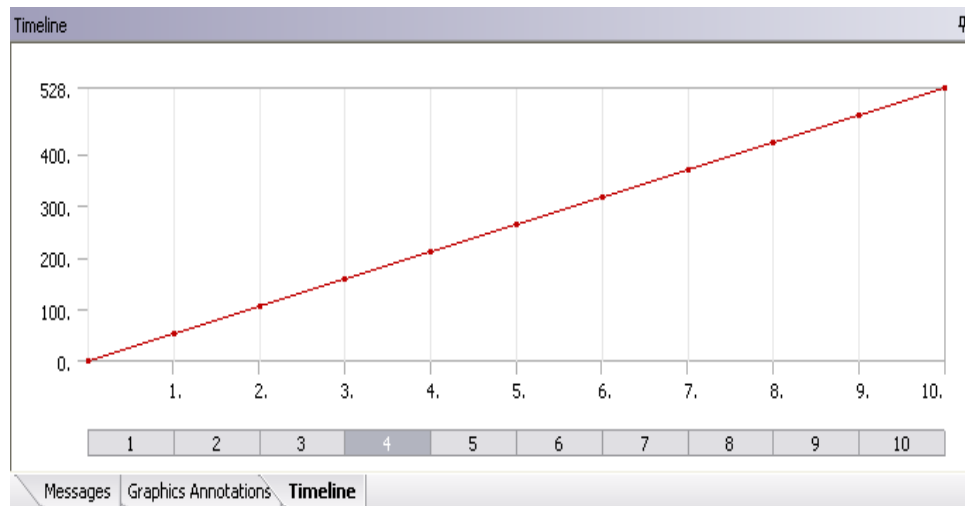
Figure 6.14 Analysis Settings for Cellular Beam

The total number of steps, number of sub steps for the initial step and maximum allowable number of sub steps are set to 10, 10 and 100 sub steps, respectively. When the load is applied to a particular point, the force stays inside meshes and sinks; however, ANSYS-workbench program does not analyze the beam model. Therefore, a maximum force with a pressure of 528 MPa is applied to the cellular beam model. The load is applied at 10 steps and at each step a 52.8 MPa incremental pressure load is applied to the NPI_240 beam. The software uses the Newton-Raphson iterative algorithm for the solution of equations.

Correct definition of boundary conditions is very important in the finite element analysis and it can greatly affect the behavior of steel cellular beam. Now that all the existing definitions about the steel cellular beam have been given, the finite element model is ready for FEM solution.

Tabular Data			
	Steps	Time [s]	Pressure [MPa]
1	1	0.	0.
2	1	1.	52.8
3	2	2.	105.6
4	3	3.	158.4
5	4	4.	211.2
6	5	5.	264.
7	6	6.	316.8
8	7	7.	369.6
9	8	8.	422.4
10	9	9.	475.2
11	10	10.	528.
*			

a) Tabular Data Pressure Steps



b) Time - Pressure Diagram

Figure 6.15 Load Diagram and Steps for NPI_240 section

According to structural definition values of steel NPI cellular beam, unlike linear analysis, plasticity properties of structural steel are also defined as bilinear isotropic hardening in nonlinear analysis in addition to alternating stress curve and strain-life parameters graphics as demonstrated in Figure 6.16.

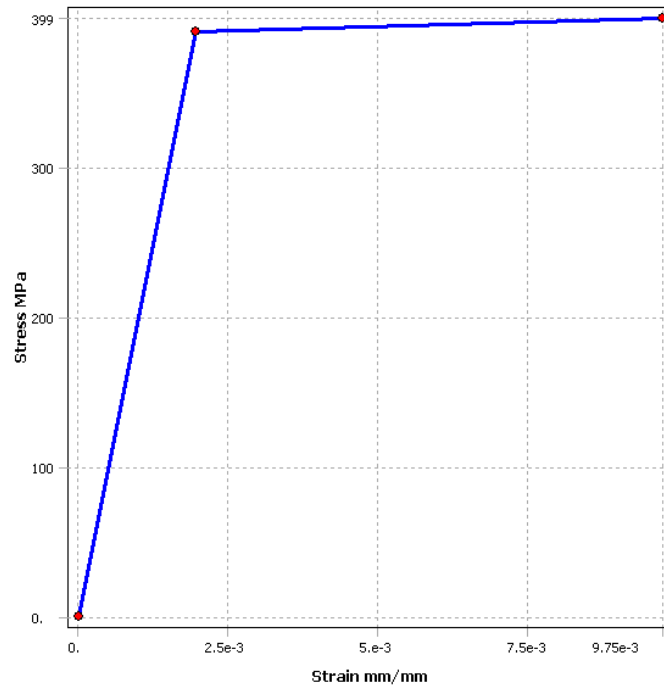


Figure 6.16 Plasticity Properties of Steel

6.3.2 Nonlinear Solution of NPI_240 Cellular Beam

Figure 6.17 demonstrates the details of analysis settings for NPI_240 beam in ANSYS Workbench. 280 kN force, the average value obtained from experimental tests of steel cellular beams, is applied to the middle of the beam as 528 MPa pressure. As explained in the previous sub section, when the load is applied to a particular point, the force stays inside meshes and sinks; however, ANSYS-workbench program does not analyze the cellular beam model. For that reason, the load is applied to the cellular beam as pressure as shown in the figure below. A bilinear isotropic material model (elastic modulus, $E = 1.9 \times 10^5$ MPa, tangent modulus, $ET = 390$ MPa) with Von-Mises yield criterion (yield strength, $F_y = 390$ MPa) was used for the steel to cellular beam model the nonlinear material behavior of the beam. The material properties used in the all NPI section beam models were determined through tensile tests of coupons taken from the test beams. Since the main objective of this finite element analysis was to determine beam failure behavior in web post regions, significant attention was paid on properly modeling the connection of the beam to the loading frame.

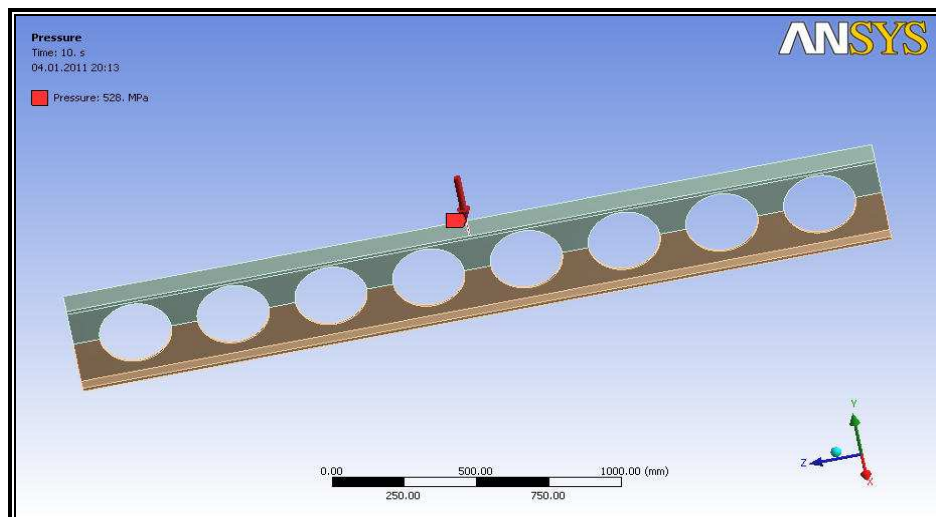


Figure 6.17 Applying Pressure to NPI_240 Cellular Beam

Different from linear solution, the material effects of cellular beam in the program are defined as nonlinear in the analysis of cellular beams. The mid-span displacement values obtained in linear and non-linear analysis of NPI-240 cellular beam is tabulated in Table 6.2 for the load increment of 28kN starting from 28kN. It is apparent from the table that when the load reaches 280 kN, which is the average value obtained from experiments, the nonlinear displacement value is 42.58% more than the linear displacement value. It is clear that after the load is increased, the axial forces increase in the beam and their effect on the flexural bending of the beam become more emphasized. As a result nonlinear displacement becomes larger. The results obtained are plotted in Figure 6.18. The effect of the geometrical nonlinearity on the values of vertical displacement at the middle of the NPI-240 steel cellular beam is also clearly seen in the same figure. Figure 6.18 clearly reveals the fact that when the vertical loads become larger in structure, the displacements also become larger and inclusion of nonlinearity in the analysis of such structures becomes a necessity.

Table 6.2 Displacement values at the mid-span of NPI-240 cellular beam

Displacements at middle part of cellular beam (mm)			
Load (kN)	Number of Steps	Nonlinear Analysis	Linear Analysis
28	1	0.8789	0.8078
56	2	1.7612	1.6157
84	3	2.6513	2.4236
112	4	3.5509	3.2314
140	5	4.5058	3.9781
168	6	5.6325	4.7859
196	7	6.6245	5.5937
224	8	7.8997	6.4017
252	9	9.8004	7.2095
280	10	14.0709	8.0785

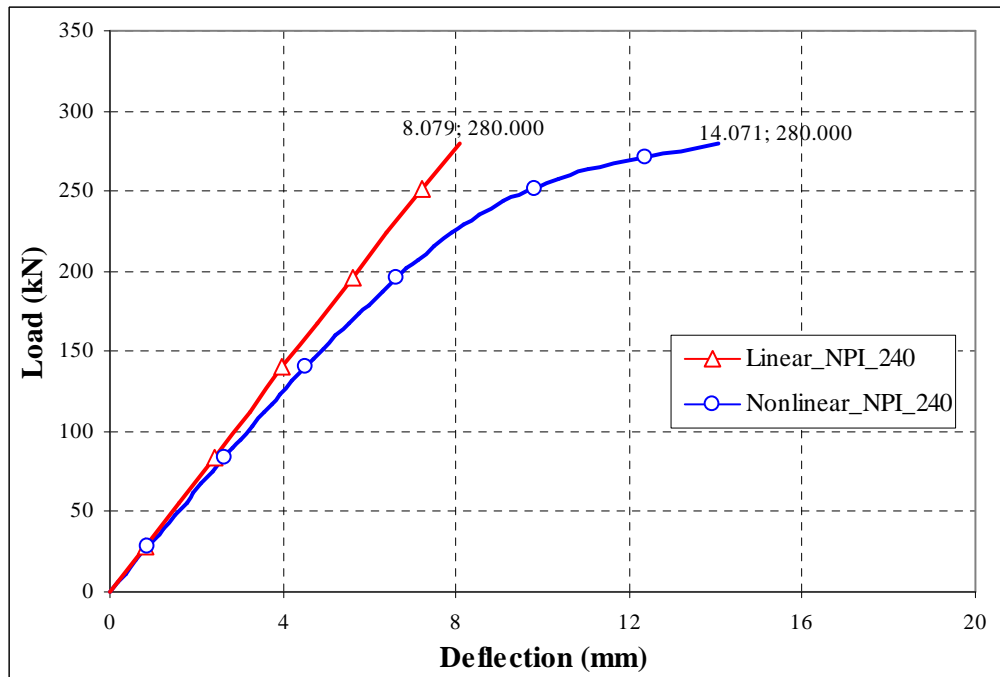


Figure 6.18 Linear and nonlinear load-deflection diagram for NPI-240 beam

When the ultimate load, 280 kN, is applied to the middle part of the beam as pressure, maximum equivalent stress which is 501.21 MPa, shown in Figure 6.19, occur around the holes. Figure 6.20 shows the maximum displacement that occurred in the middle of the beam as expected. It was measured as 15.458 mm at upper flange and 14.071 mm at lower flange.

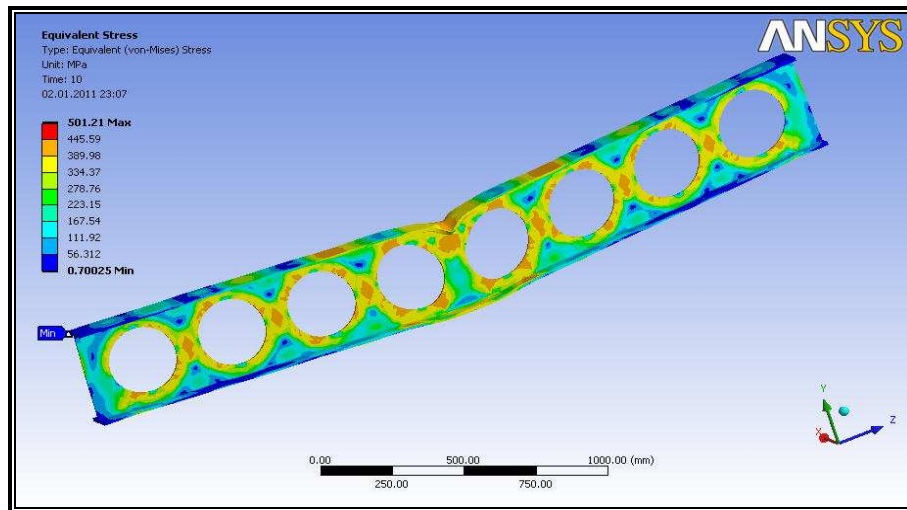


Figure 6.19 Equivalent Stress Values on NPI_240 Cellular Beam

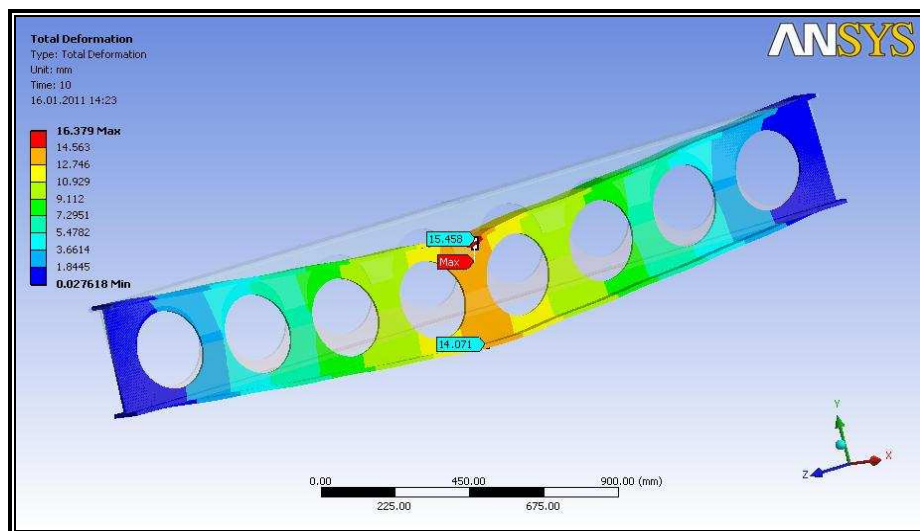


Figure 6.20 Deformation Values on NPI_240 Cellular Beam

When the same ultimate value, 280 kN, is applied to the middle part of the NPI-240 cellular beam, maximum normal stress which is 431.66 MPa, shown in Figure 6.21, occurred at web-post and maximum shear stress which is 352.0 MPa, shown in Figure 6.22, occurred around the area of support.

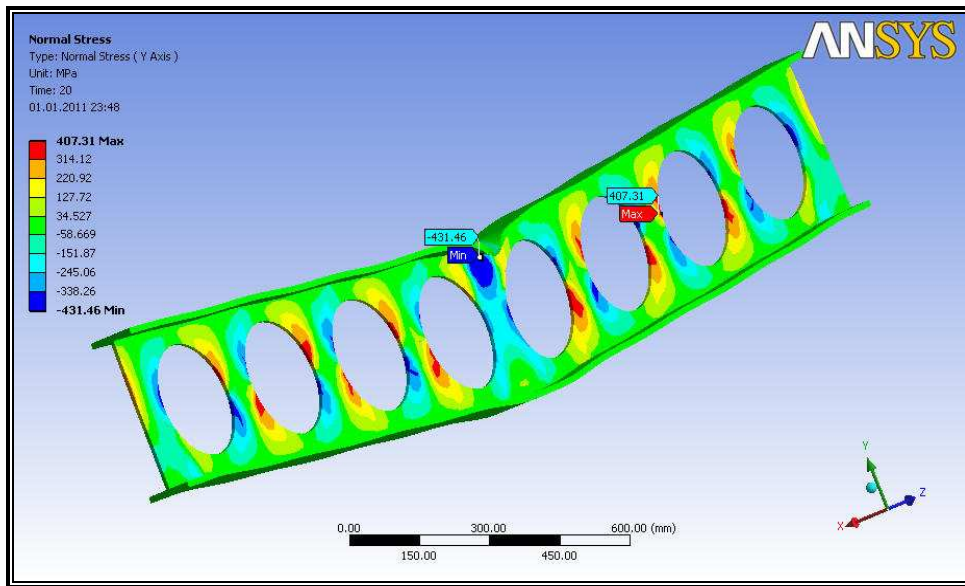


Figure 6.21 Normal Stress Values on NPI_240 Cellular Beam

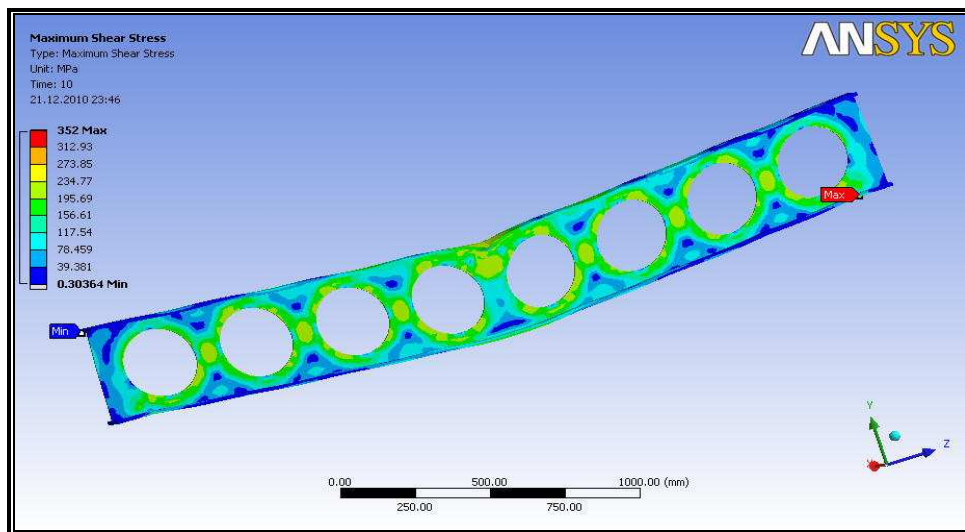


Figure 6.22 Shear Stress Values on NPI_240 Cellular Beam

When the experimental results are compared with those of nonlinear solution values, the deflection values obtained from NPI_240_TEST_3 are 10.13% lower than the nonlinear displacement value for upper flange and 7.78% lower

than the nonlinear displacement one for lower flange. Load-deflection diagrams, comparing finite element model with the curve of corresponding experimental NPI_240_TEST_3 cellular beam specimen are illustrated in Figure 6.23 and Figure 6.24, respectively.

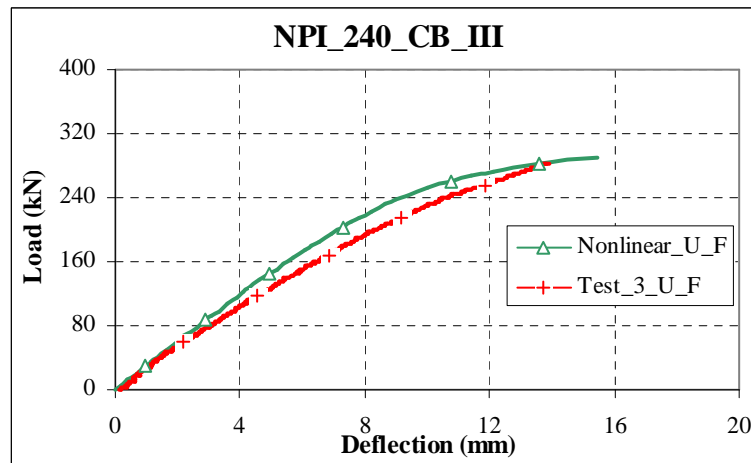


Figure 6.23 Load-deflection-curve for upper flange of NPI_240_TEST3

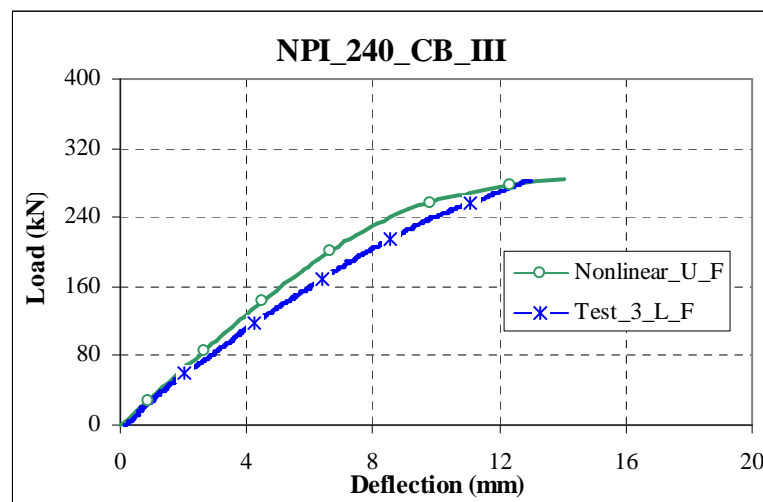


Figure 6.24 Load-deflection-curve for lower flange of NPI_240_TEST3

When the experimental results obtained are compared with those of nonlinear finite analysis values, the deflection values obtained from NPI_240_TEST_4 are 8.48% lower than the nonlinear displacement value for upper flange and 6.22% lower than the nonlinear displacement one for lower flange. Load-deflection diagram, comparing finite element model with the curve of corresponding experimental NPI_240_TEST_4 cellular beam specimen are illustrated in Figure 6.25 and Figure 6.26, respectively.

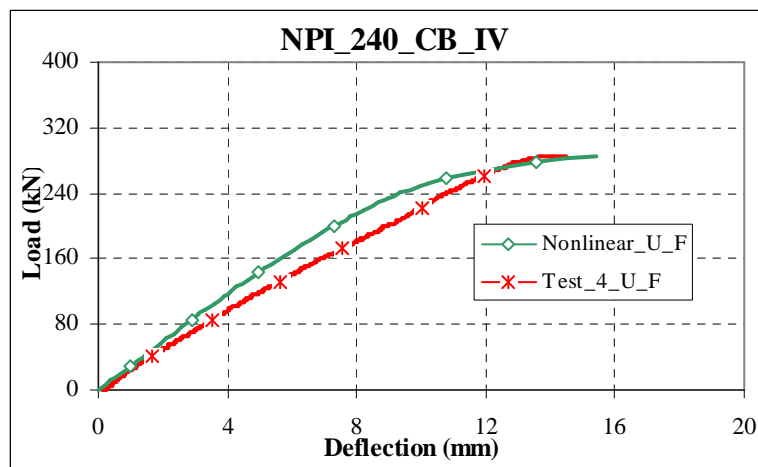


Figure 6.25 Load-deflection-curve for upper flange of NPI_240_TEST4

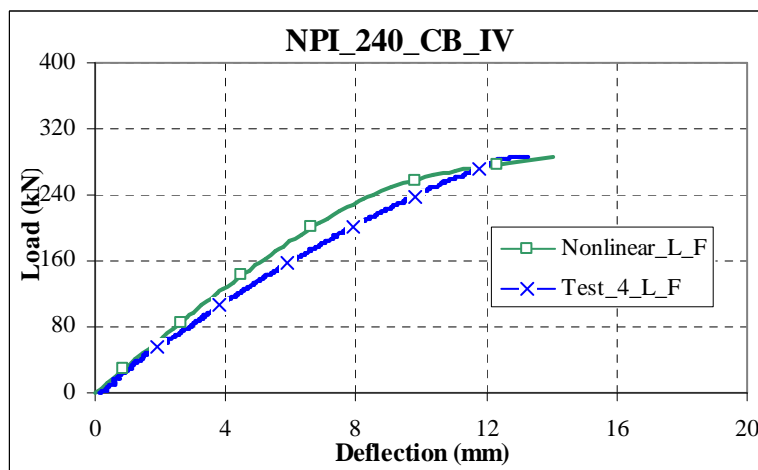


Figure 6.26 Load-deflection-curve for lower flange of NPI_240_TEST4

6.3.3 Nonlinear Solution of NPI_260 Cellular Beam

Figure 6.27 demonstrates the details of analysis settings for NPI_260 steel cellular beam in ANSYS workbench program. 220 kN force, the average value obtained from experimental tests of these steel cellular beams, is applied at the middle of the upper flange as 425 MPa pressure in 10 steps.

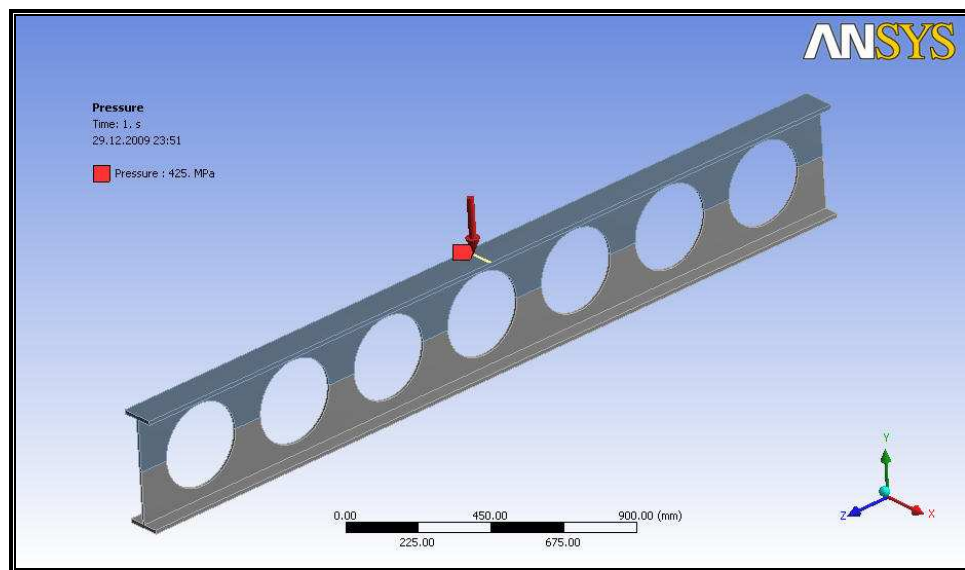


Figure 6.27 Applying Pressure to NPI_260 Cellular Beam

When 220 kN load which is obtained from experimental tests was applied to the middle of the beam as shown above, maximum equivalent stress occurred at the middle part of upper flange. It was determined as 494.42 MPa after the application of load in 10 steps as illustrated in Figure 6.28. Figure 6.29 shows the maximum displacement occurred in the middle of the beam as expected with an 18.969 mm for upper flange and 12.612 mm for lower flange. The reason for the load applied the top of web hole is that there was a 6.357 mm difference in displacement which was found between the upper flange and the lower one.

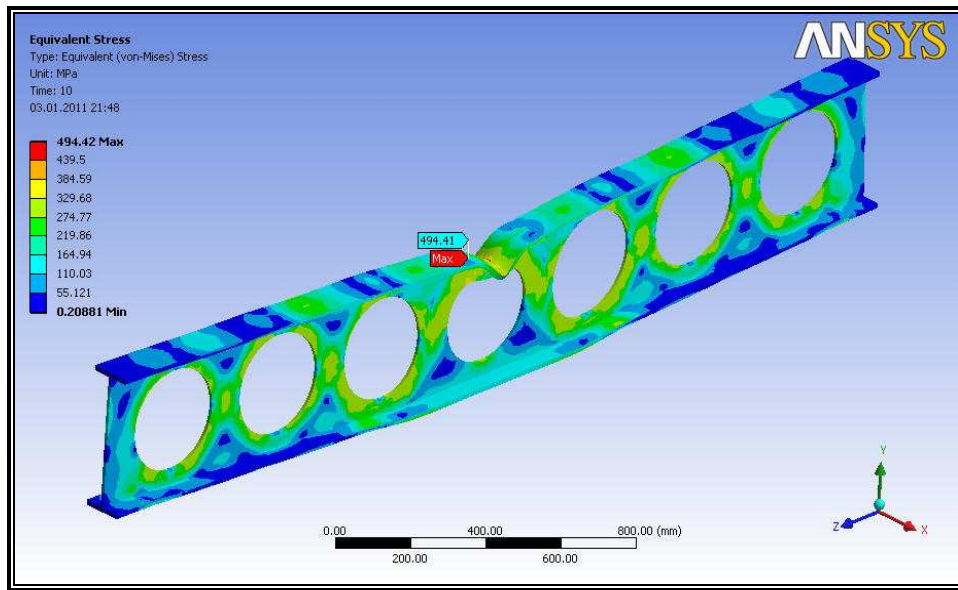


Figure 6.28 Equivalent Stress Values on NPI_260 Cellular Beam

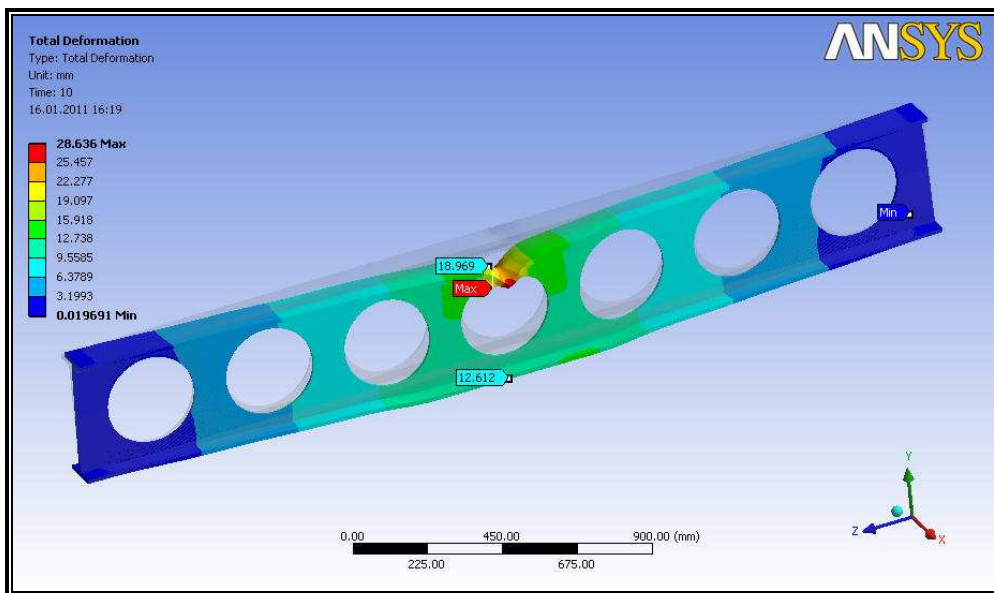


Figure 6.29 Deformation Values on NPI_260 Cellular Beam

When the same ultimate load, 220 kN, is applied to the middle part of the NPI-260 cellular beam, maximum normal stress which is 303.40 MPa, shown in Figure 6.30, occurred at web-post and maximum shear stress which is 269.06 MPa, shown in Figure 6.31, occurred around the area of support respectively.

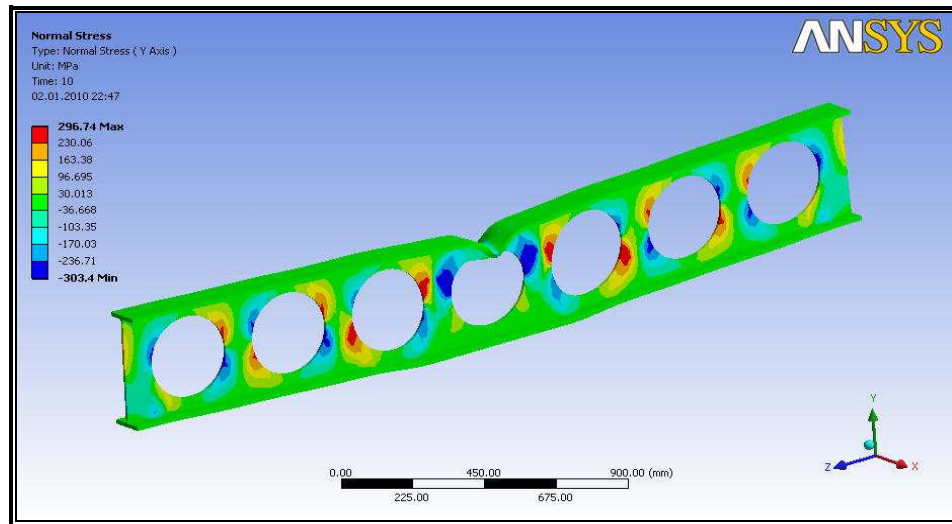


Figure 6.30 Normal Stress Values on NPI_260 Cellular Beam

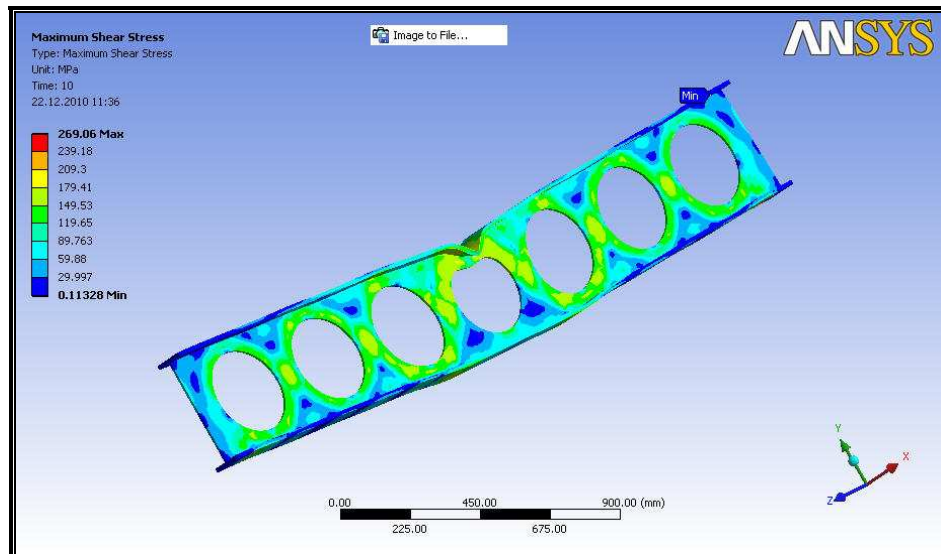


Figure 6.31 Shear Stress Values on NPI_260 Cellular Beam

When the experimental results are compared with those of nonlinear solution values, it is found that the deflection values obtained in NPI_260_TEST_1 are 9.56% more than the nonlinear displacement value for upper flange and 11.06% more than the nonlinear displacement one for lower flange. Load-deflection diagrams that are obtained by the finite element model and the experimentally for NPI_260_TEST_1 cellular beam specimen are illustrated in Figures 6.32 and 6.33, respectively.

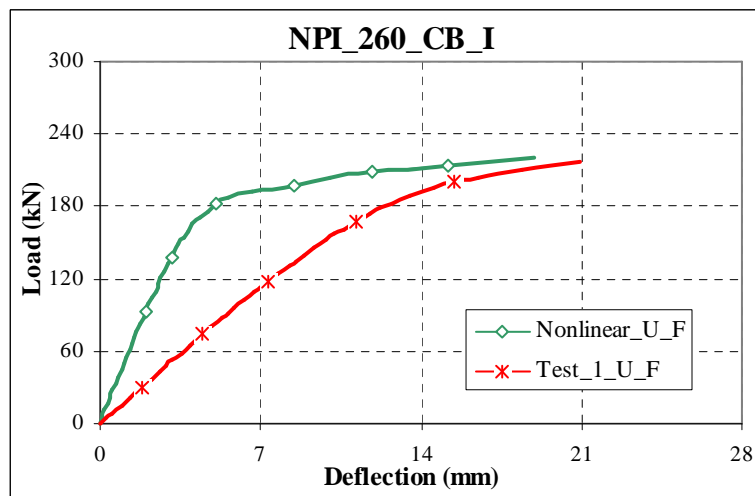


Figure 6.32 Load-deflection-curve for upper flange of NPI_260_TEST1

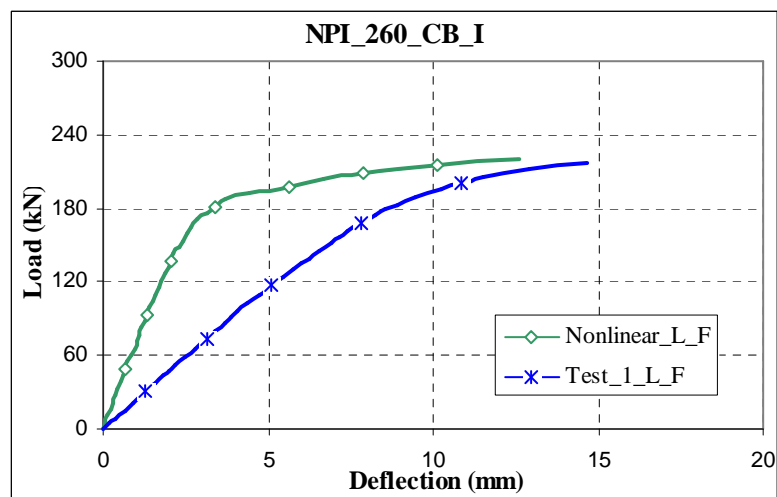


Figure 6.33 Load-deflection-curve for lower flange of NPI_260_TEST1

When the obtained experimental results are compared with those of nonlinear solution values, the deflection values obtained NPI_260_TEST_2 are 9.08% more than the nonlinear displacement value for upper flange and 8.91% more than the nonlinear displacement one for lower flange. Load-deflection diagrams that are obtained by the finite element model and the experimentally for NPI_260_TEST_2 cellular beam specimen are illustrated in Figures 6.34 and 6.35, respectively.

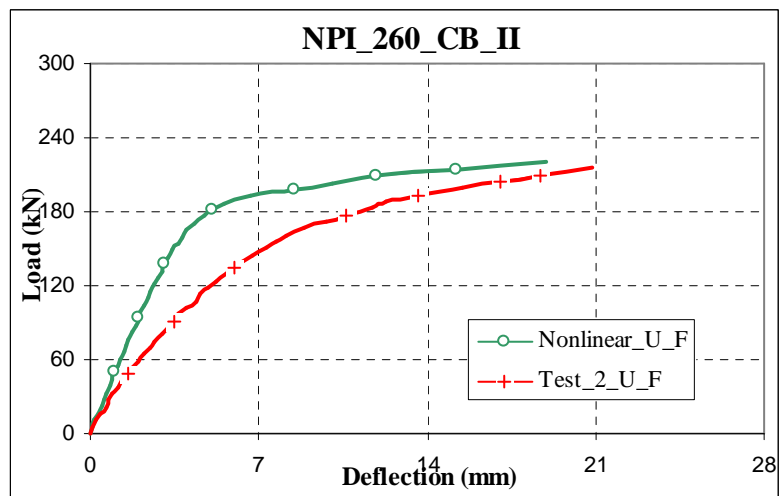


Figure 6.34 Load-deflection-curve for upper flange of NPI_260_TEST2

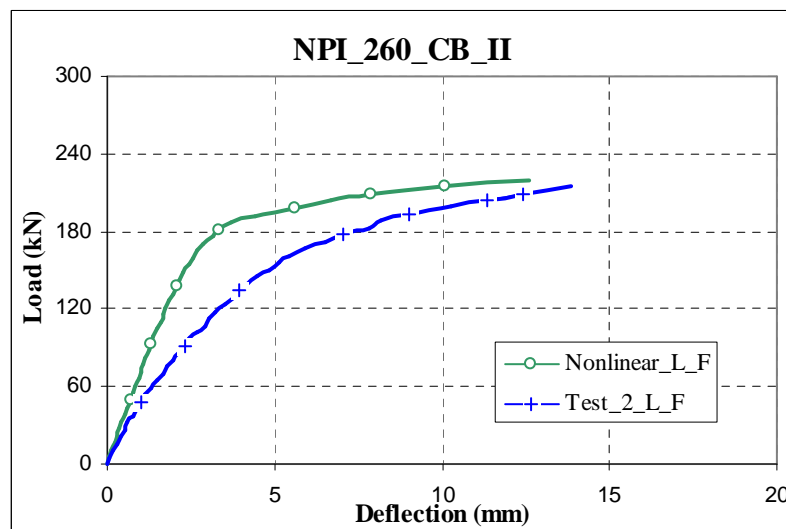


Figure 6.35 Load-deflection-curve for lower flange of NPI_260_TEST2

When the experimental results are compared with those of nonlinear solution values, it is noticed that the deflection values obtained experimentally in NPI_260_TEST_3 are 7.44% more than the nonlinear displacement value for upper flange and 7.69% more than the nonlinear displacement one for lower flange. Load-deflection diagrams that are obtained by the finite element model and the experimentally for NPI_260_TEST_3 cellular beam specimen are illustrated in Figures 6.36 and 6.37, respectively.

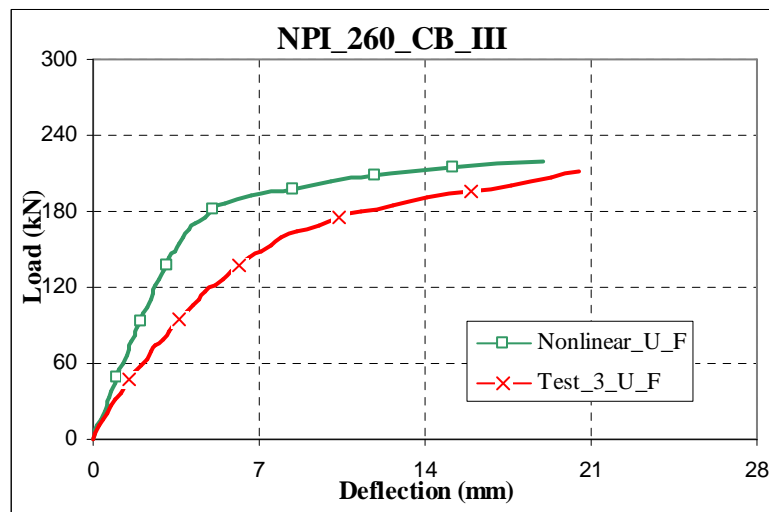


Figure 6.36 Load-deflection-curve for upper flange of NPI_260_TEST3

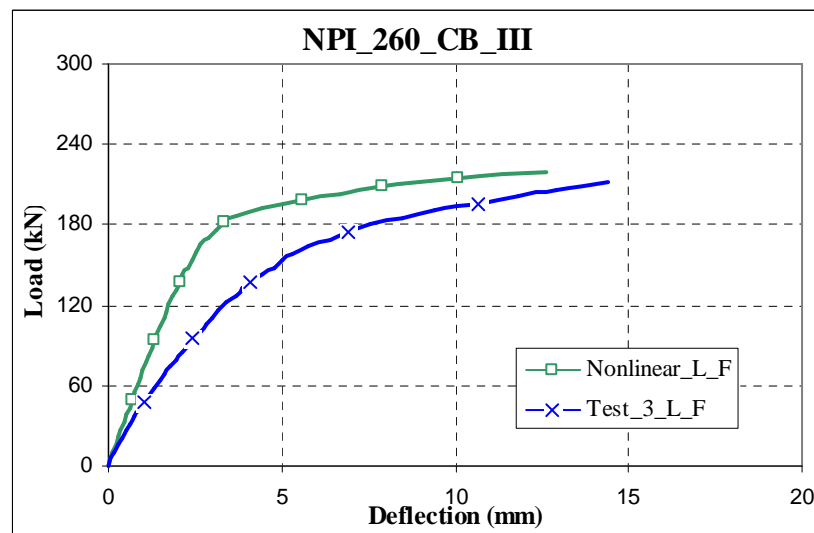


Figure 6.37 Load-deflection-curve for lower flange of NPI_260_TEST2

When the experimental results are compared with those of nonlinear solution values, it is found that the deflection values obtained experimentally in NPI_260_TEST_4 are 10.68% more than the nonlinear displacement value for upper flange and 12.59% more than the nonlinear displacement one for lower flange. Load-deflection diagrams that are obtained by the finite element model and the experimentally for NPI_260_TEST_4 cellular beam specimen are illustrated in Figures 6.38 and 6.39, respectively .

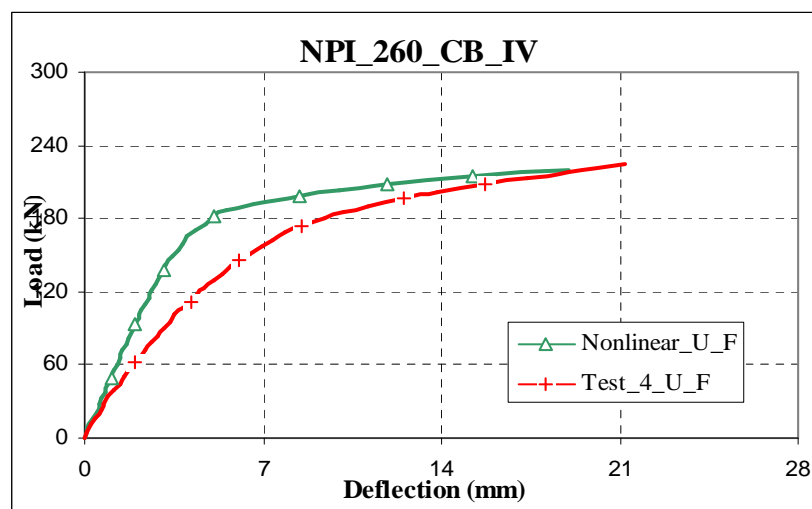


Figure 6.38 Load-deflection-curve for upper flange of NPI_260_TEST4

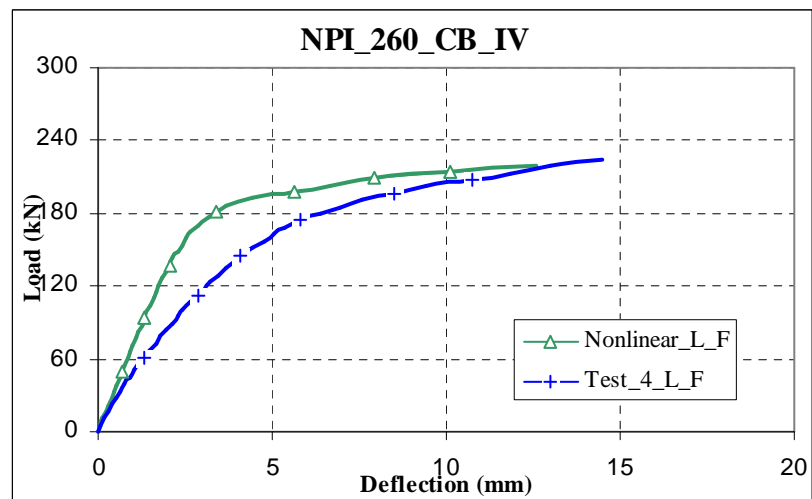


Figure 6.39 Load-deflection-curve for lower flange of NPI_260_TEST2

6.3.4 Nonlinear Solution of NPI_280 Cellular Beam

Figure 6.40 demonstrates details of analysis settings for NPI_280 beam in ANSYS Workbench. 375 kN force, obtained from experimental tests of these beams, is applied to midfield of the beam as 570 MPa pressure.

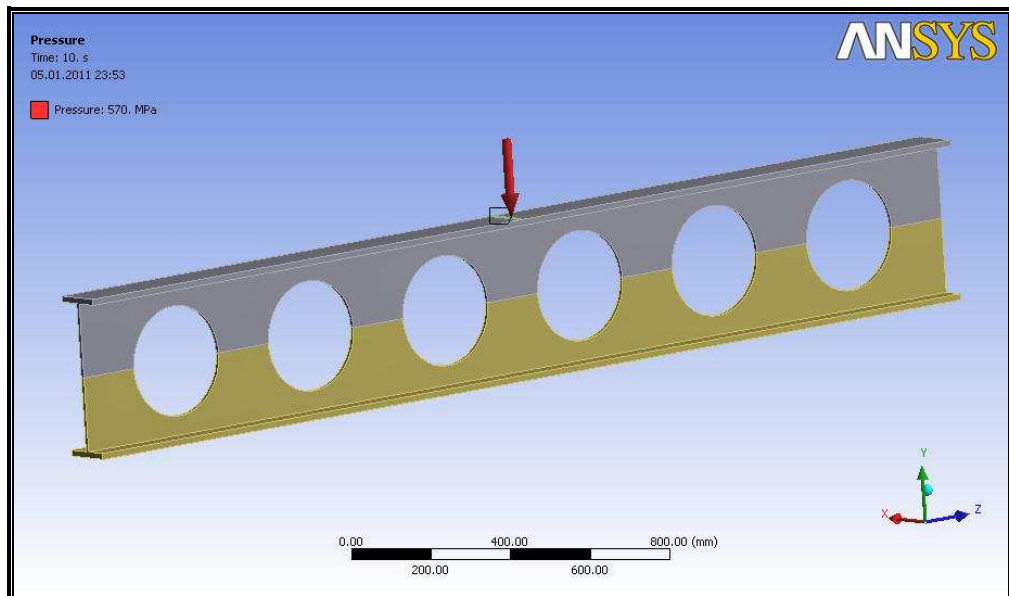


Figure 6.40 Applying Pressure to NPI_280 Cellular Beam

When 375 kN load which is obtained from experimental tests was applied to the middle of the beam as shown above, maximum equivalent stress occurred at the middle part of upper flange. It was determined as 430.82 MPa after the application of load in 10 steps as illustrated in Figure 6.41. Figure 6.42 shows the maximum displacement occurred in the middle of the beam as expected with a 17.829 mm for upper flange and 16.012 mm for lower flange.

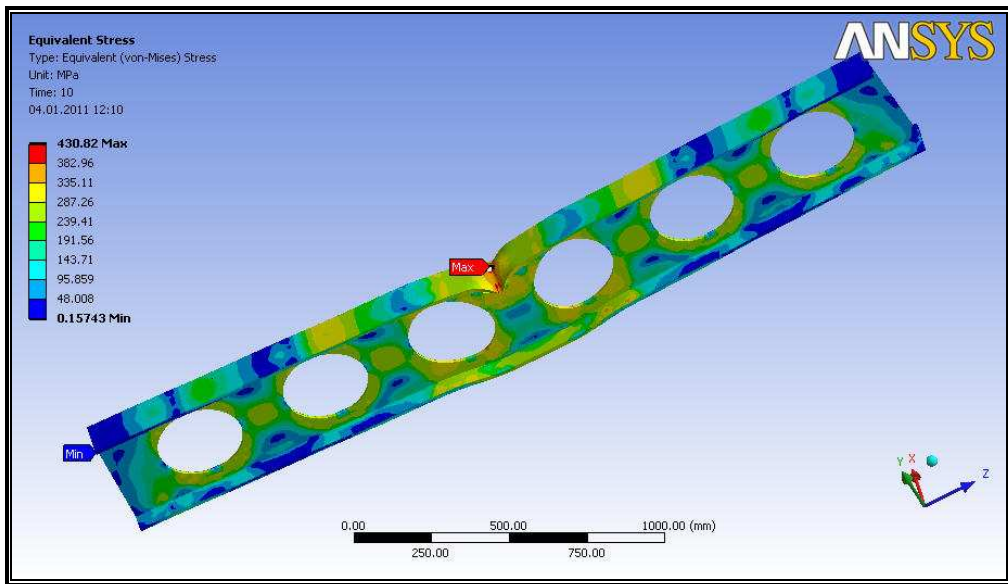


Figure 6.41 Equivalent Stress Values on NPI_280 Cellular Beam

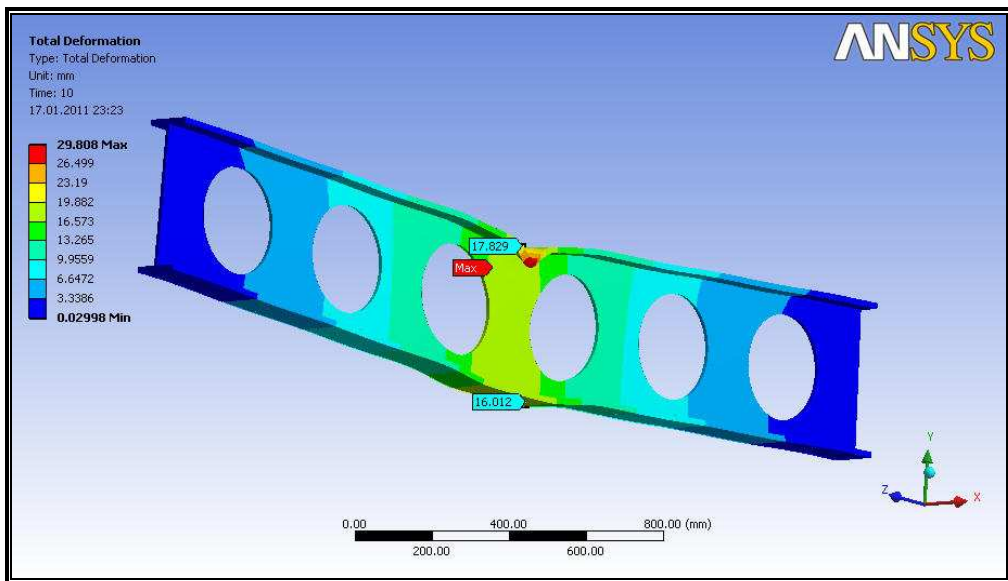


Figure 6.42 Deformation Values on NPI_280 Cellular Beam

When the same ultimate load, 375 kN, is applied to the middle part of the NPI-280 cellular beam, maximum normal stress which is 399.13 MPa, shown in

Figure 6.43, occurred at web-post and maximum shear stress which is 356.0 MPa, shown in Figure 6.44, occurred around again at web-post respectively.

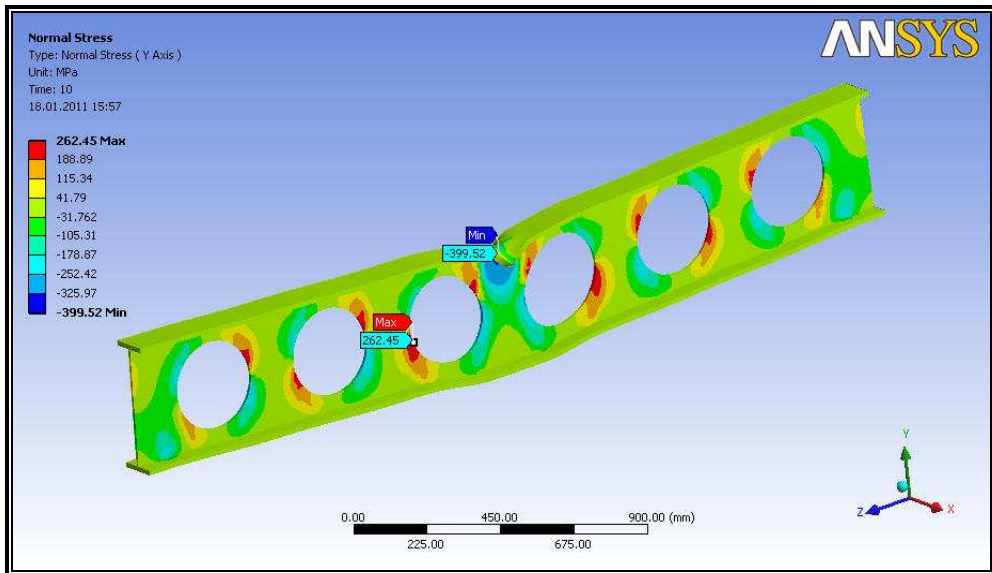


Figure 6.43 Normal Stress Values on NPI_280 Cellular Beam

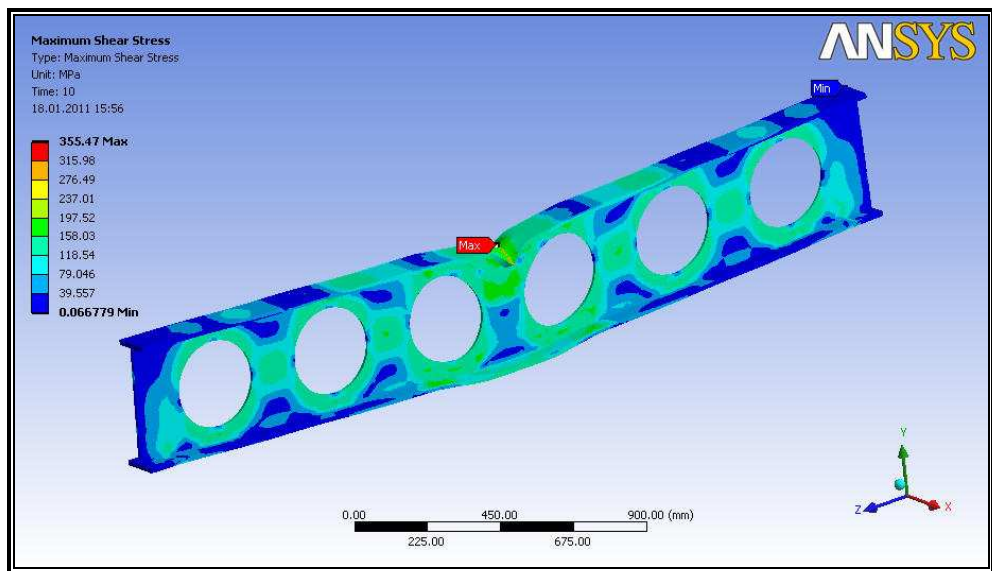


Figure 6.44 Shear Stress Values on NPI_280 Cellular Beam

When the experimental results are compared with those of nonlinear solution values, it is noticed that the deflection values obtained experimentally in TEST_1 are 11.65% more than the nonlinear displacement value for upper flange and 13.84% more than the nonlinear displacement one for lower flange. Load-deflection diagrams that are obtained by the finite element model and the experimentally for NPI_280_TEST_1 cellular beam specimen are illustrated in Figures 6.45 and 6.46, respectively.

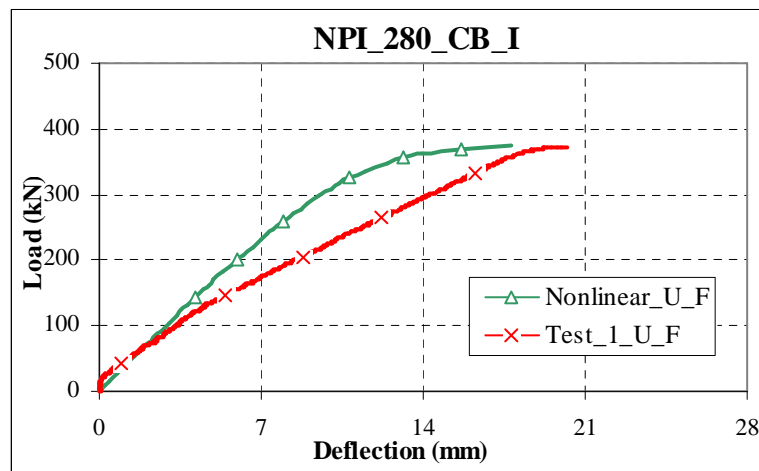


Figure 6.45 Load-deflection-curve for upper flange of NPI_280_TEST1

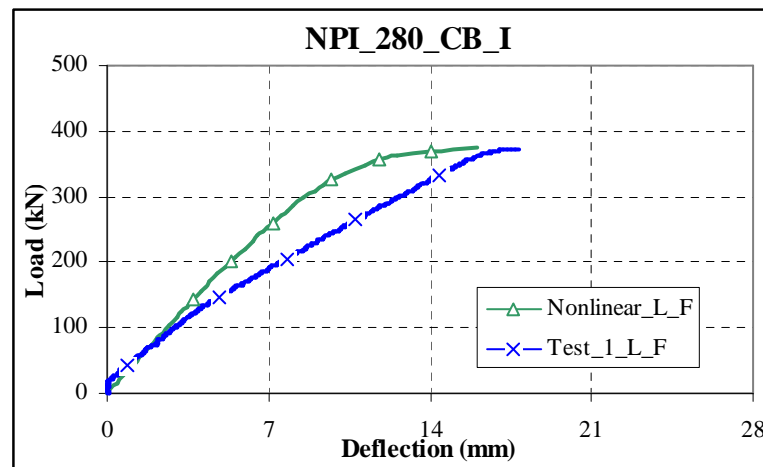


Figure 6.46 Load-deflection-curve for lower flange of NPI_280_TEST1

When the experimental results are compared with those of nonlinear solution values, it is found that the deflection values obtained experimentally in TEST_2 are 13.84% more than the nonlinear displacement value for upper flange and 12.83% more than the nonlinear displacement one for lower flange. Load-deflection diagrams that are obtained by the finite element model and the experimentally for NPI_280_TEST_2 cellular beam specimen are illustrated in Figures 6.47 and 6.48, respectively.

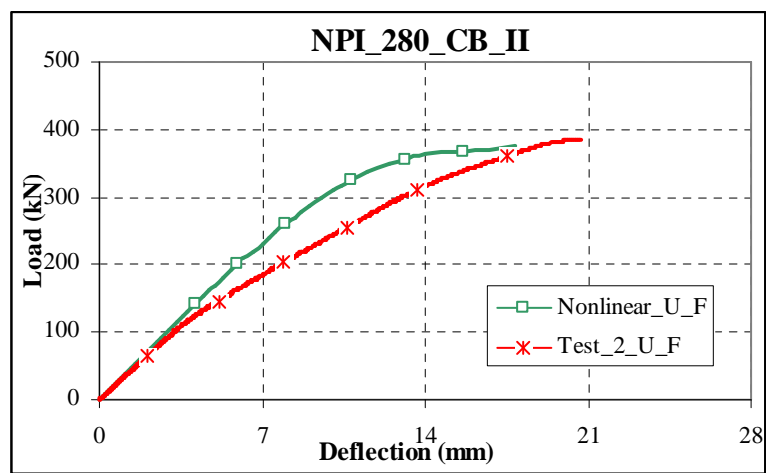


Figure 6.47 Load-deflection-curve for upper flange of NPI_280_TEST2

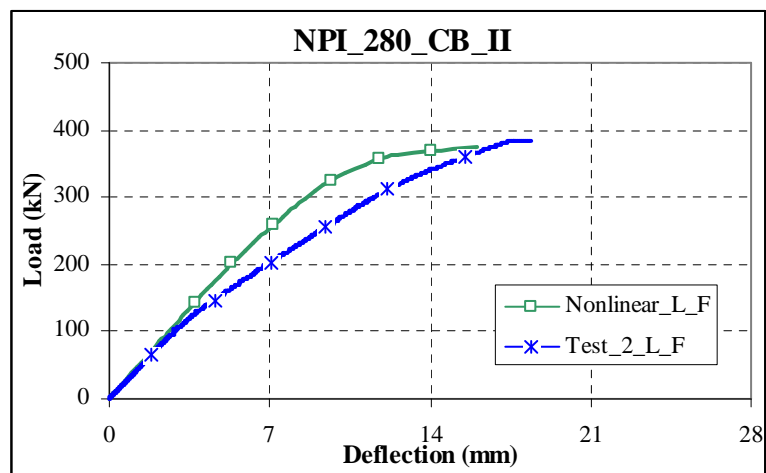


Figure 6.48 Load-deflection-curve for lower flange of NPI_280_TEST2

When the experimental results are compared with those of nonlinear solution values, it is noticed that the deflection values obtained experimentally in TEST_3 are 9.97% more than the nonlinear displacement value for upper flange and 7.89% more than the nonlinear displacement one for lower flange. Load-deflection diagrams that are obtained by the finite element model and the experimentally for NPI_280_TEST_3 cellular beam specimen are illustrated in Figures 6.49 and 6.50, respectively.

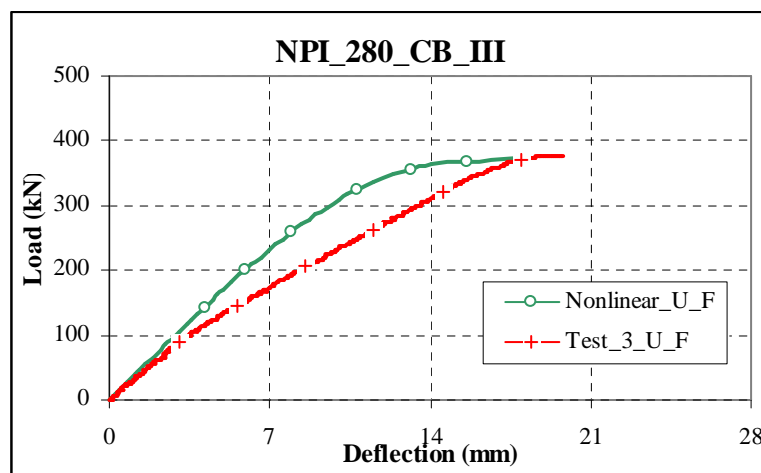


Figure 6.49 Load-deflection-curve for upper flange of NPI_280_TEST3

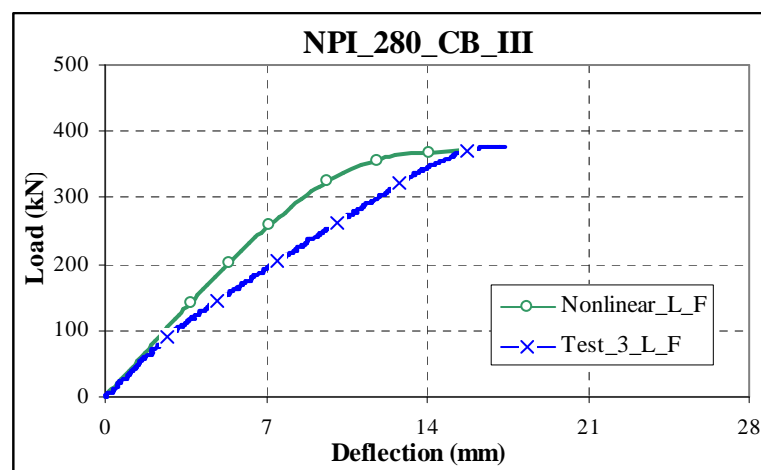


Figure 6.50 Load-deflection-curve for lower flange of NPI_280_TEST2

When the experimental results are compared with those of nonlinear solution values, it is found that the deflection values obtained experimentally in TEST_4 are 10.36% more than the nonlinear displacement value for upper flange and 6.39% more than the nonlinear displacement one for lower flange. Load-deflection diagrams that are obtained by the finite element model and the experimentally for NPI_280_TEST_4 cellular beam specimen are illustrated in Figures 6.51 and 6.52, respectively.

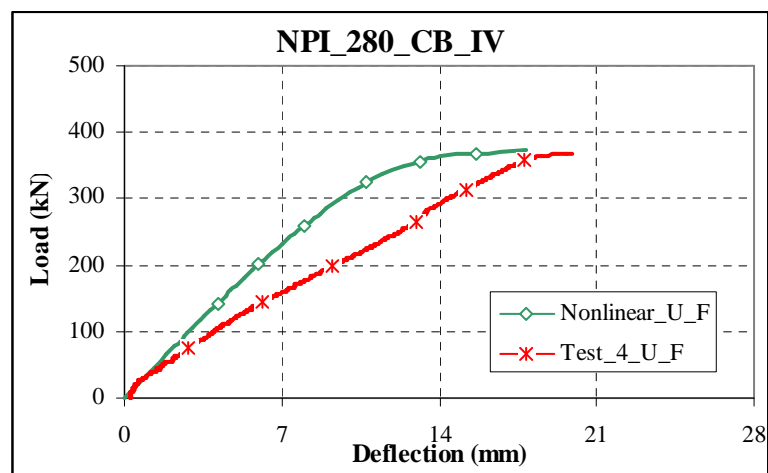


Figure 6.51 Load-deflection-curve for upper flange of NPI_280_TEST4

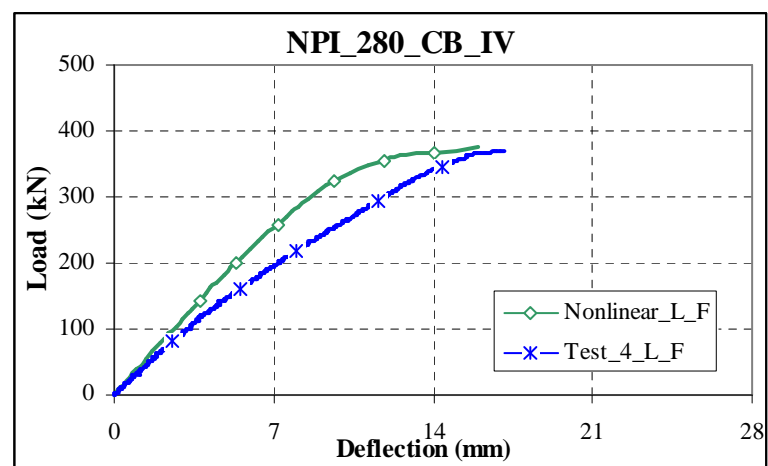


Figure 6.52 Load-deflection-curve for lower flange of NPI_280_TEST4

CHAPTER 7

SUMMARY AND CONCLUSIONS

7.1 Overview and summary of the thesis

The goal of this research presented is to investigate the ultimate load carrying capacity of optimally designed non-composite cellular beams. The study consists of three main parts: optimum design of steel cellular beams, experimental study on these beams and finite element analysis of these web-expanded beams. The results obtained in these parts are discussed in this study.

In the first part of the present study, the harmony search (HS) algorithm based optimization method and particle swarm optimization (PSO) algorithm are applied to the optimum design problems of steel cellular beams where the design constraints are implemented from BS5950 provisions. In this formulation, the sequence number of Universal Beam (UB) section, hole diameter and the total number of holes in the cellular beam are treated as design variables. The optimization problem of cellular beam with 4-m span has been solved with HS and PSO methods to illustrate accuracy and performance of methods on cellular beams. In the harmony search technique, algorithm parameters, *hms*, *hmcr* and *par* affect the value of minimum weight. For the harmony search algorithm, high *hmcr*, especially from 0.70 to 0.95 and the values of *par* ranging from 0.20 to 0.50 contribute excellently to FORTRAN

programming outputs, while *hms* demonstrates little correlation with improvement in performance. Geem's sensitivity analysis of *hmcr* and *par* is also confirmed in the optimization part of this study. In the particle swarm method, however, algorithm parameters are treated as static quantities, and thus they are assigned to appropriate values chosen within their suggested ranges of following values: Inertia of particles $w \in (0.05 \sim 0.50)$, number of particles $\mu \in (10 \sim 50)$, trust parameters in swarm c_1 and $c_2 \in (1.0 \sim 2.0)$ and time step value $\Delta t \in (1.0)$. While solving the design problem, PSO parameters are analyzed so that the most appropriate ones are identified. These observations point out that the variations in the parameter set have effect on the performance of the algorithm.

Secondly, the ultimate load carrying capacities of optimally designed steel cellular beams are tested in a self reacting frame. The tested cellular beam specimens are designed by using harmony search optimization method. The tests have been carried out on twelve full-scale non-composite cellular beams. There are three different types of NPI_CB_240, NPI_CB_260 and NPI_CB_280 I-section beams, and four tests have been conducted for each specimen. These optimally designed beams which have beginning span lengths of 3000 mm are subjected to point load acting in the middle of upper flange.

The last part of the study focuses on performing a numerical study on steel cellular beams by utilizing finite element analysis. The finite element method has been used to simulate the experimental work by using finite element modeling to verify the test results and to investigate the non-linear behaviour of failure modes such as web-post buckling and vierendeel bending of NPI_240, NPI_260 and NPI_280 section steel cellular beams. For this purpose, ANSYS-workbench finite element modeling program is used to develop a three dimensional finite element beam model. Nonlinear finite element models of these NPI section steel cellular beam specimens are built to determine and

investigate the maximum stress and displacement concentrations. While the non-linear buckling analysis of cellular beams with ANSYS software is done, the following assumptions are taken into account:

- 10-node high-order element with quadratic displacement behaviour is defined
- Geometrically as well as materially non-linear calculation is used
- Tetrahedron meshing option is selected
- Bonded contact is selected between NPI profile section parts and supporting connection plates
- Newton-Raphson iterative algorithm is used for the solution of equations
- The material properties used in all NPI section beams are determined through tensile tests of coupons taken from the test beams
- The beam geometry is based on the measured dimensions of the tested beams.
- The load is applied as pressure on the area described in the middle of the upper flange.

7.2 Conclusions

In this dissertation study, the optimum design of cellular beams turns out to be discrete nonlinear programming problem when formulated according to the constraints specified in SCI. The design optimization techniques developed are based on the harmony search and particle swarm optimization algorithms. As it is demonstrated in the cellular beam with 4-m span example, although the algorithms of HS and PSO are mathematically relatively simple, they are quite robust in finding the solutions of combinatorial optimum design problems. This design example illustrates that, in both methods, the minimum weight of the

cellular beam is obtained in relatively little number of iterations. Comparison of the optimum designs attained by harmony search algorithm and particle swarm optimizer clearly demonstrates that both techniques find almost same results but the harmony search algorithm yields a slightly better solution than the particle swarm optimizer for cellular beam with 4-m span example at the same number of structural analyses. Indeed, the minimum weight obtained with HS algorithm is 0.6% lighter than PSO algorithm. It is noticed that both the strength and geometric constraints are dominant in HS algorithm while only the strength constraints are severe in PSO algorithm in this design problem. This result also demonstrates that harmony search algorithm is a quite rapid and effective method for obtaining the optimum design of small-scale problems that consist of a small number of decision variables. Consequently, the selected method, HS algorithm, is recommended for application of the optimization of the three different NPI section cellular beams.

In the experimental part of this dissertation, the ultimate load carrying capacities of optimally designed steel cellular beams are then performed under the action of same concentrated loadings in a self reacting frame. The tests have been carried out on twelve full-scale non-composite cellular beams. The first two experiments on NPI_240 section beams have failed because of lateral torsional buckling due to a lack of lateral support. This means, even though the members relatively short spans, lateral supports are governing factor for the analysis of beams. When the lateral movement is prevented, web buckling failure mode has been described for the other two specimens on NPI_240 section beams. The results obtained from experimental tests on NPI_260 section beams, on the other hand, demonstrate that since the load is applied on the holes, in addition to web buckling, vierendeel bending has occurred on all of the four beams. This means that, when load is applied directly over the circular openings, the failure behaviour controlled by vierendeel bending mechanism. Lastly, the results obtained from experimental tests on NPI_280

section beams reveal that the failure of all four NPI_280 steel cellular beams under directly-applied concentrated loading over a web-post is defined as web-post buckling.

In the last part of the study the experimental work is simulated by using ANSYS-workbench finite element integrated software program to verify the test results and to a good degree with the non-linear behaviour of failure modes such as web-post buckling and vierendeel bending of NPI_240, NPI_260 and NPI_280 section steel cellular beams. Failure loads obtained from experimental tests are compared with finite element analysis values for these three cellular beams. Load-deflection diagrams shown in the study reveal that average deflection values obtained from experimental tests for upper and lower flange of NPI_240 section beams under 280 kN load are respectively 9.31% and %7.01 lower than finite element analyze results which is the closest value obtained between them. Moreover, the failure loads obtained from experimental tests are compared with finite element analysis values for NPI_260 cellular beam. The load-deflection diagrams shown in the study also reveal that average deflection values obtained from experimental tests for upper and lower flange of NPI_260 cellular beams under 220 kN load are respectively 9.19% and 10.06% more than from FEA results which is again within the reasonable range. Finally, obtained failure loads from experimental tests are also compared with FEA values for NPI_280 cellular beam. The load-deflection diagrams related with NPI_280 cellular beam illustrated in the study reveal that average deflection values obtained from experimental tests for upper and lower flange of NPI_280 cellular beams under 375 kN load are respectively 11.45% and 9.38% more than from FEA results which is within the acceptable range. These results demonstrate that the nonlinear analysis results correlate well with experimental ones and the discrepancy is within 10%.

REFERENCES

- [1] Macsteel Service Centers SA (Pty) Ltd., *Design of Cellular Beams*, Johannesburg, South Africa, <http://www.macsteel.zo.ca/cellbeam>, 2008.
- [2] ASD Westok Ltd. Charles Roberts Office Park Charles Street, Horbury Junction Wakefield WF4 5FH., <http://www.asdwestok.co.uk/>, 2009
- [3] M.D. Altifillisch, B.R. Cooke and A.A. Toprac, “*An investigation of open web-expanded beams*”, *Welding Research Council Bulletin*, Vol.47, pp.77-88, 1957
- [4] A.A. Toprac and B.R. Cooke, “*An experimental investigation of open web beams*”, *Welding Research Council Bulletin*, New York, Vol.47, pp.1-10, 1959
- [5] A.N. Sherbourne, “*The plastic behavior of castellated beams*”, *Proc. 2nd Commonwealth Welding Conference. Inst. Of Welding, London*, Vol.C2, pp.1-5, 1966
- [6] A. Bazile and J. Texier, “*Tests on castellated beams*”, *Constr. Métallique*, Paris, France, Vol1 (3), pp.12-25, 1968
- [7] M.U. Husain and W.G. Speirs, “*Failure of castellated beams due to rupture of welded joints*”. *Acier-Stahl-Steel*, Vol.1, 1971
- [8] Husain, M.U., and Speirs, W.G. 1973. “*Experiments on castellated steel beams*”, *J. American Welding Society, Welding Research Supplement*, Vol.52 (8), pp.329-3423, 1973

- [9] A.R. Galambos, M.U. Husain and W.G. Spin, “*Optimum expansion ratio of castellated steel beams*”, Engineering Optimization, London, Great Britain, Vol.1, pp.213-225, 1975
- [10] W. Zaarour, R.G. Redwood , “*Web buckling in thin webbed castellated beams*”, Journal of Structural Engineering (ASCE), Vol.122 (8), pp.860-866, 1996
- [11] R.G. Redwood, S. Demirdjian, “*Castellated beam web buckling in shear*” Journal of Structural Engineering (ASCE), Vol.124 (10), pp.202-207, 1998
- [12] F. Erdal and M.P. Saka, “*Optimum design of castellated beams using harmony search algorithm*”, 8th World Congress on Structural and Multidisciplinary Optimization, Lisbon, Portugal, June 1-15, 2009
- [13] R.M. Lawson, “*Design for openings in the webs of composite beams*”, Steel Construction Institute, 1988
- [14] J.K. Ward, “*Design of composite and non-composite cellular beams*”, The Steel Construction Institute Publication, 1990
- [15] M.C. Dionisio, R.M. Hoffman, J.R. Yost, D.W. Dinehart, S.P. Gross, “*Determination of Critical Location for Service Load Bending Stresses in Non-Composite Cellular Beams*” 17th ASCE Engineering Mechanics Conference June13-16, University of Delaware, Newark, DE, 2004.
- [16] R. Hoffman, D. Dinehart, S. Gross, J. Yost, “*Analysis of stress distribution and failure behaviour of cellular beams*” The Proceedings of International Ansys Conference, 2006

- [17] F. Erdal and M.P. Saka, “*Optimum design of cellular beams using harmony search algorithm*”, The Proceedings of 6th International Conference on Engineering Computational Technology, Athens, Greece, September 2-5, 2008
- [18] F. Erdal, E. Doğan and M.P. Saka “*Optimum Design of Cellular Beams Using Harmony Search and Particle Swarm Optimizers*” Journal of Constructional Steel Research Vol.67 (2), pp.237-247, February, 2011
- [19] D. Kerdal and D. A. Nethercot, “*Failure modes for castellated beams*”, Journal of Constructional Steel Research, Vol.4, pp.295-315, 1984
- [20] D. Kerdal and D. A. Nethercot, “*Lateral-torsional buckling of castellated steel beams*”, Journal of The Institution of Structural Engineers, Part A Design and Construction, Vol.60B, pp.53-61, 1982
- [21] British Standards, BS 5950, “*Structural Use of Steelworks in Building. Part 1. Code of Practice for Design in Simple and Continuous construction, hot rolled sections*”, British Standard Institution, London, U.K., 2000
- [22] H.C. Olander, “*A method of calculating stresses in rigid frame corners*”, Journal of ASCE, August, 1953.
- [23] R. Horst and H. Tuy, “*Global Optimization; Deterministic Approaches*”, Springer, 1995.
- [24] R. Paton, “*Computing with Biological Metaphors*”, Chapman & Hall, USA, 1994.

- [25] C. Adami, “*An introduction to Artificial Life*”, Springer-Verlag/Telos, 1998
- [26] C. Matheck, “*Design in Nature: Learning from Trees*”, Springer-Verlag, Berlin, 1998.
- [27] M. Mitchell, “*An Introduction to Genetic Algorithms*”, The MIT Press, 1998
- [28] J. Kennedy, R. Eberhart and Y. Shi, “*Swarm Intelligence*”, Morgan Kaufmann Publishers, 2001
- [29] G.A. Kochenberger and F. Glover, “*Handbook of Metaheuristics*”, Kluwer Academic Publishers, 2003
- [30] L.N. De Castro and F.J. Von Zuben, “Recent Developments in Biologically Inspired Computing”, Idea Group Publishing, USA, 2005.
- [31] J. Dreco, A. Petrowski, P. Siarry and E. Taillard, “*Metaheuristics for Hard Optimization*”, Springer-Verlag, Berlin, Heidelberg, 2006
- [32] S. Kirkpatrick, C.D. Gelatt and M.P. Vecchi, “*Optimization by Simulated Annealing*”, Science, Vol.220, pp.671-680, 1983.
- [33] I. Rechenberg, “*Cybernetic Solution Path of An Experimental Problem*”, Royal Aircraft Establishment, Library translation No. 1122, Farnborough, Hants., UK, 1965.

- [34] J. Kennedy and R. Eberhart, "*Particle Swarm Optimization*", IEEE International Conference on Neural Networks, IEEE Press, Vol.4, pp.1942-1948, 1995.
- [35] F. Glover, "*Tabu Search-Part I*", ORSA Journal on Computing, Vol.1 (3), 190-206, 1989.
- [36] M. Dorigo and T. Stützle, "*Ant Colony Optimization*", A Bradford Book, Massachusetts Institute of Technology, U.S.A., 2004.
- [37] K.S. Lee and Z.W. Geem, "*A New Structural Optimization Method Based on the Harmony Search Algorithm*", Computers and Structures, Vol.82, pp.781-798, 2004.
- [38] D.E. Goldberg, "*Genetic Algorithms in Search, Optimization and Machine Learning*", Addison Wesley, 1989.
- [39] M.P. Saka, "*Optimum Design of Steel Frames using Stochastic Search Techniques Based on Natural Phenomena: A Review*", Civil Engineering Computations: Tools and Techniques, Ed. B. H. V. Topping, Saxe-Coburgh Publications, pp.105-147, 2007.
- [40] O. Hasaebi , S. arbař, E. Dođan, F. Erdal, M. P. Saka, "*Performance evaluation of metaheuristic search techniques in the optimum design of real size pin jointed structures*", Computers and Structures, Vol.87 (5-6), pp.284-302, 2009.
- [41] Lee, K.S. and Geem, Z.W., "*A new meta-heuristic algorithm for continuous engineering optimization: harmony search theory and*

practice”, Computer Methods in Applied Mechanics and Engineering, Vol.194, pp.3902-3933, 2005.

- [42] LRFD-AISC, “*Manual of Steel Construction-Load and Resistance Factor Design*”, SA, 1986.
- [43] M. P. Saka, “*Optimum geometry design of geodesic domes using harmony search method*”, Advances in Structural Engineering, Vol.10 (6), pp.595-606, 2007
- [44] M. P. Saka, “*Optimum design of steel frames to BS5950 using harmony search algorithm*”, Journal of Constructional Steel Research, Vol. 65, pp.36-43, 2009
- [45] F. Erdal and M. P. Saka, “*Effect of beam spacing in the harmony search based optimum design of grillages*”, Asian Journal of Civil Engineering, Vol. 9 (3), pp. 215-228, 2008
- [46] F. Erdal and M. P. Saka, “*Optimum Design of Grillage Systems Using Harmony Search Algorithm*”, Journal of Structural and Multidisciplinary Optimization, Vol. 38 (1), pp.25-41, 2009
- [47] Manual of Steel Construction, Allowable Stress Design, 9th edition, AISC, American Institutes of Steel Construction, Inc, Chicago, Illinois, USA, 1989.
- [48] Hasańcebi, O., Erdal, F., and Saka, M.P., “*An Adaptive Harmony Search Method for Structural Optimization*”, Journal of Structural Engineering – ASCE, Vol.136 (4), pp. 419-431, April 2010.

- [49] Bonabeau E, Dorigo M and Theraulaz G, “*Swarm Intelligence: From Natural to Artificial Systems*”, Oxford University Press, U.K., 1999
- [50] Kennedy J, Eberhart R and Shi Y, “*Swarm Intelligence*”, Morgan Kaufmann Publishers, 2001
- [51] Kennedy J, Eberhart RC. “*Particle Swarm Optimization*”, In: Proceedings of IEEE International Conference on Neural Networks NJ: Piscataway; 1942-48, 1995.
- [52] Perez, R. E. and Behdinan, K., “*Particle Swarm Approach for Structural Design Optimization*”, Computers and Structures, 85 (19-20), 1579-1588, 2007.
- [53] S. He, E. Prempain and Q.H. Wu “*An Improved Particle Swarm Optimizer for Mechanical Design Optimization Problems*” , Engineering Optimization, Vol.36 (5), pp.585-605, 2004
- [54] Fourie, P. and Groenwold, A., “*The Particle Swarm Optimization Algorithm in Size and Shape Optimization*”, Structural and Multidisciplinary Optimization, Vol.23 (4), 259-267, 2002
- [55] E. Doğan, M. P. Saka, “*Optimum Design of Unbraced Steel Frames to LRFD-AISC Using Particle Swarm Optimization*”, Advances in Engineering Software (under review), 2010
- [56] D.M. Himmelblau, “*Applied Nonlinear Programming*” McGraw-Hill, New York, 1972

- [57] Runarsson, T.P. and Yao, X., “*Stochastic Ranking for Constrained Evolutionary Optimization*” IEEE Transactions on Evolutionary Computation, Vol.7 (1), pp.19-44, 2000
- [58] Venter, G. and Sobieszczanski-Sobieski, J., “*Multidisciplinary Optimization of a Transport Aircraft Wing Using Particle Swarm Optimization*”, Structural and Multidisciplinary Optimization, Vol.26, pp.121-131, 2004.
- [59] Steelwork design Guide to BS 5950: Part 1, “*Section Properties, Member Capacities*”, Vol.1, 4th edition, The Steel Construction Institute, U.K., 1990.
- [60] W.F. Chen and E.M. Lui. “*Structural stability: theory and implementation*”, Elsevier, New York, 1987
- [61] “*Standart Test Methods and Definitions for Mechanical Testing of Steel Products*”, Designation A 370-07a, ASTM International, 100 Barr Harbor Drive, West Conshohocken, PA 19428-2959, United States

VITA

Ferhat Erdal

Middle East Technical University
Department of Engineering Sciences
Ankara, 06531, Turkey, Phone: +90-312-2104459
Email: eferhat@metu.edu.tr

INTERNATIONAL JOURNAL PAPER

Erdal F., Saka M.P. and Doğan E. “*Optimum Design of Cellular Beams Using Harmony Search and Particle Swarm Optimizers*” Journal of Constructional Steel Research Vol. 67, No: 2, Pp: 237-247, February, 2011

Hasançebi, O., Çarbaş, S., Doğan, E., **Erdal, F.** and Saka, M.P., “*Comparison of non-deterministic search techniques in the optimum design of real size steel frames*”, Computers and Structures, Vol. 88 No: (17-18), Pp: 1033-1048, September, 2010.

Hasançebi, O., **Erdal, F.**, and Saka, M.P., “*An Adaptive Harmony Search Method for Structural Optimization*”, Journal of Structural Engineering – ASCE, Vol. 136, No. 4, Pp: 419-431, April 2010.

Hasançebi, O., **Erdal, F.**, and Saka, M.P., “*Optimum Design of Geodesic Steel Domes under Code Provisions using Metaheuristic Techniques*” Journal of Engineering and Applied Sciences, Vol.2 Issue 2, Pp: 88-103, 2009

Saka M.P. and **Erdal F.** “*Harmony Search Algorithm Based Optimum Design of Grillage Systems.*” *Structural and Multidisciplinary Optimization*, Vol. 38, No: 1, Pp: 25-41, 2009.

O. Hasaebi , S. arbař, E. Dođan, **F. Erdal**, M. P. Saka, “*Performance evaluation of metaheuristic search techniques in the optimum design of real size pin jointed structures*”, *Computers and Structures*, Vol. 87 No: (5-6), Pp: 284-302, 2009.

F. Erdal and M. P. Saka, “*Effect of Beam Spacing in the Harmony search based optimum design of grillages*”, *Asian Journal of Civil Engineering*, Vol. 9, No: 3, Pp: 215-228, 2008.

E. Dođan, **F. Erdal**, and M. P. Saka, “*Optimum Design of Grillage Systems using Improved Particle Swarm Optimization Method*”, *Automation in Construction*, An International Journal, (under review)

NATIONAL JOURNAL PAPER

F. Erdal and M. P. Saka, “*Petek Kiriřlerin Yapılarda Kullanılması*” *Yapı Dünyası*

F. Erdal and M. P. Saka,” *Dairesel Gözenekli Petek Kiriřlerin BS řartnamesi kullanılarak Boyutlandırılması*” *Yapı Dünyası*

INTERNATIONAL CONFERENCE PAPER

F. Erdal and O. Hasaebi, “*Optimum Design of Geodesic Steel Domes under Code Provisions using Metaheuristic Techniques*”, 9th International Congress on Advances in Civil Engineering, September 27-30, 2010, Trabzon, Turkey

E. Doğan, **F. Erdal**, and M. P. Saka “*Optimum Design of Grillage Systems under Code Provisions using Particle Swarm Optimization*” *GECCO’10*, July 7–11, 2010, Portland, Oregon, USA. ACM 978-1-4503-0072-8/10/07

F. Erdal and M. P. Saka, “*Optimum Design of Castellated Beams Using Harmony Search Method*”, Proceedings of The Eight International Conference on Structural and Multidisciplinary Optimization, 1-5 June, 2009, Lisbon, Portugal.

F. Erdal and M. P. Saka, “*Optimum Design of Cellular Beams Using Harmony Search Method*”, Proceedings of The Ninth International Conference on Computational Structures Technology, 2-5 September, 2008, Athens, Greece.

F. Erdal and M. P. Saka, “*Optimum Design of Grillage Systems Using the Harmony Search Algorithm*”, The Eighth International Conference on Computational Structures Technology, CST 2006, Las Palmas de Gran de Canarias, Spain, 12-15 September 2006

NATIONAL CONFERENCE PAPER

F. Erdal ve M.P. Saka “*Dairesel Gözenekli Petek Kirişlerin Harmoni Arama Yöntemi Kullanılarak Optimum Boyutlandırılması*” XVI. Ulusal Mekanik Kongresi, UMK-2009, Kayseri, 22-26 Haziran 2009

RESEARCH PROJECTS

O. Hasaңebi, M. P. Saka, **F. Erdal**, S. Çarbaş, E. Doğan, and Ö. Kurç, “*Optimum Design of Three Dimensional Steel Skeleton Structures Using Stochastic Search Techniques and its National Structural Engineering Applications*”, Turkish Scientific and Technical Research Council

(TUBITAK), Ankara, Turkey, Project No: 108M070, (75000 US\$), started on: 1st June 2008, To be Completed on: 1st December 2010.

O. Hasaebi, M. P. Saka, **F. Erdal**, S. arbař ve E. Dođan, “*Stokastik Optimizasyon Yöntemleri Kullanılarak Ü Boyutlu elik Tařıyıcı Sistemlerin Optimum tasarımı ve Ülkemiz Yapı mühendisliğine Uygulanması*” Thesis Project BAP Project Code: BAP-2008-03-03-02

COURSE CERTIFICATES

“*High Performance Computations for Engineering*”, A Five Day Course for Engineering PhD Students, 17th May - 22nd May 2009 , Pollack Mihály Faculty of Engineering, University of Pécs, Hungary.

“*RC Structures under Extreme Loading Course Certificate*”, TMMOB Civil Engineering Organization 19-20 February 2009, METU, Ankara, Turkey.

EDUCATIONAL BACKGROUND

Middle East Technical University, Ankara, Turkey
2007- Department of Engineering Sciences, PhD.
2011 Thesis Title : “Ultimate Load Capacity of Optimally Designed Cellular Beams”

Middle East Technical University, Ankara, Turkey
2005- Department of Engineering Sciences, Msc.
2007 Thesis Title : “Optimum Design of Grillage Systems Using Harmony Search Algorithm”

1999-2003 Akdeniz University, Antalya, Turkey
Department of Civil Engineering

EMPLOYMENT RECORD

Research Assistant - METU, Engineering Sciences mechanical laboratory.

TEACHING EXPERIENCE

ES 202 - Mathematics for Engineers

ES 221 - Engineering Mechanics

ES 223 - Statics and Strength of Materials

ES 224 - Strength of Materials

ES 361 - Computing Methods in Engineering

COMPUTER SKILLS

Application Development-Engineering: MATLAB, MathCAD, FORTRAN

Package Software: AutoCAD, Solidwork, SAP2000, ANSYS-Workbench,

ABAQUS, STA4CAD